A NOISE SPECTRUM ANALYZER FOR FREQUENCIES LESS THAN ONE HERTZ AND INVESTIGATION OF LOW FREQUENCY ZENER DIODE NOISE

By

TELVA JOE BOEHM

Bachelor of Science in Electrical Engineering
The University of Texas - Austin
Austin, Texas
1965

Master of Science
Oklahoma State University
Stillwater, Oklahoma
1970

Submitted to the Faculty of the Graduate College
of the Oklahoma State University
in partial fulfillment of the requirements
for the Degree of
DOCTOR OF PHILOSOPHY
December, 1975

A NOISE SPECTRUM ANALYZER FOR FREQUENCIES LESS THAN ONE HERTZ AND INVESTIGATION OF LOW FREQUENCY ZENER DIODE NOISE

Thesis Approved:

Thesis Adviser

Dean of the Graduate College

ACKNOWLEDGEMENTS

I wish to express thanks and sincere gratitude to my thesis adviser, Dr. Hans R. Bilger, for the original idea of this research. His interest, guidance, encouragement and expert assistance were instrumental in making this thesis possible.

A very special thanks to Dr. B. L. Basore for his advice, help, and personal interest in my welfare during my graduate studies.

I wish also to thank Professor Paul McCollum and Dr. Don Holbert, the other members of my committee, for their interest and advice.

The contributions of Dr. J. A. Ringo of Washington State University, who provided the Zener diodes used in this study and made the initial measurements on these devices are here acknowledged.

Finally, to my wife Elizabeth I give my warmest appreciation, for without her assistance, understanding, and encouragement this endeavor would have not been possible. My children, Gwen and Trudy are here thanked for their patience and understanding.

TABLE OF CONTENTS

LIST OF TABLES

LIST OF FIGURES

Figure Page

CHAPTER I

INTRODUCTION

The term "noise" is a generic word and therefore has physical meaning only when defined in the context of the specific system to which it is applied. This thesis concerns itself entirely with the measurement and evaluation of very low frequency (frequencies less than 1 Hz) electronic noise arising in electronic systems and devices.

Electronic noise generally takes on the character of very small and random fluctuations in the measurable parameters of the device or system under consideration. The parameter most often measured in a study of this type is usually either an output voltage or current.

Various types of electronic noise have been postulated, observed, and to an extent clearly understood in the past. Examples of these types are Nyquist or thermal noise, generation-recombination noise, and shot noise (for discussion of these see [33]). There is at least one type of noise referred to as 1/f or excess noise for which no generally acceptable theory has yet been presented. In addition the physical process which gives rise to this type of noise remains to be clearly identified. The reference to this noise as 1/f is loose. The 1/f term arises from the observed properties of the power spectral density of this noise.

From the standpoint of its power spectrum, 1/f noise can be regarded as a low frequency phenomenon which usually is observed at frequencies less than 10 Hz. It has been observed in numerous devices (for examples

see [31], [4], [23], and [7]) and in fact no device as yet has been shown to be 1/f noise free. As its name implies, the character of this noise is such that its power spectral density increases with decreasing frequency. A more precise form for describing this noise is

$$S(f) = \frac{K}{f^a} \tag{1-1}$$

where

$S(f)$ = noise power spectral density (V^2/Hz),

f = frequency (Hz), and

K and a = constants.

The constant "K" varies widely (several orders of magnitude) depending on the device being studied and the value of "a" generally lies between 0.8 and 2.

Since there is no generally accepted theory or explanation for the 1/f noise phenomenon, the case for 1/f noise rests solely on empirical evidence and its documentation. (In fact it is the empirical evidence which makes it difficult to find an appropriate theory.)

The essence of this thesis is to make reliable and calibrated measurements of noise at frequencies below 1 Hz thereby adding to the information available on this phenomenon. It is hoped that such measurements would contribute to the development of a satisfactory model for this noise and an understanding and identification of the physical process responsible for the phenomenon.

Techniques which provide for a reliable and calibrated measurement of low frequency noise are in themselves of practical importance. Since noise imposes limits on sensitivity and accuracy in the measurement of physical quantities, its identification and minimization are of primary

concern to the solid state physicist or semiconductor device design engineer. Here measured data is the only means available by which the noise characteristics of a new process or device may be evaluated.

Conventional analog techniques for measuring noise become impractical at frequencies less than 1 Hz. As a result digital recording and processing of noise data is used in this study. A substantial portion of this thesis is devoted to a description and discussion of the equipment which was designed and constructed to make low frequency noise studies possible. This equipment was used to investigate the low frequency noise behavior of Zener diodes in the frequency range of 0.4 Hz to 8×10^{-5} Hz. Reports on Zener diode noise have previously appeared in the literature (see Haitz [16] and Ringo [28]); however, this investigation is apparently the first at frequencies below 0.1 Hz.

There are two important reasons for choosing to investigate the noise characteristics of Zener diodes. First, these devices are basically used as secondary voltage references. These noise measurements can be used as a measure of the stability of these devices, at least in the short term sense, thereby giving an indication of their quality as references. Also, these devices have the semiconductor phenomenon of "avalanching" as the physical mechanism basic to their operation. An investigation of the noise characteristics of this type of device below 0.1 Hz provides primary information on the noise behavior of such in this frequency range.

Chapters II, III, and IV of this thesis discuss the electronic equipment that was designed and constructed for the study of low frequency noise. The processing techniques used on the measured data are treated in Chapter V. Calibration information of the noise measuring

system is in Chapter VI. Chapters VII and VIII are devoted to the Zener diode noise measurements and their evaluation. Chapter IX covers the concluding remarks.

CHAPTER II

SPECTRUM ANALYZER

Introduction

This chapter concerns itself with a description of the data spectrum analyzer that was designed and constructed for the low frequency noise measurements reported in this work. Figure 1 shows a simplified block diagram of this analyzer which may be divided into three major parts. The first of these is a sensitive moving mirror galvanometer whose output is a beam of light. It is to this device that the data signals to be measured are fed. The second and most complex part of the system is the positional scanner. The function of this part is to periodically measure the deflection of the light beam from the galvanometer. The third part is composed of the digital timer, card punch interface, and card punch shown in Figure 1, and is referred to simply as the digital recorder. The function of this part is to permanently record the output from the positional scanner. The subsequent sections of this chapter deal with the details of each of these parts.

Galvanometer

Physical Description

A moving coil, mirror type, galvanometer is used to detect the input to the spectrum analyzer. The galvanometer used here is a modified Lange

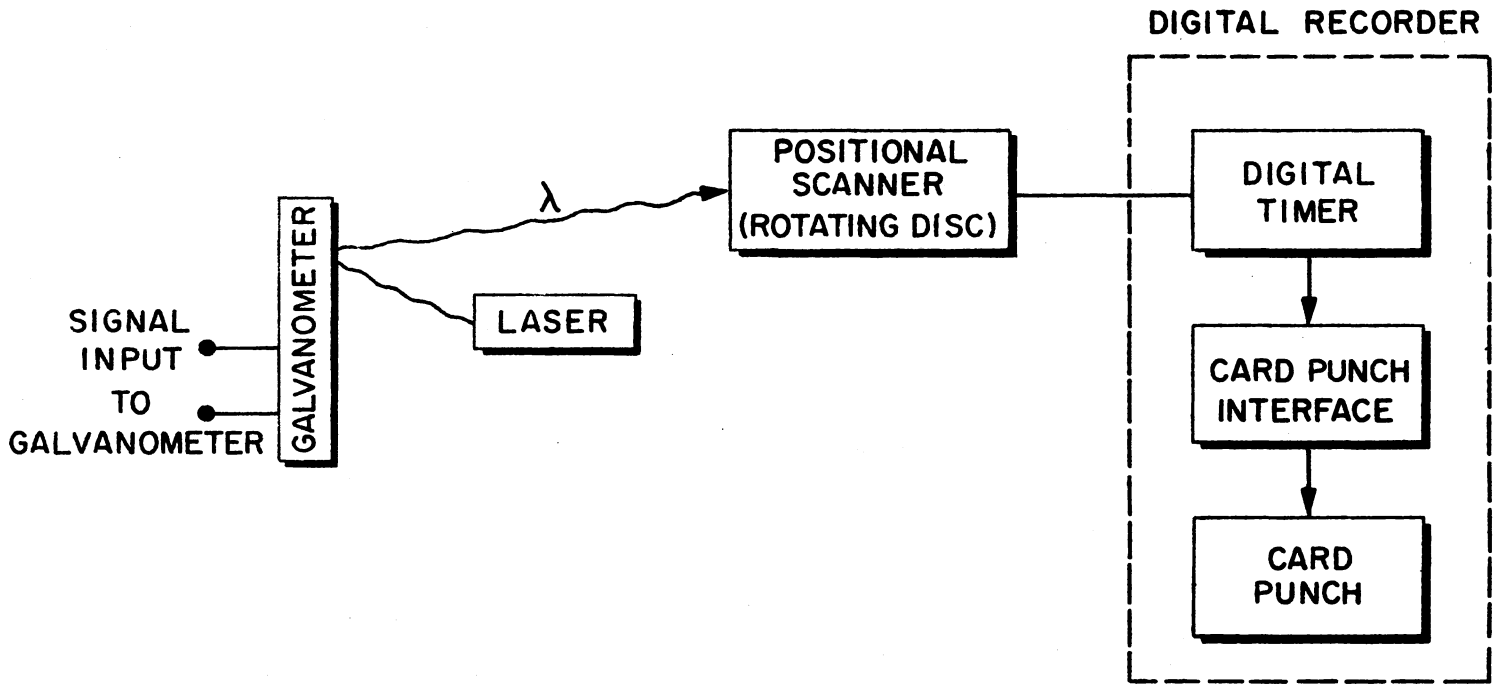

Figure 1. Block Diagram of the Spectrum Analyzer

model MG2 manufactured by the Dr. B. Lange Company of Berlin, Germany. Modifications were made to this instrument to make it compatible with the rest of the system. The built in optical system consisting of several fixed mirrors was disabled and the self contained light source removed. The light source that is now used is a low power He-Ne gas laser (University Laboratories Model 200). The galvanometer mirror is not optically flat. To compensate for the resulting light beam divergence, a 15 mm diameter, 101 mm focal length, positive meniscus lens was positioned between the laser and galvanometer. The galvanometer and lens assembly is contained in a metal box that was constructed to minimize air drafts, dust, and 60 Hz hum effects. Figure 2 shows a view of the box containing the galvanometer and lens assembly with its cover removed. The front portion of the laser can also be seen.

Specifications

The optical arm length of the galvanometer was measured and found to be 2.89 ± 0.01 m with a beam diameter at the end of the arm of 3.0 ± 0.5 mm. At this arm length, the sensitivity of the beam position to variations in room temperature was found to be less than 0.1 mm/°C.

The input resistance of this instrument was determined to be 1330 Ω ± 1% and its input voltage sensitivity is 1.56 ± 0.03 μV/mm. The frequency response of the spectrum analyzer is determined by that of the galvanometer. Figure 3 shows this response for four different values of external damping. These curves are closely approximated by a second order, low pass, filter function of the following form,

$$|A| = \frac{1}{\left[1 + \left(\frac{f}{f_c}\right)^2 + \left(\frac{f}{f_o}\right)^4\right]^{1/2}} \quad , \qquad (2\text{-}1)$$

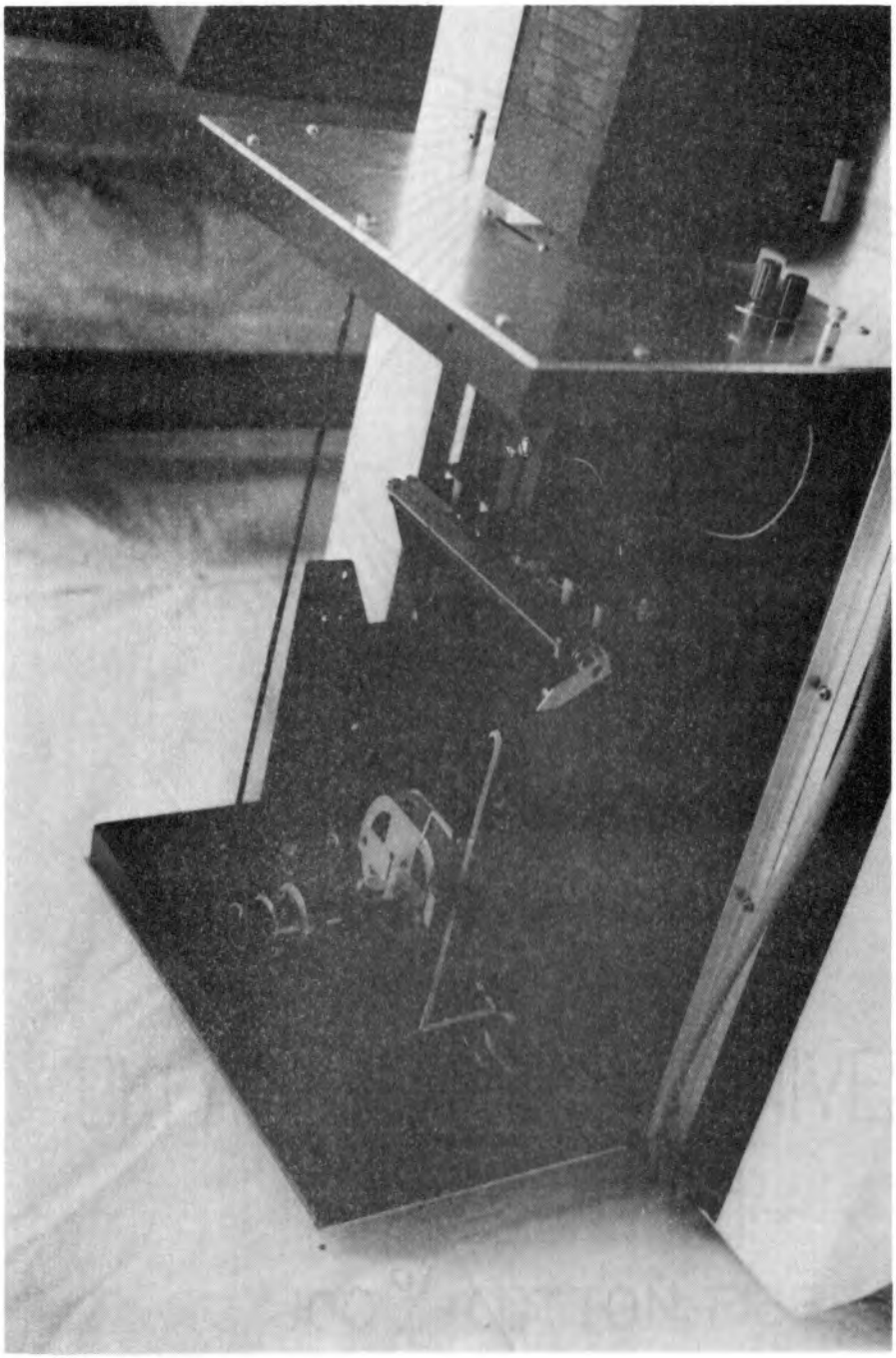

Figure 2. Galvanometer and Lens Assembly

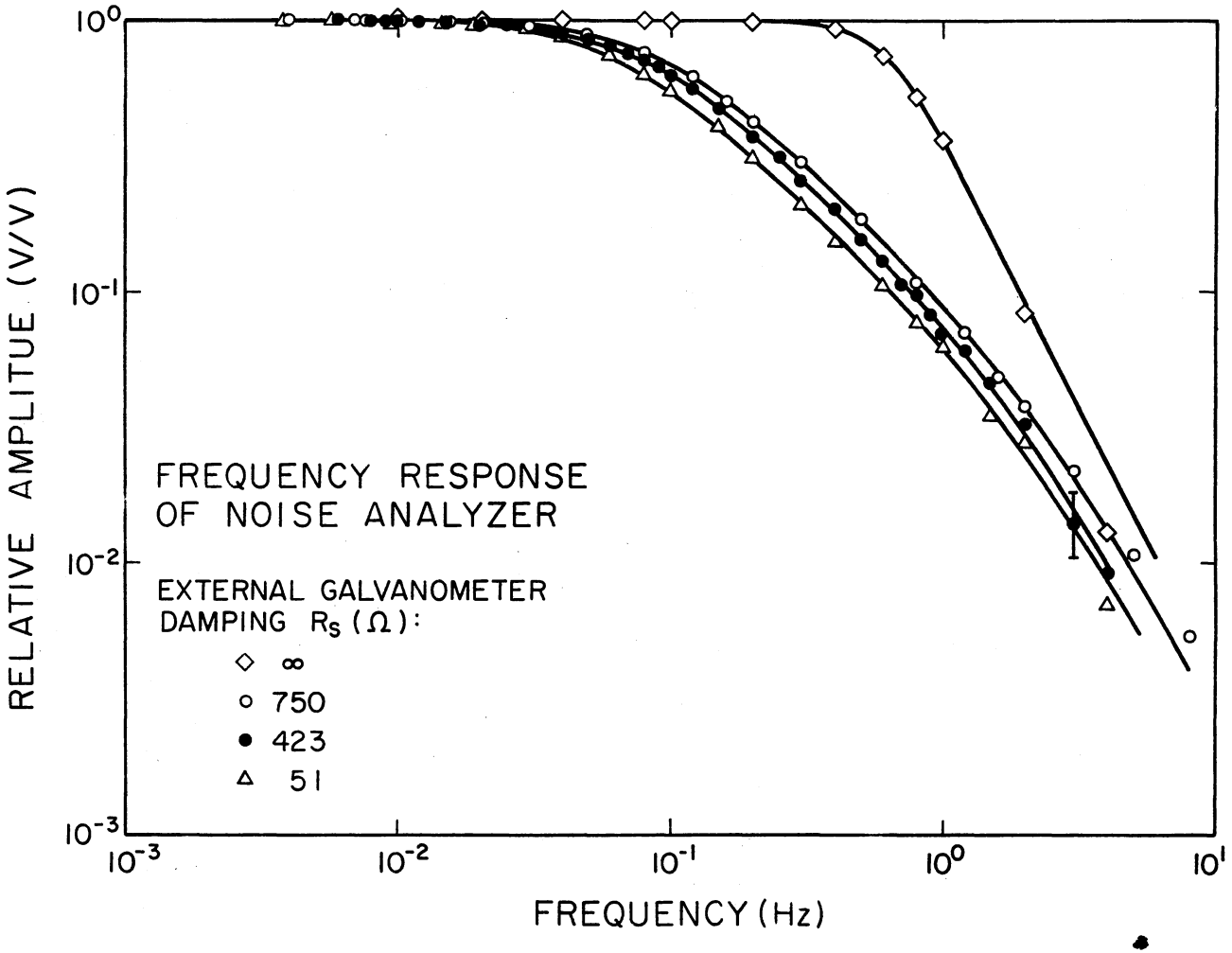

Figure 3. Frequency Response Characteristics of the Galvanometer and Spectrum Analyzer

where

$|A|$ = magnitude of the voltage response,

f = frequency (Hz), and

f_c and f_o = parameters determined by the galvanometer and its external damping.

For an external damping of 750 Ω the value of f_c and f_o are:

$$f_c = 0.0937 \pm 0.0004 \text{ (Hz)}$$
$$f_o = 0.51 \pm 0.02 \text{ (Hz)} \quad . \tag{2-2}$$

Additional detail regarding the measurement results presented in this section will be found in Chapter VI.

Positional Scanner

Introduction

The positional scanner is optically connected to the galvanometer through the reflected light beam. The function of the scanner is to periodically measure the position of the beam. The output from this device is a rectangular pulse whose width is a measure of the beam's position, and a momentary switch closure between each of these measurements. The switch closure is part of the required interface to the digital recorder discussed in the next section of this chapter.

Physical Description

A rear view of the positional scanner is shown in Figure 4. As can be seen in the figure, the scanner is basically a disc of 24 cm radius which rotates with constant speed. The mechanical drive for the disc is

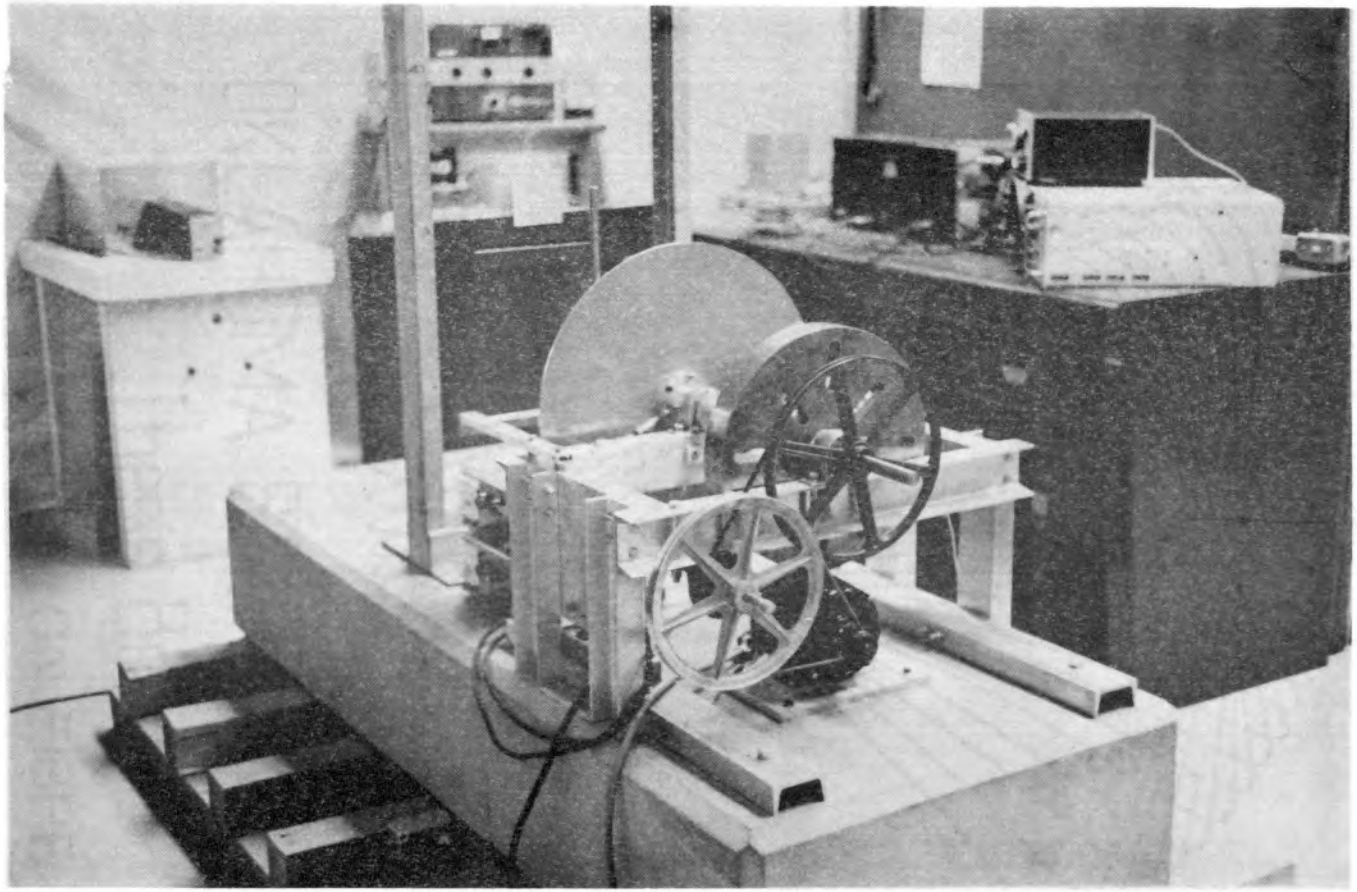

Figure 4. Rear View of the Positional Scanner

provided by a 3 phase, 1800 rpm synchronous motor. This motor is coupled to the disc through a speed reducing arrangement consisting of two "0" belts and two pairs of sheaves. The minor output requirement of a momentary switch closure is simply accomplished by a mechanical switch mounted to the frame supporting the disc. This switch is actuated by a cam on the axle of the rotating disc once for each revolution.

Principles of Operation

The geometry of the undeflected galvanometer light beam and the disc is such that the beam is roughly parallel to the disc's axis of rotation and strikes the disc 20.7 cm directly above this axis. The beam's path of travel for the driven galvanometer is along a horizontal line near the top of the disc. Near the edge of the disc and along a line of radius is a 24.6 mm long and 0.79 mm wide slit. This slit will be irradiated by the light beam once for each revolution of the disc for a time t_d approximately given by the following equation,

$$t_d = \frac{d}{\omega r} \tag{2-3}$$

where

ω = the angular velocity of the disc,

r = the distance from the axis of rotation to the point where the beam and slit intersect, and

d = diameter of the galvanometer beam.

There will always be this slit-beam intersection once each revolution so long as the beam falls on the disc and gets no nearer than 8 mm to the edge of the disc. The slit is coupled to a light sensitive photodiode operational amplifier combination (United Detector Technology Inc.

UDT-400) by means of optical fibers. This light sensitive device is rigidly mounted in front of the disc and along the disc's axis of rotation. The optical fibers are used to mechanically decouple the rotating disc from this light detector.

A fixed reference point is established on the disc by means of a small hole. This hole is 1.6 mm in diameter and is located opposite the center of the disc and along the diagonal which contains the slit. This hole together with an incandescent light source and a phototransistor, provide a means of detecting the instant a particular angular position of the rotating disc occurs during each revolution. An equation of the same form as (2-3) gives the time that this light source irradiates the phototransistor each revolution. Figure 5 shows the dimensional layout of the disc along with the relative locations of the slit, reference hole, and beam path.

The light sensitive device coupled to the slit, and the phototransistor associated with the reference hole, provide input signals to an electronic circuit. During the course of each disc revolution the phototransistor produces a pulse when the reference hole passes between it and its light source. Similarly the photodiode operational amplifier produces a pulse when the slit intersects with the galvanometer light beam. The risetime associated with both of these pulses is primarily governed by the angular velocity of the disc. For the rotational speed of 0.89 rps, these risetimes were measured and found to be on the order of 300 μs. The pulse arising from the reference hole, "start-pulse", is used to set a flip-flop circuit. The pulse due to the slit, "stop-pulse", is used to reset this flip-flop. Referring again to Figure 5, the physical location of the phototransistor is such that the start-pulse

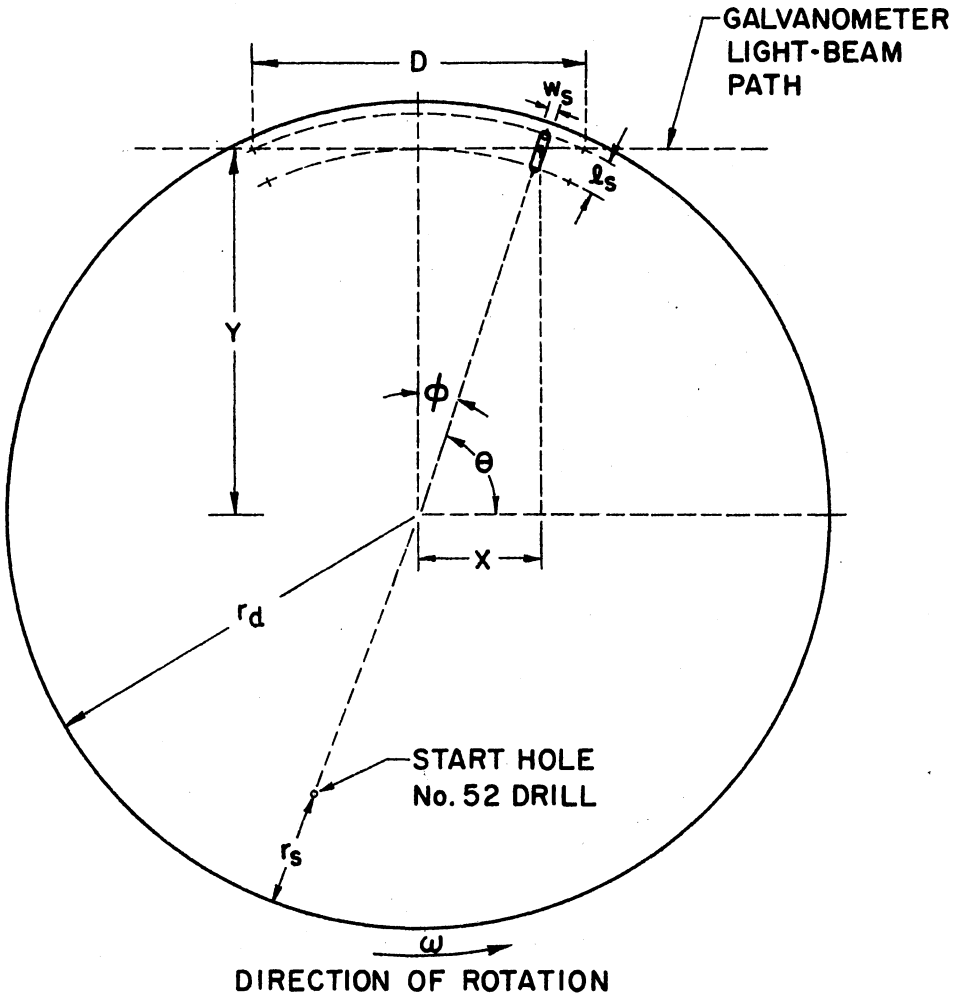

r_d = 24.00 ±0.05 cm

Y = 20.72 ±0.05 cm

ℓ_s = 2.46 ±0.03 cm

W_s = 0.79 ±0.03 cm

D = 20.40 ±0.05 cm

r_s = 7.30 ±0.03 cm

Figure 5. Dimensional Layout of the Rotating Disc

defines $\theta = 0$. The stop-pulse occurs at the value of θ corresponding to the beam-slit intersection. This value is clearly related to the time the flip-flop is in its set condition by the following formula,

$$\theta = \frac{2\pi t_s}{\tau} \qquad (2\text{-}4)$$

where

t_s = the time the flip-flop is in its set state, and

τ = rotational period of the disc.

From this and Figure 5, it follows that the horizontal position X of the beam at the time it intersects with the slit is given by

$$X = Y \text{ Cot } (\theta) = Y \text{ Cot } (\frac{2\pi t_s}{\tau}) \quad ; \qquad (2\text{-}5)$$

here

X = horizontal displacement of the beam with zero being defined as X_o when $\theta = \pi/2$, and

Y = a length parameter which is defined in Figure 5.

Thus the flip-flop's output, after suitable buffering, provides the primary output from the positional scanner. A circuit diagram of the electronics associated with the positional scanner is given in Appendix A.

There is a detail to be noted with regard to this positional measuring scheme. The rotating disc produces a measurement for each revolution. However, the time at which this measurement is made corresponds to exactly when the beam intersects the slit. Therefore, if the beam moves during a rotational period of the disc, the time between successive measurements fluctuates accordingly. This phenomenon is systematic and is accounted for in the data processing procedures discussed in Chapter V.

Specifications

The rotational frequency of the disc was measured and found to be 0.8902 ± 0.0006 rps. This was determined by measuring the time for the disc to make 3200 revolutions. Eight such measurements were made amounting to just under eighty hours of observation.

The dominant source of noise in the data acquisition system is traceable to fluctuations in the rotational period of the disc. These fluctuations were observed to be random with an effective rms value of 180 ± 10 μs. This number was obtained by fixing the beam from the galvanometer and taking 240 measurements of the width of the output pulse from the positional scanner. The relationship of these fluctuations to the measurement of the beam's position can be expressed using Equation (2-4).

$$X + \Delta X = Y \cot\left[\frac{2\pi(t_s - \Delta t_s)}{\tau}\right] \qquad (2\text{-}6)$$

where

Δt_s = effective rms fluctuation in the disc period, and

ΔX = the equivalent rms fluctuation in the position of the beam.

If the value of Δt_s is small then ΔX can be approximated by the following expression,

$$\Delta X \approx Y\left(\frac{2\pi\Delta t_s}{\tau}\right) \qquad . \qquad (2\text{-}7)$$

ΔX in turn can be related to an input voltage to the galvanometer by the equation

$$\Delta V = S\Delta X = SY\left(\frac{2\pi\Delta t_s}{\tau}\right) \qquad (2\text{-}8)$$

where

ΔV = the equivalent rms fluctuation of an input voltage to the galvanometer (μV), and

S = sensitivity of the galvanometer (1.56 μV/mm).

Measurements of Δt_s (Δt_s = 180 μs) show that these fluctuations correspond to 0.21 mm (Equation 2-7) or to 325 nV (Equation 2-8).

The maximum peak-to-peak detectable excursion of the galvanometer beam was measured and found to be 204.0 ± 0.5 mm. This corresponds to a maximum measurable peak-to-peak voltage signal of 312 μV referred to the input of the galvanometer.

Digital Recorder

Physical Description

Three commercially available electronic instruments comprise the digital recorder section of the spectrum analyzer. They are a Dymec 2401A Integrating Digital Voltmeter, a Dymec 2526A Card Punch Interface Unit, and an IBM 526 Assembly Keypunch. This equipment performs the function of encoding onto punch cards the information output from the positional scanner. Figure 6 shows the physical appearance of the digital recorder.

Principles of Operation

The rectangular pulse output from the positional scanner is used as an input signal to the digital voltmeter. The digital voltmeter, which is also a frequency counter, is used as a time measuring device, which measures the width of this pulse. The voltmeter's internal oscillator serves as a time base which is gated to its counting circuits by the pulse from the scanner. This timing information is routed through the

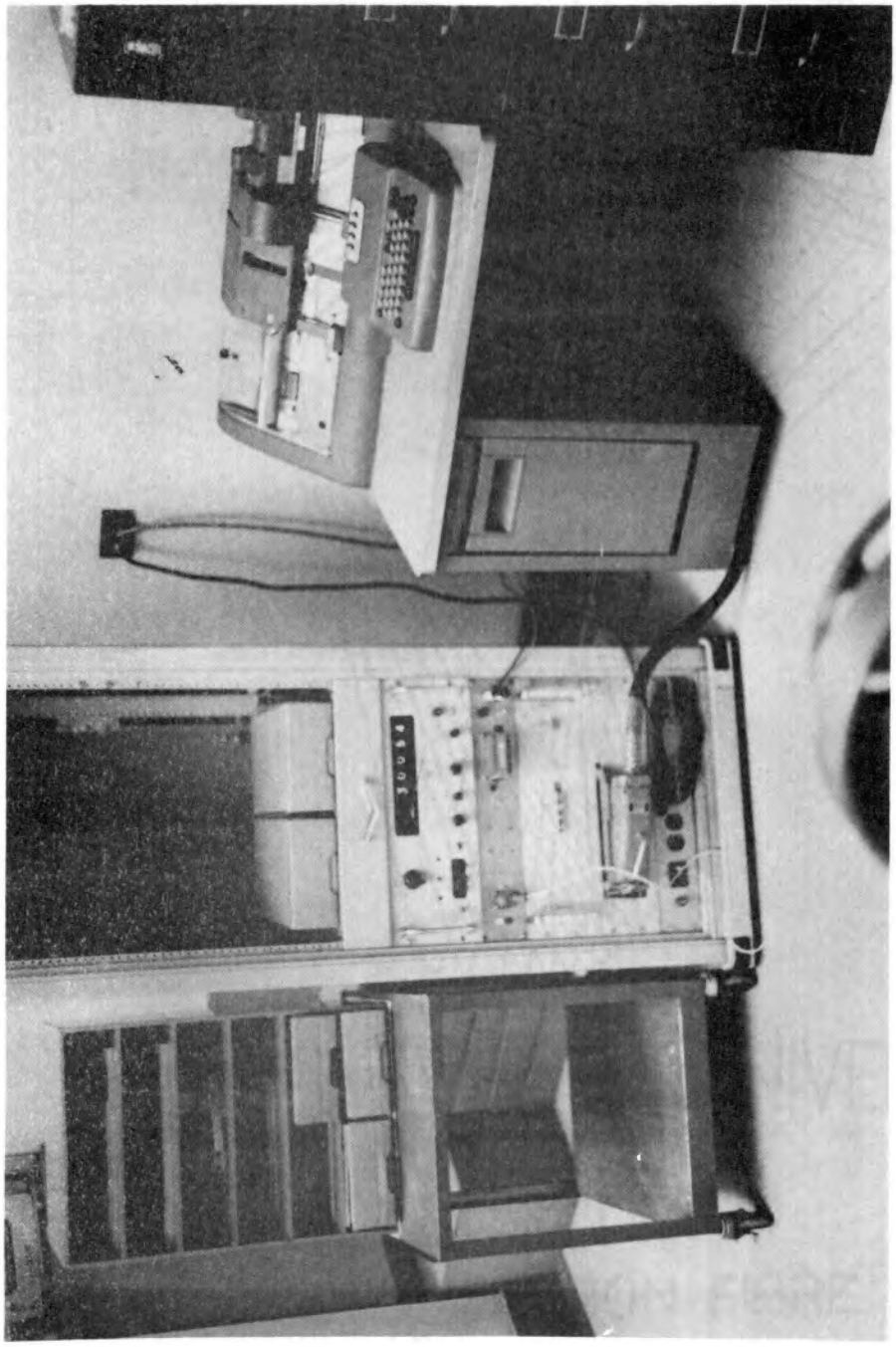

Figure 6. Digital Recorder

interface unit to the keypunch where it is recorded on cards. The switch closure provided by the positional scanner resets the counting circuits between each successive timing measurement.

Specifications

The internal time base for the digital voltmeter is a 100 kHz quartz crystal oscillator. Five digits of timing information are capable of being recorded. The accuracy of this unit is specified by the manufacturer as ± 1 digit in the least significant place which clearly implies ± 10 μs accuracy on the width measurement of the pulse from the positional scanner.

The interface unit is operated solely as intended by its manufacturer and therefore will not be further discussed.

The maximum rate with which the keypunch can encode data is eleven digits per second. Thus the maximum sample rate for the spectrum analyzer is about two samples per second. The punch cards used for storing the data are the standard IBM eighty column type. The format used for storing data on these cards is sixteen, five digit data samples per card.

CHAPTER III

CONSTANT TEMPERATURE THERMOSTAT

Introduction

A major problem that generally occurs in making low level, low frequency measurements is the effect of fluctuations in the ambient temperature on those measurements. This can readily be seen by comparing the Nyquist noise voltage of a 10 kΩ resistor, in a 1 Hz bandwidth, to its noise resulting from a fluctuating temperature. If the current through this resistor is 1.0 mA and the temperature coefficient of its resistance is $\Delta R/R\Delta T$ = 10 ppm = 10^{-5}/°C, then the resulting voltage due to an effective temperature variation of 1 x 10^{-3} °C will be about 10 times larger than its Nyquist noise voltage.

A simple approach to the temperature control problem is to well insulate the device under study thereby attenuating the effects of the outside fluctuations to the point where they are negligable. Ringo [28] had success with this technique in his Zener diode power spectral studies; however he restricted himself to frequencies above 0.1 Hz. On the other hand, Blakemore, in similar studies on operational amplifiers found it to be useless at frequencies below 1 x 10^{-3} Hz due to the practical considerations involved [10].

A second, but considerably more complicated, approach to the problem involves the use of electronically controlled fluid bath type thermostats. At least two such thermostats with rather impressive

specifications have been reported in the literature (see Baldinger and Nüesch [3] and Harvey [17]).

The thermostat constructed for this study is similar to those cited in the above references. However, it differs from that reported by Baldinger and Nüesch in that it is a single thermostat (Baldinger and Nüesch used a thermostat within a thermostat arrangement). It differs from Harvey's in that his thermostat involved forced cooling whereas this one does not. Obviously since no forced cooling is utilized, the operating temperature of the termostat is necessarily above that of the environment because its heat losses are depended on to prevent thermal run-away. Figure 7 shows the physical appearance of the thermostat used in this study.

Physical Description

Mechanical Construction

Figure 8 shows a cross-sectional view of the thermostat. As can be seen, the thermostat basically is composed of a fluid container isolated from the environment by a thick layer of insulation.

The fluid container is fabricated with 18 gauge (1.27 mm) stainless steel. The ductwork is entirely aluminum (for a similar mechanical lay-out see reference [18], pp. 295-296). The purpose of the ductwork is to direct the flow and prevent vortexing of the fluid which is stirred during operation.

A minimum thickness of 10 cm of formed-in-place polyether urethane foam is used to insulate the fluid container from the environment. The chemicals used to make this foam are manufactured by the Upjohn Company, and marketed as type 323. The specified thermal conductivity "k" for

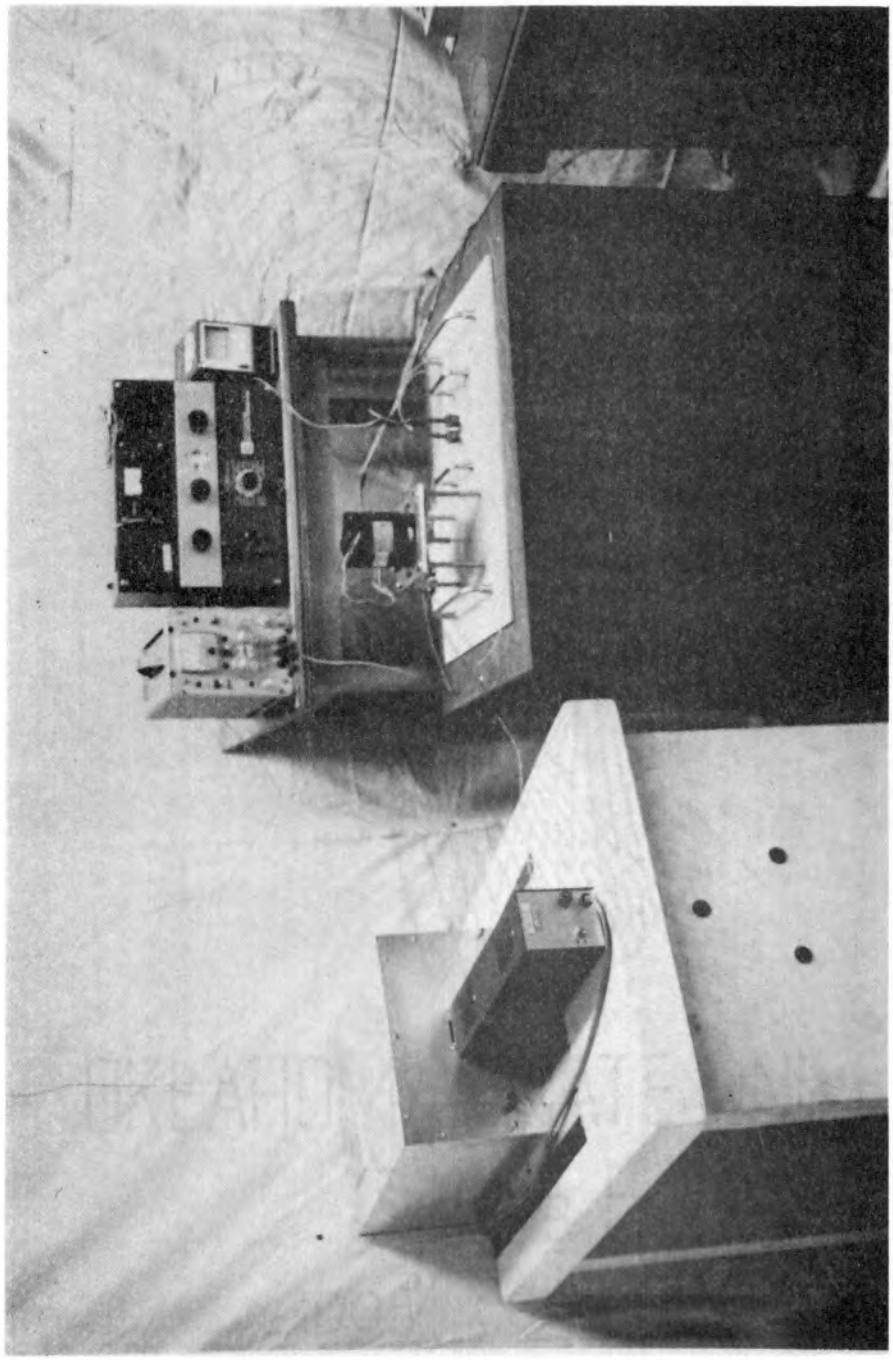

Figure 7. Constant Temperature Thermostat

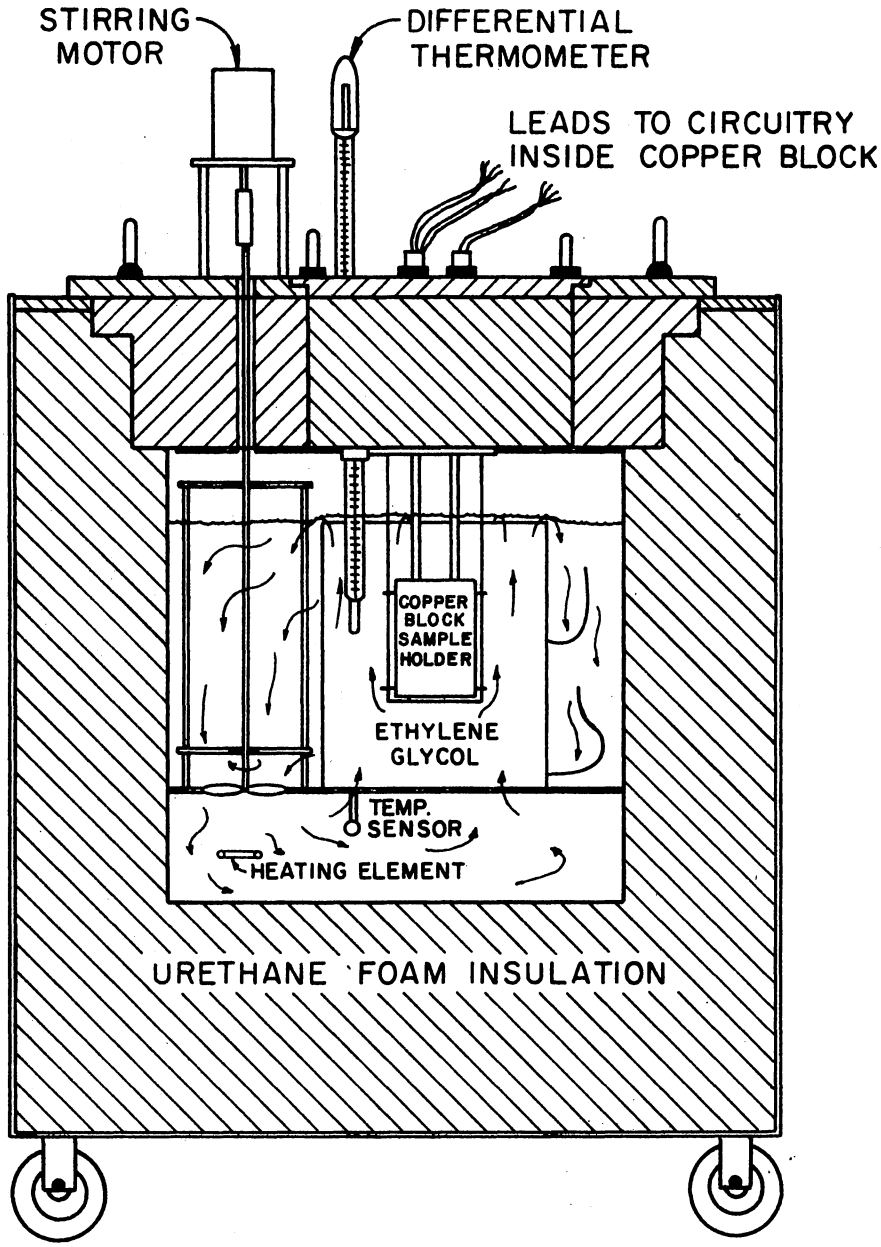

Figure 8. Cross-Section View of the Thermostat

this insulation is 0.11 to 0.14 BTU in/(ft^2 h °F) [21] (this can be expressed as 0.016 to 0.020 W/(m °C)). It is used because it is rigid, providing support for the fluid and its container, and because of its excellent insulating properties compared to other materials [32]. An estimate of the heat loss through the insulation is given later in this chapter.

The cover for the thermostat is a two lid structure as is shown in Figure 8. The larger of the two covers the entire fluid bath container and provides mechanical support for the stirring motor. Within this lid is a smaller cover. It is through this smaller cover that access to the working volume of the thermostat is provided while it is in operation. This smaller lid also provides mechanical support for a differential thermometer which is used to monitor the bath temperature at a location within the flow duct.

Fluid Bath and Stirring Motor

Ethylene glycol is used for the bath fluid. Reasons for choosing it for the bath include: it is non-corrosive; it is non-volatile; and it has a relatively high specific heat, C_p = 0.56 cal/(g °C) [C_p = 2340 W s/(kg °C)] [24]. The density ρ of ethylene glycol is 1.113 kg/ℓ with the thermostat bath using 23.8 ℓ. Thus a thermal capacity of 6.21 x 10^4 W s/°C is achieved with this bath fluid.

The fluid circulating motor is a 600 rpm, 1/300 HP hysteresis synchronous motor (Ashland Electric Products Inc., number C73EZU-1). This motor drives a 6.2 cm diameter propeller located near the botton of the fluid container. A crude estimate of the pumping action of this motor with its propeller, based on rpm and pitch, is about 0.5 ℓ/s.

Bath Heater and Temperature Sensor

The heating element is a conventional resistive type manufactured for home water heaters. It is rated at 1500 W although in this application it is operated at considerably reduced power levels (details are given later in this chapter). The location of this element is just below the fluid propeller, and close to the temperature sensing element. It is generally desirable to have the heating and sensing elements in close proximity to minimize the response time between these elements [17]. The response time for this thermostat based on an estimated fluid velocity of 2.5 cm/s and the sensor characteristics is about 11 seconds. The location of the temperature sensor is about 10 cm downstream from the heating element.

The temperature sensor is a dual 100 Ω (at 0 °C) platinum wire resistive element, type 8922, supplied by the Leeds & Northrup Company (for information on choice of sensors see Larsen [20]). It has a specified temperature coefficient of 0.00385 Ω/(Ω °C). Both of these elements are contained in a single sealed stainless steel tube which is 6.4 mm in diameter and 10 cm long. Its thermal time constant is specified as 7 seconds and its resistance change is less than 0.05 Ω over 10000 hours of operation (this may be expressed as 1.4×10^{-11}/s). It is assumed that this instability in the resistance value is largely due to a drift resulting from incomplete annealing in manufacturing (see "Mechanisms Affecting Resistance" in platinum resistance thermometers [18]). Based on this assumption, an absolute drift of no more than 1.2×10^{-4} Ω is expected in any 24 hour period. This value corresponds to an equivalent temperature drift of 300 μ °C/day.

Copper Block Sample Holder

The working volume of the bath is located in the center of the fluid flow duct. In order to immerse devices into the bath it was necessary to construct an enclosure to protect those devices from the fluid (cursory checks showed low values of electrical resistance of about 150 kΩ/cm and therefore direct immersion of devices is not allowed).

This enclosure was machined from two solid copper blocks which are fastened together with screws forming a sealed container. Entry into the enclosure is through two small holes connected to the smaller lid of the thermostat with rubber surgical tubing. The outside dimensions of this container are 5.92 cm x 8.2 cm x 1.9 cm. The inner volume is about 34 cm^3. A view of this copper enclosure can be seen in Figure 9.

Contained in this enclosure is a precision platinum resistance thermometer. This thermometer was a model S1061, obtained from Minco Products, Inc. It has a specified R_o of 470.40 Ω at 0 °C with a maximum fluctuation of 10 ppm per year (3.2×10^{-13}/s). This thermometer is snugly fitted into a groove that was machined into the copper block and is used to monitor the block's temperature.

The devices that are normally contained in this enclosure are connected to the outside by wires. To estimate the thermal loss through these wires, calculations were made based on a perfectly thermally insulated copper wire whose ends are maintained at temperatures which differ by 10 °C (the typical temperature differential between the room and the fluid is about 8 °C). The results of these calculations show that a heat out-flow of about 270 μW/wire can be expected.

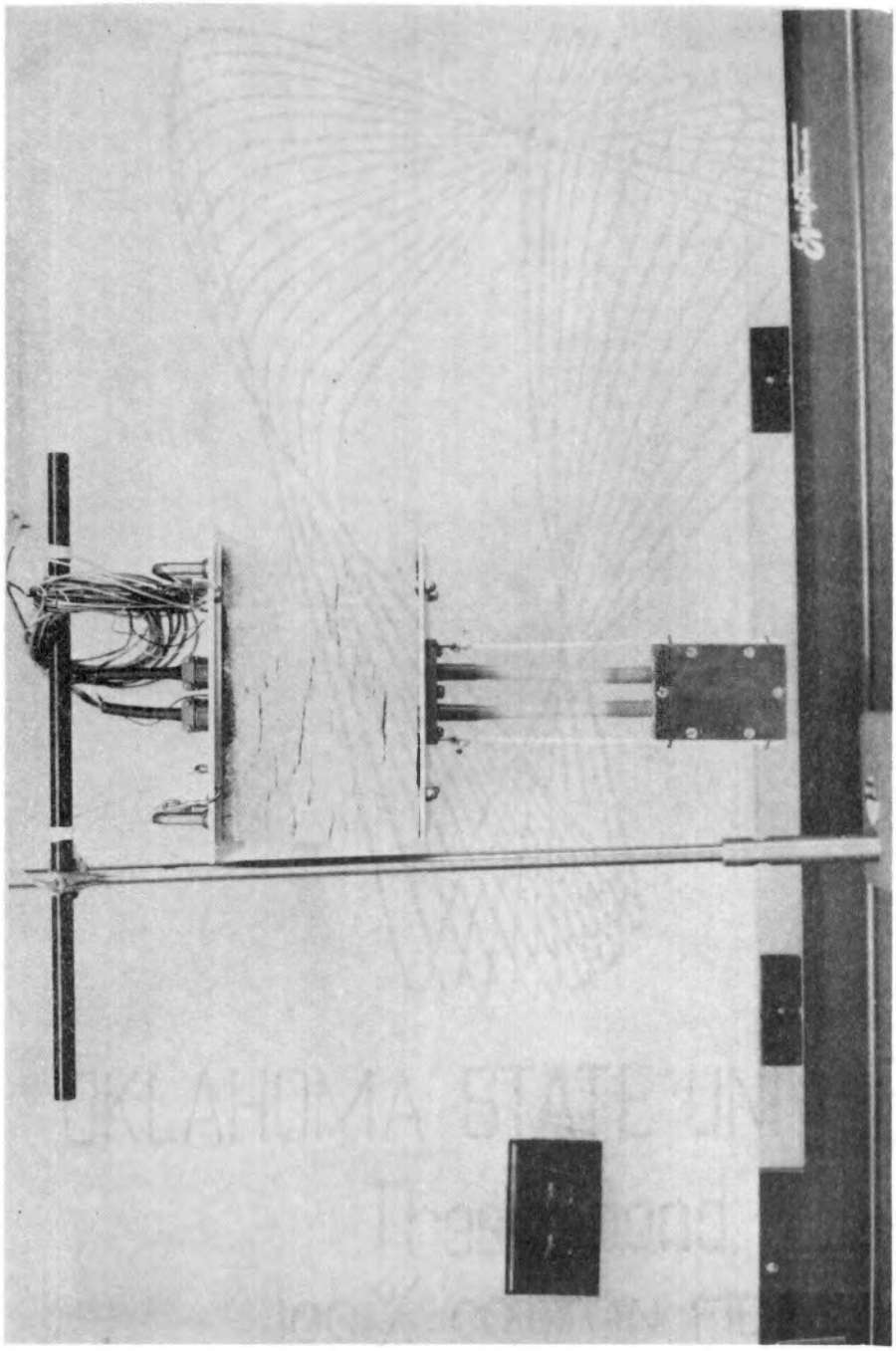

Figure 9. Copper Enclosure Shown Suspended From the Small Thermostat Lid

Bath Temperature Control

Introduction

The control of the bath temperature is done with electronic circuitry. Precision control of temperature generally reduces to the problem of small signal detection [17]. The circuitry that was designed for this thermostat can be broken into four major groups: (1) an a.c. bridge temperature sensor; (2) a high gain tuned error signal amplifier; (3) a phase detector and control signal source; and (4) a controlled d.c. bath heater power supply. Figure 10 is a block diagram showing the relation of the above to the system and Figure 11 shows the physical appearance of this equipment. The remainder of this section will discuss each of the above groups. Complete schematic diagrams will be found in Appendix B.

Bridge

A basic diagram of the temperature sensing bridge is included in Figure 10. The two temperature sensitive elements are the platinum wire resistance elements previously described and the other two resistors are each 113 Ω ± 0.01% with temperature coefficients of 1 ppm (Vishay type S102). A 2.0 V pp, 102 Hz sinusoidal oscillator provides the input power to the bridge. There are several reasons for choosing a.c. as a bridge power source. Thermocouple effects can be eliminated; transformer coupling the error signal from the bridge is permitted, thus avoiding ground loop problems; and narrow bandwidth a.c. high gain amplifying techniques can be used in handling the output error signal. For additional information see Baldinger and Nüesch [3].

For the input voltage V_{osc} of 2.0 V pp, the corresponding bridge

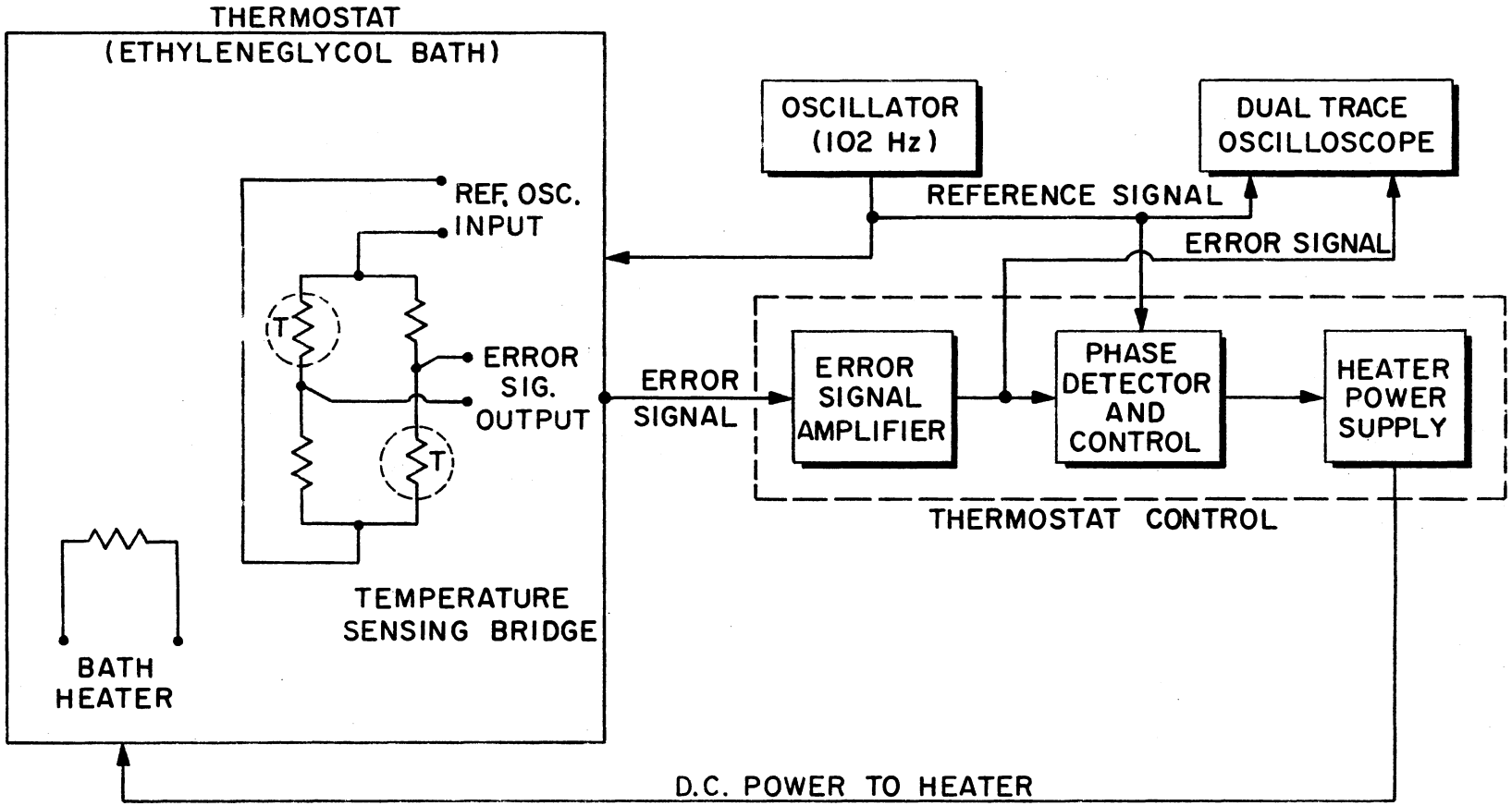

Figure 10. Block Diagram of the Bath Temperature Control System

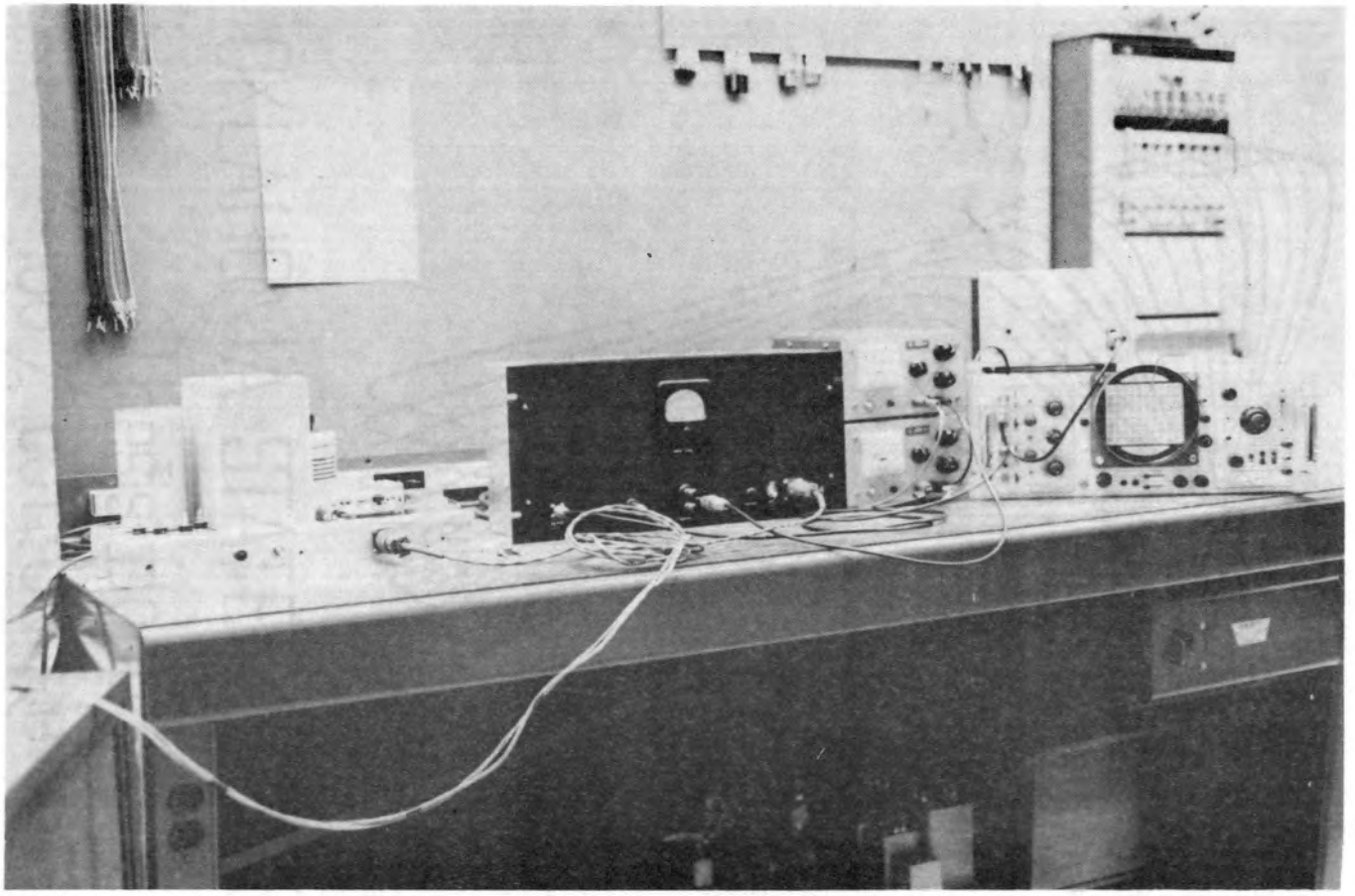

Figure 11. Physical Appearance of the Bath Temperature Control System

output error signal ΔV_B, for a $\Delta T = 1.0 \times 10^{-3}$ °C temperature excursion, is given through

$$\Delta V_B = (\delta B_r)(\Delta T)(V_{osc}) = 3.41 \ \mu Vpp \qquad (3\text{-}1)$$

where

$\delta B_r = 1.71 \times 10^{-3}/°C$, the sensitivity of the bridge determined through its parameters.

This error signal, for 1.0×10^{-3} °C, is sufficiently high to make detection and amplification achievable with standard techniques.

There are two details with regard to using an a.c. bridge to sense temperature variations worth noting. The first is that the bridge must be balancable in the a.c. sense. To achieve this it was found necessary to pad each of the platinum elements with a small capacitor. The required capacitor values were determined by trial and error and found to be on the order of 10 pF. The second detail involves the nature of the output error signal. The magnitude of this signal gives only information about the excursion of the temperature from balance. To be able to tell if an excursion represents an excess or under temperature condition, it is necessary to compare the phase of the error signal to that of a fixed reference. Thus, for an a.c. temperature sensing bridge scheme, an added requirement of phase sensing must be incorporated into the control system.

Error Signal Amplifier

Four commercially available IC operational amplifiers make up the error signal amplifier. The front end is a low noise (10 $nV/\sqrt{Hz}$ @ 100 Hz) model AD504M unit supplied by Analog Devices. This amplifier is

transformer coupled to the temperature sensing bridge and is followed by another "op-amp" whose purpose is additional gain. The remaining units form a two stage, bridge-tee, band pass gain section. The combination of these units provide for a measured voltage gain of $G = 3.5 \times 10^6 \pm 10\%$ at a tuned frequency of 102 Hz with a 4 Hz half-power bandwidth. The output of the error signal amplifier along with the oscillator signal supplying the bridge are displayed by a dual trace oscilloscope for monitoring purposes during thermostat operation.

Phase Detector and Control Signal Source

The output from the error signal amplifier goes to the phase detector circuit where its phase is compared to that of a reference oscillator. If the phase relation between these two signals indicate an under temperature condition exists in the thermostat, a d.c. control signal is developed whose value is proportional to the magnitude of the amplified error signal. This control signal, through an incandescent lamp and photo-conductive resistor arrangement, is used to control the power supplied to the thermostat heater.

Heater Power Supply

The thermostat heater is supplied d.c. current from the heater power supply. The level of current, during thermostatic operation, supplied to the heating element ranges from a maximum value of about 0.6 A to a minimum value of a few milliamperes. The 0.6 A value corresponds to a heater power dissipation of 3.7 W.

When the thermostat is initially being brought up to its operating temperature, a manual switch allows for an increase in supply current

output to about 4.5 A. At this current level in heater power is about 200 W. A 2.7×10^{-3} °C/s temperature rise in the bath is observed when the heater is supplying 200 W.

Performance of the Thermostat

Bath Temperature Stability

Direct observation of the differential thermometer, resistance measurements of the platinum resistance thermometer contained in the copper block, and error signal measurement from the bridge in the control circuitry were used to estimate the fluctuation of the bath temperature (see the previous sections of this chapter for the physical locations and specifications for the above).

The differential thermometer has 10×10^{-3} °C graduations. A small fixed telescope was used to observe the height of its mercury column. No observable change in its height was noted in 17 readings taken over a period of 3 days ($| \Delta T | < 3 \times 10^{-3}$ °C).

Six resistance measurements on the platinum wire thermometer over a period of 10 hours indicated a 2.5×10^{-3} Ω peak excursion in the resistance from its mean value. This corresponds to a maximum variation of approximately $\pm 1.4 \times 10^{-3}$ °C from the mean temperature of the bath. This result can be considered an upper limit on the bath variation in that it includes thermocouple effects and systematic errors due to thermometer self heating. The manufacturer specified this thermometer's self heating effect to be negligable if the measuring current was kept below 0.5 mA. However, in this installation, on the order of 2 mA was used.

The output signal from the error signal amplifier contained in the control circuitry was measured with a true rms voltmeter (HP 3400A). The

The output from the voltmeter was recorded by a strip chart recorder. Figure 12 shows about 15 minutes of a 4 hour recording. This curve indicates the rms value of the error signal as it varies about the balance point of the sensor bridge. The temperature calibration is based on the bridge transfer function, the reported gain of the error signal amplifier, and the temperature coefficient of the platinum wire sensors.

Based on the fact that the error signal is sinusoidal, it is a simple matter to estimate the peak bath temperature excursion from the curve shown in Figure 12 over the time interval shown. The temperature sensitivity of the error signal amplifier output signal, δV_{eo}, is given by

$$\delta V_{eo} = (G)(\delta B_r)(V_{osc}) = 1.20 \times 10^4 \ V_{pp}/°C \qquad (3\text{-}2)$$

where

G = gain of the error signal amplifier.

From Equation (3-2), the temperature sensitivity δT can be expressed in terms of the output error signal voltage as

$$\delta T = [\delta V_{eo}]^{-1} = 83.5 \ \mu \ °C/V_{pp} \quad . \qquad (3\text{-}3)$$

The result of Equation (3-3) may be expressed in terms of the rms value of the error signal amplifier output voltage as

$$\delta T = \sqrt{8} \ [\delta V_{eo}]^{-1} = 236 \ \mu \ °C/V_{rms} \quad . \qquad (3\text{-}4)$$

Although the curve in Figure 12 does not give a voltage scale, an equivalent temperature excursion is shown. From this curve the peak temperature excursion is seen to be less than 1×10^{-3} °C.

Variations in room temperature were recorded during thermostat

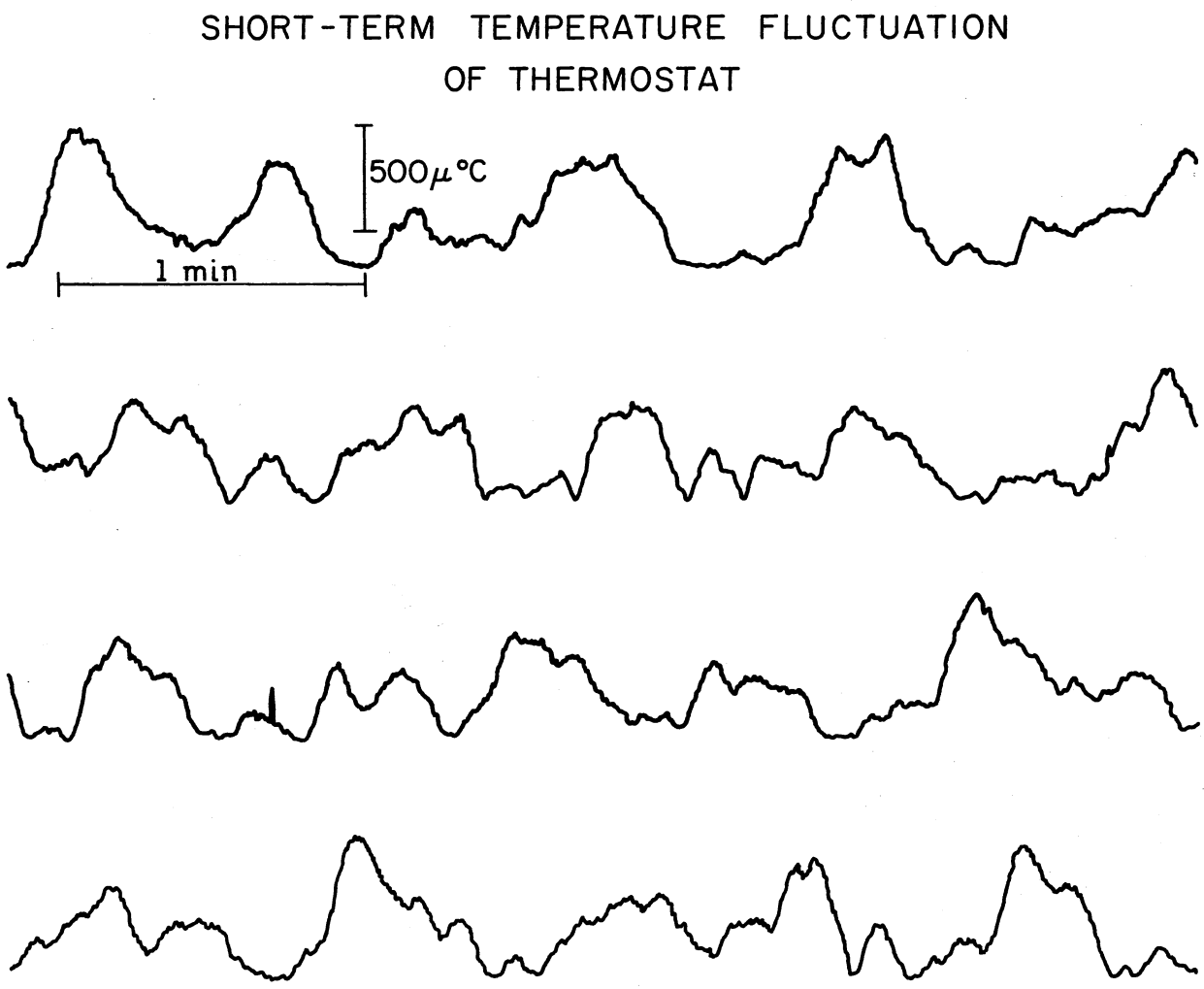

Figure 12. Short Term Temperature Fluctuation of the Thermostat

operation. These records show that room temperatures have a total variation of as much as 4 °C over a period of 24 hours. Assuming that the bath temperature variation given above holds for the same length of time, a thermostat to room temperature stability factor of 5×10^{-4} can be given. The above assumption appears to be valid in that continuous operation of the thermostat for a period of 4 days gave no indication of any changes in stable operation or thermal drift.

Absolute Bath Temperature

The absolute bath temperature is not an important consideration for the study for which this thermostat was constructed. An indication of the bath temperature was obtained by measurements made with two mercury column thermometers with 0.1 °C graduations. Both thermometers indicated temperatures of about 32.26 ± 0.03 °C.

Thermostat Heat Losses

The following technique was used to estimate the heat losses of the bath to the environment. Stable thermostatic conditions were established. The thermostat was switched off and the time required for the bath temperature to drop one degree was noted. This was done three times with an average time of about 16 hours resulting. The room temperature during these checks was monitored. A maximum variation of about 2 °C occurred during each of the 16 hour periods. This variation was always in the form of slow drifts which seemed to track the daily temperature variations of the building in which the thermostat is located. For a temperature differential of 8 °C (maximum bath temperature minus the average room temperature) a bath heat loss time constant of approximately 120

hours can be inferred assuming a simple exponential decay in temperature.

The heat loss of the bath to the environment can be estimated with the following formula,

$$\frac{\Delta Q}{\Delta t} = m\, C_p \frac{\Delta T}{\Delta t} \approx 1 \text{ W} \quad . \qquad (3\text{-}5)$$

Here

$\frac{\Delta Q}{\Delta t}$ = heat loss (W),

$\frac{\Delta T}{\Delta t}$ = rate of temperature change (°C/s),

[1 °C/16 h = 1.7 x 10^{-5} °C/s],

m = mass of glycol bath (kg),

[(1.113 kg/ℓ)(23.8 ℓ) = 26.5 kg], and

C_p = glycol specific heat = 2340 W s/(kg °C).

CHAPTER IV

SPECTRUM ANALYZER PREAMPLIFIER

Introduction

A preamplifier was constructed for the low frequency spectrum analyzer described in Chapter II. Its purpose is to provide the input signals to the analyzer with a voltage gain and to isolate the input source from the 1330 Ω input resistance of the galvanometer (see Galvanometer, Chapter II). Measuring the Nyquist noise of a 10 MΩ resistor is an example of a case for which both the input signal levels are too low and the impedance matching requirements are too severe for the analyzer to handle directly. The use of a preamplifier makes this measurement possible (see Nyquist Noise, Chapter VI). A side benefit connected with preceding the spectrum analyzer (galvanometer) with a preamplifier is that it makes it possible to fix the external damping on the galvanometer independent of the signal source. The analyzer's frequency response is thereby independent of the signal source's output impedance which simplifies interpreting measured results (for details concerning spectrum analyzer frequency response and galvanometer damping see Galvanometer, Chapter II).

Physical Description

Figure 13 shows a schematic diagram of the preamplifier. It is a two stage, differential-input differential-output, circuit with the

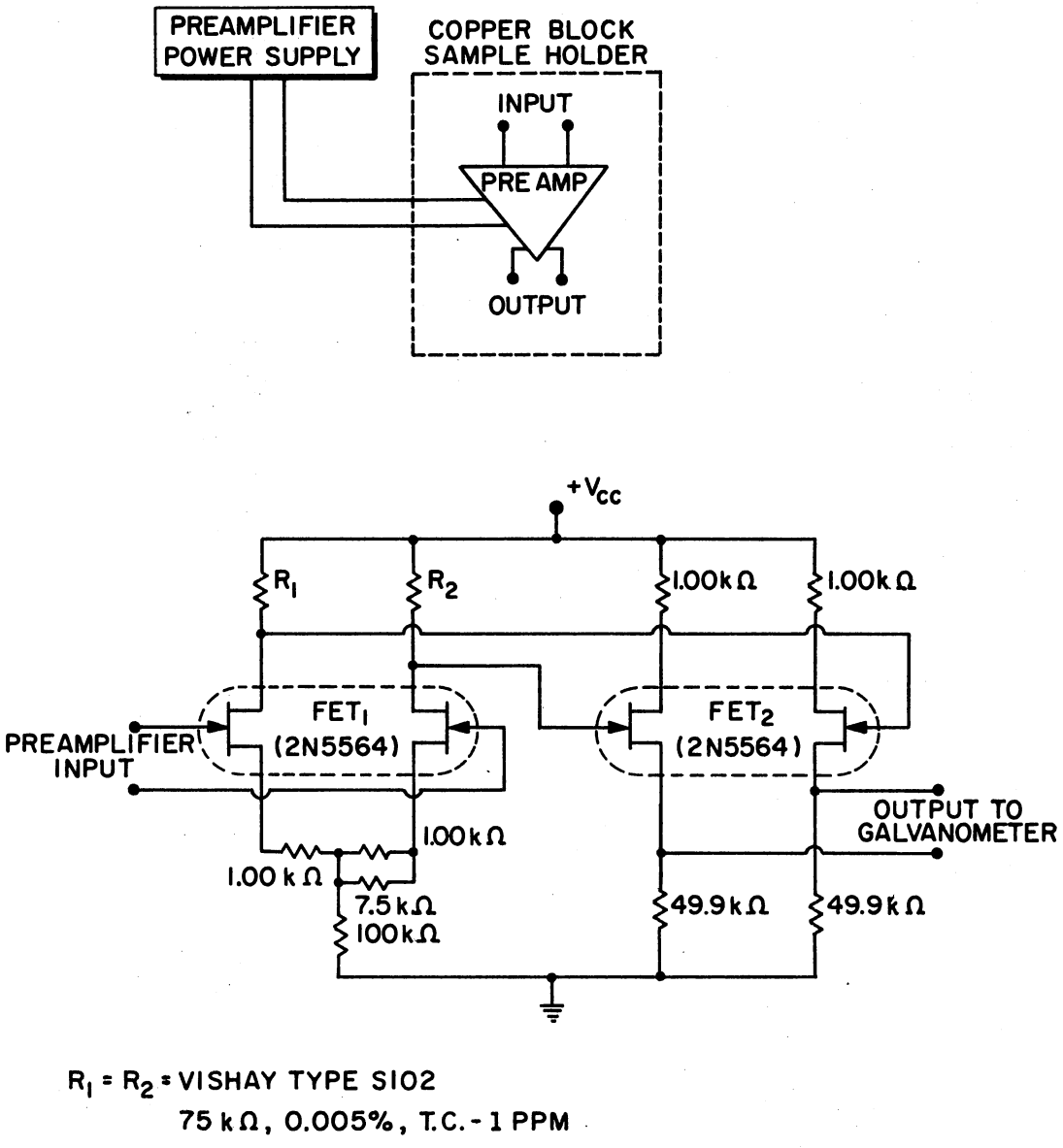

Figure 13. Preamplifier: Block Diagram Showing Relation to the Spectrum Analyzer and Circuit Diagram

first stage providing the voltage gain and the second serving as a buffer. The dual field effect transistors (FET) are similar in characteristics to 2N5564's. They are selected low noise units that were provided by National Semiconductor. The required gate bias for the input FET's is a detail which is taken care of when connection to a particular source is considered. The drain resistors used in the first stage are bulk metal (Vishay S102). Their resistance values are matched to 0.01% with a specified temperature coefficient of 1 ppm/°C or less. The measured noise index (NI) of these units are -50.1 db and -49.7 db based on measurements in the frequency range of 12 to 250 Hz (for details on NI see Motchenbacher and Fitchen [25]). The other resistors used in the circuit are precision metal film ± 1%.

The preamplifier is assembled on an epoxy glass printed circuit board which is mounted in the copper block sample holder described in Chapter III (see Copper Block Sample Holder, Chapter III). The FET's are thermally tied to, but electrically insulated from, the copper block with beryllium copper cup clips (Wakefield 2604SH18B). The power supply for the preamplifier is discussed later in this chapter.

Specifications

The preamplifier operates with a nominal supply voltage of 13 V to 16 V. A voltage gain of 20.9 was measured for the preamplifier with the output loaded with 1300 Ω (approximate load represented by the galvanometer). The output impedance was determined to be approximately 680 Ω based on loaded and unloaded gain measurements. A common mode rejection ratio (CMRR) of approximately 1200 for the preamplifier was determined based on the following method: The gates of the input FET's were

connected to a common potential provided by a simple voltage divider connected from the power supply to ground. The power supply voltage was increased in 100 mV steps from 15.0 V to 15.6 V. A change in output voltage of 1.8 mV was observed for each of these steps. The CMRR follows directly from

$$CMRR = \left(\frac{\Delta V_{ps}}{\Delta V_o}\right)\left(\frac{\Delta V_o}{\Delta V_{in}}\right) = \left(\frac{\Delta V_{ps}}{\Delta V_o}\right) A_V \approx 1200 \qquad (4\text{-}1)$$

where

$\left(\frac{\Delta V_{ps}}{\Delta V_o}\right)$ = change in power supply voltage for a corresponding change in output voltage, and

$\left(\frac{\Delta V_o}{\Delta V_{in}}\right) = A_V$ = voltage gain of preamplifier (1300 Ω load).

The input impedance was not measured but it is assumed to be at least several hundred MΩ due to the general characteristics of FET's. Due to the narrow bandwidth and low frequency nature of the spectrum analyzer (low pass frequency response with a bandwidth less than 1 Hz) the frequency response of the preamplifier is not seriously considered since a cursory check indicated an upper cut-off frequency in the 100 kHz range.

Power Supply

The preamplifier's power supply is a commercially available unit manufactured by "Power Designs Incorporated" model 2020. This supply is specified to have an internal resistance whose value is less than 0.001 Ω at d.c. with a maximum noise level at its output, including 60 Hz ripple, less than 100 μV pp. A noise power spectrum in the frequency range of 80 μHz to 0.4 Hz was measured for this supply and is reported in Chapter VI (see Power Supply Noise, Chapter VI). The instability of the output

voltage is given as 0.001% + 100 μV per 8 hour period or 0.005% + 250 μV per week, for constant load, line voltage, and temperature. The voltage temperature coefficient is specified to be less than 0.001% or 50 μV, whichever greater, per °C in the temperature range of 15 °C to 45 °C.

CHAPTER V

SPECTRAL ESTIMATION OF SAMPLED WAVEFORMS

Introduction

The output of the data acquisition system is a set of numbers which represent the time-amplitude history of a random waveform. These data are transformed and operated on such that an estimate of their power spectral density results. This chapter discusses the particular method used to estimate the power spectral density along with the other numerical procedures necessary in preparing the data for transformation.

Power Spectral Density Estimation: The General Problem

There are three generally accepted digital procedures for estimating the power spectral density given a finite length random data record. These are: (1) the Blackman-Tukey method which involves taking the Fourier transform of the data's autocorrelation function; (2) the direct method which involves taking the Fourier transform of the time domain data; and (3) the method of using digital filters which simulate the techniques common to conventional analog measurements. A detailed description of these procedures may be found in Otnes and Enochson [26] and a comprehensive comparison is given by Mansour, Hawkins, and Bloodworth [22].

In this study, the direct method is used to obtain the power

spectral density estimates. This choice was made for the following reasons. First, the computational efficiency of this method is the highest [26]. This is due primarily to the development of an algorithm which minimizes the number of required mathematical operations required to perform the Fourier transform [14]. This algorithm is commonly referred to as the "Fast Fourier Transform" (FFT) and specifics regarding the properties of it can be found in the text by Brigham, "The Fast Fourier Transform" [12]. Also, this method is basically a one-step operation in that only the transform of the recorded data is required as opposed to first having to obtain the autocorrelation function as in the Blackman-Tukey method. Finally, this method has the advantage that different bandwidths may be chosen for each spectral estimate [26].

The primary disadvantage of the FFT is that in order for it to be indeed fast, it is desirable that the input data record be composed of exactly 2^K samples where K is an integer. Thus data acquisition times are fixed to periods corresponding to the above number of samples.

Power Spectral Density by Direct Fourier Transform

The Fourier transform of a record of x(t) is defined by the following relation

$$X(f) = \int_{-\infty}^{\infty} x(t)e^{-j2\pi ft}\, dt \qquad (5\text{-}1)$$

where

f = frequency, and

t = time.

In practice the record x(t) represents the measured data. Realistic

constraints placed on any physical measurement force this record to be finite in length. Therefore, a more appropriate form of the Fourier transform is the finite-range Fourier transform which is defined as

$$X(f,T) = \int_0^T x(t)e^{-j2\pi ft}\,dt \tag{5-2}$$

where

T = length of the data record x(t).

Now in a sampled data system only discrete values of x(t) are known. Hence, the data record x(t), frequency f, and time t are expressed as

$$x_n(t) = x(n\,\Delta t) \qquad n = 0,1,2,\cdots,N-1, \tag{5-3}$$

$$f_k = \frac{k}{T} = \frac{k}{N\,\Delta t} \qquad k = 0,1,2,\cdots,N-1, \tag{5-4}$$

$$t_n = n\,\Delta t \qquad n = 0,1,2,\cdots,N-1. \tag{5-5}$$

In these

Δt = the interval between individual data points (samples) commonly referred to as the sample period,

T = length of the data record, and

N = the number of samples in the data record.

From this it follows that the discrete version of Equation (5-2) is

$$X(f_k,T) = \Delta t \sum_{n=0}^{N-1} x(n\,\Delta t)e^{-j2\pi kn/N} \qquad k = 0,1,2,\cdots,N-1\ . \tag{5-6}$$

Normalizing the scale factor in front of the summation in Equation (5-6) yields

$$X_k = \sum_{n=0}^{N-1} x_n e^{-j2\pi kn/N} \qquad k = 0,1,2,\cdots,N-1 \tag{5-7}$$

where

$$X_k = \frac{X(f_k,T)}{\Delta T}, \text{ and}$$

$$x_n = x(n\ \Delta t).$$

Equation (5-7) is the generally accepted defining relation for the discrete finite Fourier transform. The FFT is an efficient algorithm which evaluates the X_k's of this equation.

For a finite data record x(t) from the stationary random process {x(t)}, the one-sided power spectral density of the process is defined as

$$S_x(f) = 2 \lim_{T\to\infty} \frac{1}{T} E[|X_\ell(f,T)|^2] \qquad (5\text{-}8)$$

where

$E[|X_\ell(f,T)|^2]$ = the expected value operation over the ensemble index ℓ, and

T = time interval or period of each data record x(t).

If only a single data record of finite length is considered, then an estimate of $S_x(f)$ at any frequency f is given by the following,

$$\tilde{S}_x(f) = \frac{2}{T} |X(f,T)|^2 \quad . \qquad (5\text{-}9)$$

Here the tilde implies that this is an estimated quantity. Using Equation (5-7), the discrete version of (5-9) can be expressed as

$$\tilde{S}_k = \tilde{S}(f_k) = \frac{2}{T} |X_k\ \Delta t|^2 = \frac{2\ \Delta t^2}{N\ \Delta t} |X_k|^2 = \frac{2\ \Delta t}{N} |X_k|^2 \quad . \qquad (5\text{-}10)$$

Here the individual spectral estimates are interpreted to be at the discrete frequencies f_k given by Equation (5-4). The equivalent bandwidth BW of each of these estimates is given by

$$BW = \frac{1}{T} = \frac{1}{N\ \Delta t} \quad . \qquad (5\text{-}11)$$

The formula (5-10) is used to arrive at the power spectral estimates

presented in later chapters. A detailed development of Equations (5-1) through (5-11) can be found in Bendat and Piersol [6]. Given a data record of N samples and Equation (5-7), it can be seen that only N distinct frequency components are evaluated (the interpretation of these components is such that they are symmetrically spaced in frequency about f = 0). Thus the one sided power spectral density estimates $\tilde{S}_k$ of Equation (5-10) will have N/2 components with the highest frequency f_k of estimation being at $1/(2\ \Delta t)$ (for details on the interpreted location in the frequency domain of the spectral components see Brigham [12]).

Problems Related to the Finite Fourier Transform Method

Introduction

Two problems arise in using a finite transform to estimate the power spectral density of a random process. The first is related to the fact that only a finite length sampled data record can be practically considered. This fact gives rise to a phenomenon called leakage [26]. The second problem is associated with the statistical error of the spectral estimate produced by the transform method. This section discusses these problems and the steps that can be taken to minimize their effects.

Leakage

Leakage is a phenomenon which arises in practice because only a finite length data record x(t) can be measured of a given random process {x(t)}. Mathematically the restriction of finite length on the data record shows up as

$$X(f,T) = \int_{-\infty}^{\infty} x(t)u_T(t)e^{-j2\pi ft}\,dt \qquad (5\text{-}12)$$

where

$$u_T(t) = 0 \quad \text{for} \quad t < 0,$$
$$= 1 \qquad\qquad 0 \leq t \leq T$$
$$= 0 \qquad\qquad t > T.$$

The $u_T(t)$ function expresses the fact that $x(t)$ is a finite length data record. Making use of the convolution theorem [12], Equation (5-12) becomes

$$X(f,T) = X(f) * U_T(f) \qquad (5\text{-}13)$$

where

* = the convolution operation.

The $U_T(f)$ function that appears in Equation (5-13) is the Fourier transform of the "box-car" $u_T(t)$ time function. Thus, $U_T(f)$ is of the general [sin (Y)/Y] form (for a derivation of this see any elementary text on Fourier transforms). In the transform method of evaluating $\tilde{S}_x(f)$, the main lobe of the $U_T(f)$ function centers on the frequency at which $\tilde{S}_x(f)$ is being evaluated. In addition, the width of this lobe, which is measured between the first zeros of $U_T(f)$, corresponds to twice the bandwidth of the estimate specified in Equation (5-11). Unfortunately however, $U_T(f)$ has significant side lobes which extend from both sides of this main lobe. The presence of these side lobes do have a decided effect on $\tilde{S}_x(f)$ and its relation to $S_x(f)$ [26]. The effect of leakage on $\tilde{S}_x(f)$ can be reduced by modifying $u_T(t)$ in some way such that the magnitudes of these side lobes are reduced. This modification is commonly referred to as tapering the data record $x(t)$ or simply as "windowing". The Hann window [26] is but one example of how $u_T(t)$ may be modified to reduce

leakage (this particular window was not used in this study because of computational efficiency reasons). This window has the following form

$$u_{T_H}(t) = 0 \qquad \text{for} \qquad t < 0$$

$$= \text{Sin}\left(\frac{\pi t}{T}\right) \qquad 0 \leq t \leq T \tag{5-14}$$

$$= 0 \qquad t > T.$$

This window function does reduce the side lobes to a certain extent. However, the price which is paid for this is that the width of the main lobe is increased. This increase reduces bandwidth resolution of $\tilde{S}_x(f)$. This side lobe verses bandwidth trade off is in general common to all such leakage reducing recipes [26].

It should be noted that this problem of side lobes is common to all finite power spectral density estimation methods. Their suppression is a subject on which much has been written. Further details can be found in Akaike [2], Blackman and Tukey [9], Jenkins and Watts [19], and Parzen [27] to cite but a few of the available sources.

In the case where x(t) represents a noise voltage measurement, this corresponds to a decrease in the power represented by the data record. This reduction in power can be expressed as

$$\frac{\frac{1}{T}\int_0^T [u_{T_W}(t)]^2 \, dt}{\frac{1}{T}\int_0^T [u_T(t)]^2 \, dt} = A \tag{5-15}$$

where

$u_{T_W}(t)$ = modified window function used to reduce leakage, and

$u_T(t)$ = boxcar window associated with Equation (5-12).

The power spectral density of x(t) is multiplied by 1/A in order to

restore this loss in power (see Parseval's theorem [12]).

Statistical Error

The second problem which arises in using the direct finite transform method for calculating the power spectral density estimates is the statistical error associated with these estimates. Assuming that the sampled data record is from a gaussian distributed random process, the individual spectral estimates $\tilde{S}_k$ will be χ^2_ν (chi-square) distributed with two degrees of freedom. Therefore, the relative mean-square error will be given by

$$\varepsilon_r^2 = \frac{\sigma^2_{\tilde{S}_k}}{\bar{\tilde{S}}_k^2} = \frac{2\nu}{\nu^2} = 1 \qquad (5\text{-}16)$$

where

$\bar{\tilde{S}}_k$ = mean value of $\tilde{S}_k$ (expected value),

$\sigma^2_{\tilde{S}_k}$ = variance of $\tilde{S}_k$, and

ν = degrees of freedom in the χ^2_ν statistic = 2.

The relative rms (root-mean-square) error ε_r in this case is also unity implying that the standard deviation of the estimate is equal to the quantity being estimated.

The error can be improved by averaging neighboring spectral estimates. This operation is commonly referred to as frequency smoothing (see Bendat and Piersol [6]). If "m" spectral components are averaged, the number of degrees of freedom of the χ^2_ν statistic will be 2m. From Equation (5-16) it follows that

$$\varepsilon_r^2 = \frac{2(2m)}{(2m)^2} = \frac{1}{m} \qquad . \qquad (5\text{-}17)$$

Thus the averaged spectral estimate $\hat{S}_k$ which is given by

$$\hat{S}_k = \frac{1}{m} [\tilde{S}_k + \tilde{S}_{k+1} + \cdots + \tilde{S}_{k+m-1}] \qquad (5\text{-}18)$$

will have a relative rms error ε_r given by

$$\varepsilon_r = \frac{1}{\sqrt{m}} \quad . \qquad (5\text{-}19)$$

The bandwidth associated with each $\hat{S}_k$ will now be

$$BW' = (m)(BW) \quad . \qquad (5\text{-}20)$$

This represents a trade-off between statistical accuracy of the spectral estimates and the frequency resolution. A more detailed discussion on statistical error may be found in Otnes and Enochson [26].

Power Spectral Density Estimation From a Recorded Sampled Data Record

Introduction

The previous sections of this chapter introduced a method and its associated problems of power spectral density estimation from a finite length data record. This section deals with the specific operations done on the recorded data whose spectra are reported in later chapters.

The data which are recorded by the apparatus of Chapter II appear as digital numbers encoded on standard IBM eighty column punch cards. This allows for direct processing of this data by digital computing techniques. The digital computer that was used here is an IBM 360/65 system. The program used to process the data was written in the FORTRAN IV language compatible with the G-level compiler supplied by IBM (the FFT algorithm was available as a subroutine from the computer system library). A complete listing of this program is included in the appendices. Figure 14

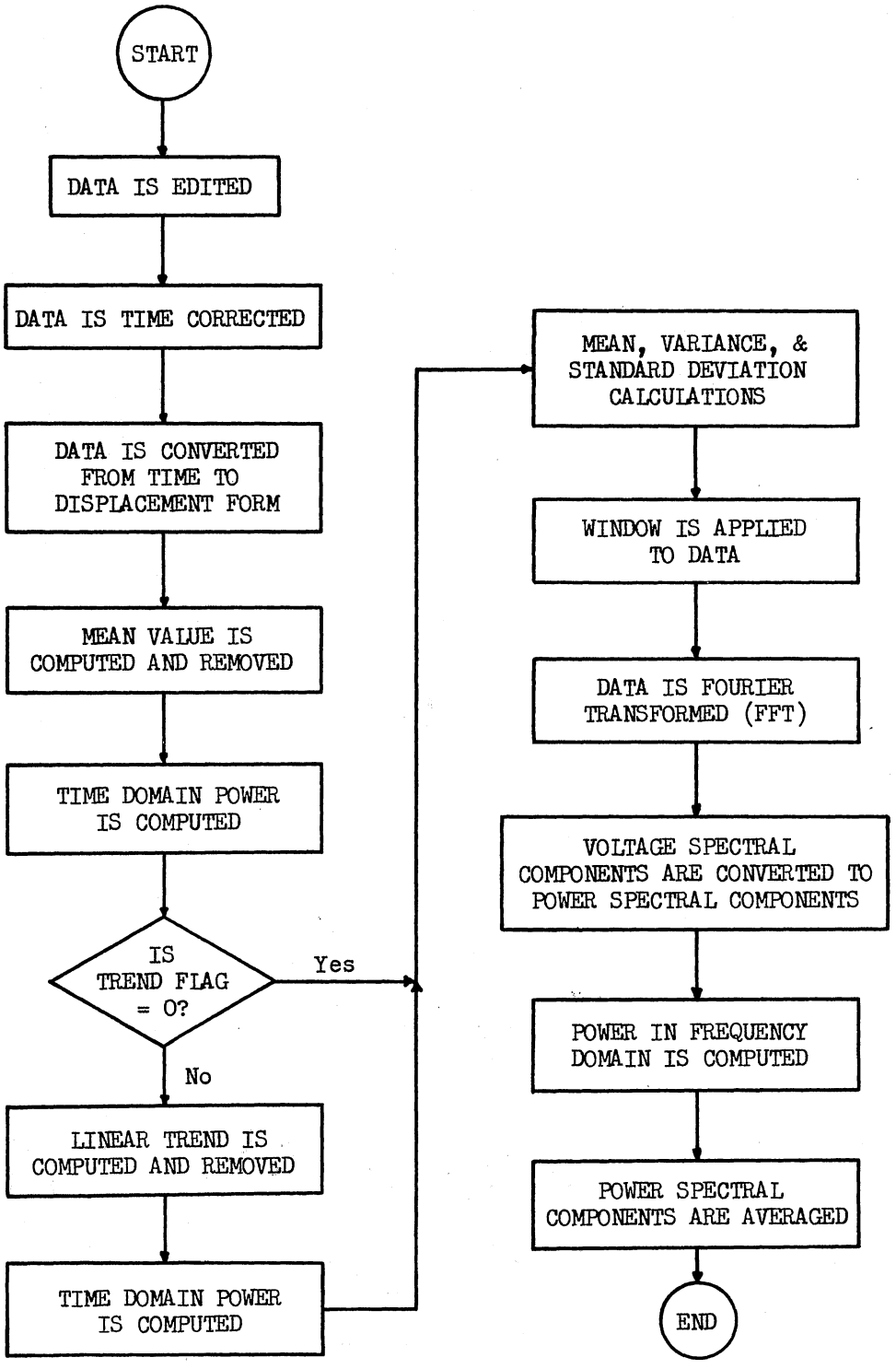

Figure 14. Flow Diagram Showing Major Steps Used in Processing a Data Record

shows in flow diagram form the major operations done on each data set in order to obtain its spectrum. Details of each of these steps will now be given. For the purposes of this description each $x(n\ \Delta t)$ will be identified as x_i where the index "i" equals "n". Also the number of data samples per record is required to be equal to 2^K where K is an integer. As mentioned earlier, this condition arises from the FFT algorithm which is used in obtaining the spectral estimates.

Data Editing

The first step in the processing sequence is to edit each individual x_i. Each x_i value is checked to see if it falls within the allowable range of the sampling system. Occasionally the keypunch unit fails to properly record a data value. In this case, the value that is punched generally turns out to be outside the possible numeric range for the data set by the characteristics of the spectrum analyzer (see Chapter II). If a particular x_i is outside its permissible range, it is "corrected" according to the formula

$$x_i = \frac{[x_{i-1} + x_{i+1}]}{2} \quad . \qquad (5\text{-}21)$$

As can be seen, this is a simple linear interpolation correction. Three assumptions go with the use of (5-21). The first is that the most probable value of x_i is given by it. The second is that the first value x_i is correctly recorded. And finally, if x_i is in error, x_{i+1} and x_{i-1} are not. Preliminary tests of the data acquisition system and processing program included spectrum sensitivity to omitted data points. It was found that for random data with a stationary mean as much as a 1% sequence of the record could be omitted without noticable effects on the

resulting spectrum. Therefore, the validity of the first assumption is thought to be secondary in importance. Assumptions two and three are mechanical and easy to check. These checks amount to visually inspecting the first data point of each record and having the computer print the value of the index "i" on all corrected points. If all the printed values of "i" differ from each other by at least two then the conditions imposed by the third assumption are satisfied.

Time Correction

Recalling the discussion in Chapter II on the disc sampler, it should be remembered that the resulting data record is composed of samples which are not uniformly spaced in time. This timing error is systematic and can be corrected. The method used for correcting this error is a second order (three point) Lagrange interpolation routine [1]. This is represented mathematically as

$$x_i \leftarrow \sum_{k=i-1}^{i+1} \left[\prod_{\substack{j=i-1 \\ j\neq k}}^{i+1} \frac{(t_{i-1} + \Delta t) - t_j}{t_k - t_j} x_k \right] \qquad (5\text{-}22)$$

$$i = 2,3,\cdots,N$$

where

$t_{i-1} = x_{i-1}$,

$t_i = x_i + \Delta t$,

$t_{i+1} = x_{i+1} + 2\,\Delta t$,

Δt = the sampling period, and

N = total number of data points in the record.

The $\leftarrow$ symbolizes a "redefining" type of operation. In the above it is interpreted to mean that x_i is redefined to have the value resulting from

the evaluation of the expression to the right of this symbol. This symbol, with the same meaning attached, will be used throughout this section.

Here again the first value of the data record is taken to be correct. This routine starts by considering the values of the first three x_i's. This allows x_2 to be interpolated. Then x_1 is dropped and x_4 is added to the group allowing x_3 to be interpolated. The routine continues in this fashion until all N values of the data record are corrected. To accommodate the last point x_N, the value of x_{N+1} is assumed equal to the uncorrected value of x_N.

Voltage Conversion and Mean Removal

The data are now converted into equivalent voltage samples according to the following expression

$$x_i \leftarrow Y \text{ Cot } (\frac{2\pi}{\Delta t} x_i) \quad . \qquad (5\text{-}23)$$

This expression was developed in Chapter II and will not be rediscussed here.

The mean value of the data record is computed in the standard fashion (see section on Mean, Variance, and Standard Deviation) and this value is subtracted from each x_i. The presence of a non-zero mean is considered to be systematic and its removal is straight forward.

Time Domain Power

Power in the time domain P_{td} represented by the data record is now computed. It is evaluated by the following formula

$$P_{td} = \frac{1}{N} \sum_{i=1}^{N} (x_i)^2 \quad . \qquad (5\text{-}24)$$

This formula is taken from the discrete data version of Parseval's theorem which is found in Brigham [12].

Removal of a Linear Trend

At this point in the data processing a linear trend can be removed from the data. Whether or not this is done is dependent on the value of a variable, called a flag, which is defined at the time the data are read by the computer. The trend of the data is computed by finding the linear mean square fit to all the x_i. The trend is then removed from the data by subtracting this straight line from the record. The formulas used in finding the best fitted straight line are the standard ones found in most elementary texts on statistics and therefore will not be given here.

There are reasons why it is generally desirable to remove any discernible trend from the data record. First, note that it is impossible to make a meaningful spectral estimate at frequencies whose periods are longer than that represented by the data record. Also a property of the discrete Fourier transform is that it imposes periodicity on the data record [12]. As far as the transform is concerned, a linear trend in the data has the same effect as if a sawtooth type function with period equal to that of the record were present. This has the effect of increasing the power density estimates at the low end of the spectrum. Therefore, the removal of any linear trend is considered both warranted and justified. As a matter of routine, if a linear trend is removed from the data, the power in the time domain is then recomputed.

Mean, Variance, and Standard Deviation

At this point the record is in a uniformly time sampled data form with zero mean and no linear trend, assuming any trend was removed. This record is now divided into groups of 256 data points (the program assumes that a data record contains at least this many points). The purpose for doing this is to be able to investigate the time history of the data record to see if any peculiar or interesting variation is present in any of these quantities. In addition, the mean, variance, and standard deviation of the complete record is also computed. The standard statistical formulas shown below are used in these computations.

$$\bar{x}_i = \frac{1}{N} \sum_{i=1}^{N} x_i \tag{5-25}$$

$$\sigma^2_{x_i} = \frac{\sum_{i=1}^{N} (x_i - \bar{x}_i)^2}{N - 1} \tag{5-26}$$

$$\sigma_{x_i} = [\sigma^2_{x_i}]^{1/2} \tag{5-27}$$

Window Function and Power Spectral Density Estimates

The particular leakage reducing window function used in this program has been referred to in the literature as the "Tukey interim recipe" [26]. For a discussion of this window see Bingham, Godfrey, and Tukey [8]. This windowing operation has the functional form

$$x_i \leftarrow (x_i)(u_i) \qquad i = 1,2,3,\cdots,N \tag{5-28}$$

where

$$u_i = \frac{1}{2}\{1 - \text{Cos}\,[\frac{10\pi}{N-1}(i-1)]\} \quad \text{for} \quad 1 \leq i \leq \frac{N+9}{10}$$

$$= 1 \qquad \frac{N+9}{10} < i < \frac{9N+1}{10}$$

$$= \frac{1}{2}\{1 - \text{Cos}\,[\frac{10\pi}{N-1}(i-1)]\} \qquad \frac{9N+1}{10} \leq i \leq N \quad .$$

The factor by which each spectral estimate is multiplied to account for the resulting decrease in variance is 8/7 (see Equation (5-15)).

The data record is now transformed according to Equation (5-7). A standard FFT subroutine that is provided by our computational center is used. Information on this subroutine is given in Brenner's paper, "Fast Fourier Transform of Externally Stored Data" [11].

The power spectral density estimates are now computed by Equation (5-10) with the constant multiplier of 8/7 associated with the window included.

Frequency Domain Power

Power in the frequency domain, P_{fd}, is evaluated according to the following equation

$$P_{fd} = \frac{1}{2N\,\Delta t}\left[\tilde{S}_1 + \left(2\sum_{i=2}^{N/2}\tilde{S}_i\right) + \tilde{S}_{(N/2)+1}\right] \quad . \qquad (5\text{-}29)$$

This formula is obtained from the discrete data version of Parseval's theorem [12].

Spectral Component Averaging

The final step in the processing program is spectral averaging. The averaging begins at the low end of the spectrum. The first 16 components are averaged in groups of 4. The next 144 in groups of 8. This is followed by 18 groups of 16, and 18 groups of 32. The group number is now

changed to 16 with the number of components averaged doubling each time the components contained in the 16 groups are exhausted. This procedure continues until all spectral estimates are considered. The reason that this particular scheme is used is as follows. For all but the first 22 averaged estimates, the resolution bandwidth is at least 10 times narrower than the center frequency of the estimate. Of the first 22, all but the first 2 have bandwidths which are at least twice as narrow. This is a reasonable compromise where both statistical accuracy and low frequency spectral estimation are important. From the section on statistical error, the probability density of one estimate is assumed to follow a χ^2_ν distribution with 2 degrees of freedom ($\nu = 2$). Averaging over several neighboring estimates one uses the fact that the rms error associated with this average will be given by $1/\sqrt{m}$ (see Equation (5-19)) where m is the number of individual components over which the average is computed. In addition the bounds of an averaged estimate $\hat{S}_i$ at a chosen level of confidence can be found using a table of percentage points of the chi-square distribution (for such a table see reference [26]). This can be expressed as the following relation

$$\text{(lower bound) } \hat{S}_i \leq S_i \leq \text{(upper bound) } \hat{S}_i \quad . \tag{5-30}$$

In words, the relation expressed in (5-30) may be stated as follows. At the level of confidence chosen, the true spectral value S_i lies within the interval determined by (lower bound) $\hat{S}_i$ and (upper bound) $\hat{S}_i$ where $\hat{S}_i$ is the averaged estimate of S_i. Table I lists these bounds at the 90% confidence level for the number of spectral components averaged in the program. Also listed is the relative rms error of these averages.

TABLE I

UPPER AND LOWER BOUNDS AND RELATIVE RMS ERROR OF AVERAGED SPECTRAL ESTIMATES

Number of Spectral Components Averaged m	Relative RMS Error $\varepsilon_r = \frac{1}{m}$	Degrees of Freedom (χ^2_ν) $\nu = 2m$	90% Level of Confidence $(\text{Lower Bound})\ \hat{S}_i \leq S_i \leq (\text{Upper Bound})\ \hat{S}_i$	
			(Lower Bound)	(Upper Bound)
1	1	2	0.334	19.4
2	0.707	4	0.421	5.63
4	0.500	8	0.516	2.93
8	0.354	16	0.608	2.01
16	0.250	32	0.751	1.44
32	0.177	64	0.764	1.37
64	0.125	128	0.824	1.24
128	0.0884	256	0.870	1.16
256	0.0625	512	0.905	1.11
512	0.0442	1024	0.931	1.08

System Frequency Response and Aliasing

Considerations

The frequency response of the system was shown in Chapter II. The attenuation has the effect of lowering the spectral estimates at the corresponding frequencies. Correcting for it is a simple matter. Each averaged spectral estimate is multiplied by the reciprocal of the function describing the system response squared (for a description of the frequency response of the spectrum analyzer used in this study see Chapter II).

The problem of aliasing is more complex. From the sampling theorem it is known that a continuous waveform can be uniquely determined from its sample values if the sampling frequency is at least twice the highest frequency component contained in the waveform [12]. This frequency requirement is expressed in the following relation

$$f_s = \frac{1}{\Delta t} \geq 2f_m \tag{5-31}$$

where

f_s = the sampling frequency, and

f_m = the highest frequency component contained in the sampled waveform.

The sampling rate corresponding to $f_s = 2f_m$ is known as the "Nyquist sampling rate" [12] and will be denoted as f_n.

When (5-31) is not satisfied aliasing occurs. Aliasing is the phenomenon by which energy contained at frequencies greater than f_n masquerade at frequencies lower than f_n. This apparent low frequency energy shows up directly in the power spectral estimates. The aliased spectral

components can be expressed as [22]

$$\hat{S}_A(f_k) = \hat{S}_T(f_k) + \sum_{n=1}^{\infty} [\hat{S}_T(nf_s + f_k) + \hat{S}_T(nf_s - f_k)] \qquad (5\text{-}32)$$

where

$\hat{S}_A(f_k)$ = spectral estimate at f_k which contains aliasing contributions, and

$\hat{S}_T(f_k)$ = spectral estimate at f_k if there were no aliasing.

The problem with the practical use of Equation (5-32) is that it assumes prior knowledge of the spectral characteristics. Nevertheless, a hypothetical spectrum can be considered and the effect of aliasing can then be determined. As an example two such spectra along with the system frequency characteristic were considered. One of the spectra was specified to be independent of frequency (white) and the other to be inversely proportional to frequency (1/f). Table II summarizes the results obtained, where the hypothetical spectra are assumed to be filtered by a second order low-pass filter with f_c = 0.094 Hz and f_o = 0.51 Hz (see Chapter II, Equation (2-1)).

The results given in Table II show that for the recording system used in this study, the effects of aliasing are dominant only at high frequency ends of the assumed spectra. In particular, at frequencies a decade or more below the Nyquist frequency, aliasing can be expected to contribute no more than 3% to an estimated spectrum. This of course assumes that an estimated spectrum is closely represented by one of the hypothetical spectra.

The procedural steps that are taken to correct for aliasing in computed spectra are straight forward. First the shape of the spectral density a decade below the Nyquist frequency is determined. This shape

TABLE II

RELATIVE EFFECT OF ALIASING ON BANDLIMITED POWER SPECTRAL DENSITY ESTIMATES

Relative Frequency of Estimate $\frac{f^{**}}{f_n}$	$\frac{S_A(f)^*}{S_T(f)}$	
	$S_T(f) = K^{***}$	$S_T(f) = \frac{K^{***}}{f}$
1	2.20	2.00
0.8	1.62	1.35
0.6	1.27	1.09
0.4	1.13	1.03
0.2	1.04	1.01
0.1	1.03	1.00
0	1.03	1.00

*The entries were based on a bandwidth limited measuring system whose frequency response is determined by a second order low-pass filter. f_c = 0.094 Hz and f_o = 0.51 Hz were used as the filter parameters in preparing this table (see Equation (2-1), Chapter II).

**The Nyquist sampling frequency for the system described in this study is f_n = 0.89 Hz.

***K is a constant.

is assumed not to change in the decade just below f_n or above. The factor by which each estimate should be corrected is then determined by Equation (5-32). The series in the equation is evaluated term by term until the contribution of the next term is less than 0.5%.

A FORTRAN program was written to make the corrections discussed in this section. Since it is relatively simple and straight forward the details of it will be omitted.

CHAPTER VI

CALIBRATION OF SPECTRUM ANALYZER

Introduction

This chapter deals with calibration and performance tests which were run on the spectrum analyzer described in Chapter II. These tests can be broken into three categories. They are: (1) those involving deterministic waveforms, (2) measurements to determine the ambient noise level of the system, and (3) spectral measurements of known input noise sources.

Calibration Using Deterministic Waveforms

Introduction

The initial calibration of the system was done with a low frequency function generator. A Wavetek model 133 was used for this purpose. This generator was connected to the galvanometer through a balanced resistive voltage divider. The reason for the voltage divider is twofold. It allows for adjustment of source resistance which in turn determines the external damping on the galvanometer, and it allows the generator to operate at an output level which is in the range of easy adjustment.

All measurements were performed with the system in its normal operating configuration. The output signals from the function generator for these tests were measured and monitored with an oscilloscope (HP 141B) which was calibrated before the tests. The accuracy to which

these output signals were known approaches 1%. The resistors used in the voltage divider were precision types, with 1% resistance tolerances. Therefore, the accuracy with which the amplitude of the input signals to the galvanometer were known are about 2%. The galvanometer output signals were measured by observing beam displacements at the positional scanner (see Chapter II). For the signal levels used in these tests, the accuracy with which the beam displacement was measured was better than 1%.

Sinusoidal Waveform Measurements

Low frequency sinusoidal waveforms were used to determine the frequency response of the galvanometer. Response measurements were made for source resistances of 1300, 1000, 750, 423, 100, and 51 Ω. These source resistances are accurate to 1%. These measurements are the basis for the selected galvanometer relative response curves that were included in Chapter II. In addition to relative response measurements, absolute measurements were also made. From these, the input resistance of the galvanometer was determined to be 1330 Ω ± 1% and the system sensitivity, S = 1.56 ± 0.03 μV/mm, established. Also it was verified that in the useful operating range of the system, the frequency response of the galvanometer is insensitive to amplitude.

System Noise Measurements

Positional Scanner and Galvanometer Noise

Figure 15 shows the results of two different system spectral noise measurements. The first is a spectrum of the noise of the positional scanner alone. To obtain this result, the beam from the galvanometer was

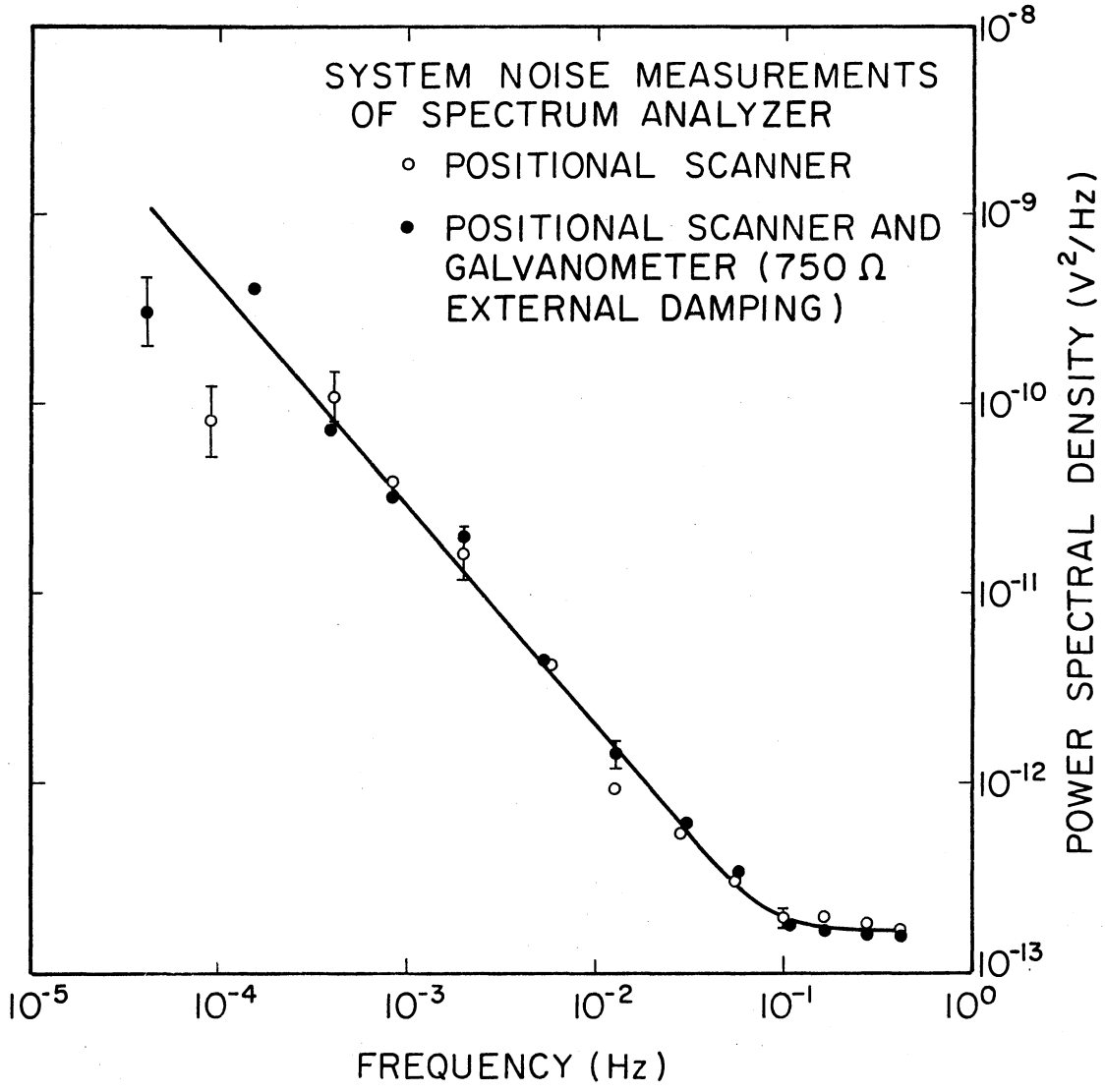

Figure 15. Positional Scanner, Positional Scanner and Galvanometer Noise Power Spectra

positionally fixed. This was accomplished by allowing the beam to pass through a small hole in a mechanically fixed metal plate. The location of this plate was about 3 cm in front of the positional scanner. The data record from which this spectrum was computed consisted of 16384 = 2^{14} samples with a sample period of 1.12 second (1.12 s = $1/f_s$ = 1/0.89, see Chapter II). The spectrum shown represents an average of all of the "raw" averaged spectral components resulting from processing the data. There was no discernible drift in the data and no system frequency response or aliasing corrections were applied as described in the section on "System Frequency Response and Aliasing" in Chapter V.

Also included in this figure is a spectrum representing the noise of the galvanometer and positional scanner combination. For this measurement, the input to the galvanometer was shorted through a 750 Ω resistor. The data record contained 32768 = 2^{15} points and the sample period was 1.12 second. Here again there was no discernible drift in the data and no corrections for system frequency response or aliasing were used.

A comment at this point appears to be in order. An inspection of Figure 15 shows that for all practical purposes the two spectra are identical. This implies that the intrinsic noise of the galvanometer plays little if any part in the system's overall noise characteristic.

Power Supply Noise

Figure 16 shows the power spectral density estimates for the power supply (Power Designs Inc., model 2020) used to power the preamplifier described in Chapter IV. This supply was also used to power the devices and input circuits used in later measurements. To make the measurements, the input circuit shown in Figure 17 was used, with output connected

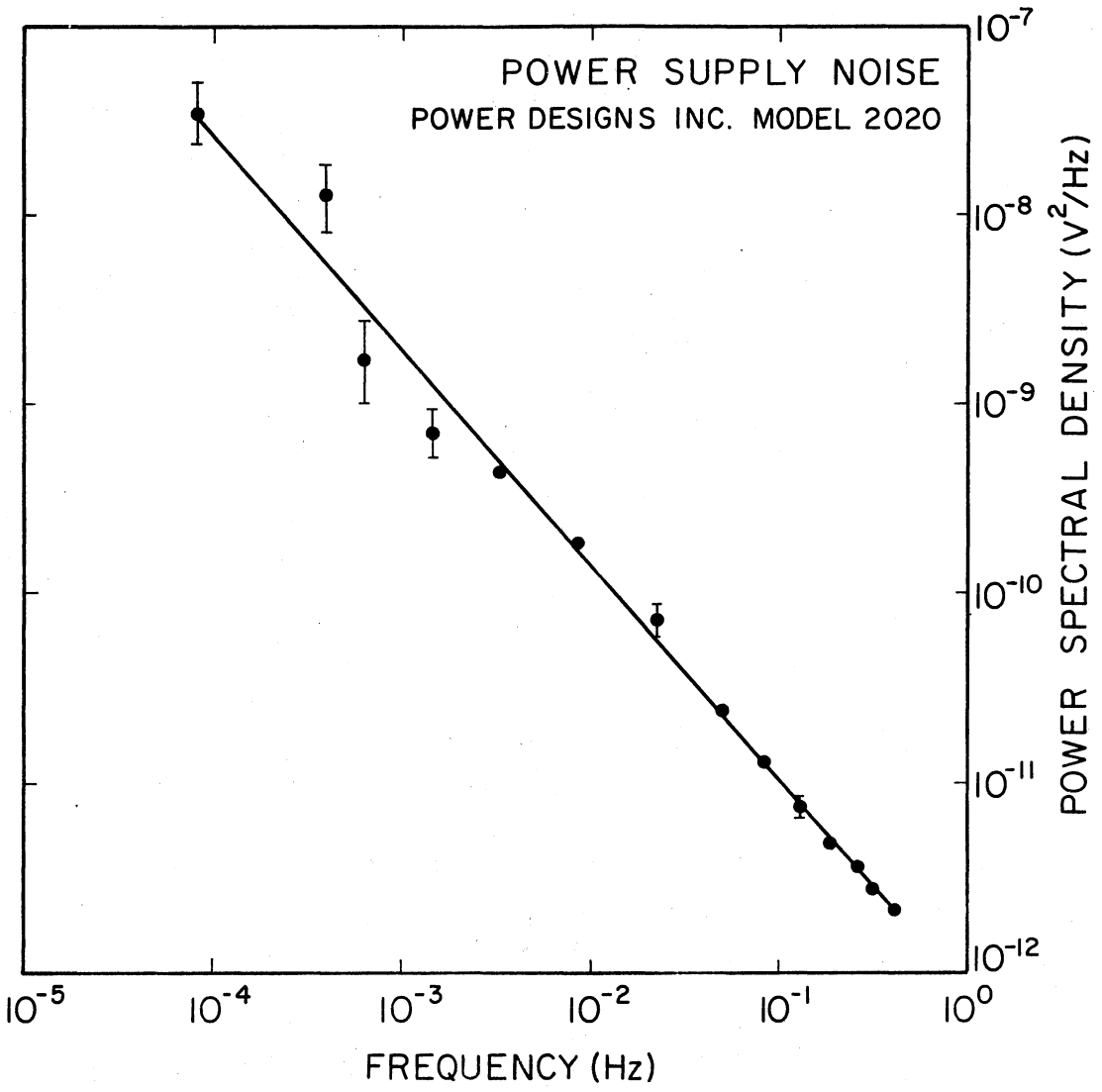

Figure 16. Power Supply Noise Power Spectrum

directly to the galvanometer. This provided an external damping on the galvanometer of 750 Ω. A two power supply configuration was used to keep the d.c. offset to the galvanometer at a minimum. The output voltage of supply 1 and 2 was set to a nominal 14.134 V and 14.121 V, respectively, to null the d.c. output to the galvanometer (see Chapter IV). This null was achieved by noting the position of the galvanometer beam before the power supplies were connected and then adjusting the supply voltages to return the beam to that position after connection. These supplies are "identical" units of the same model supplied by the same manufacturer (see Chapter IV for their specifications).

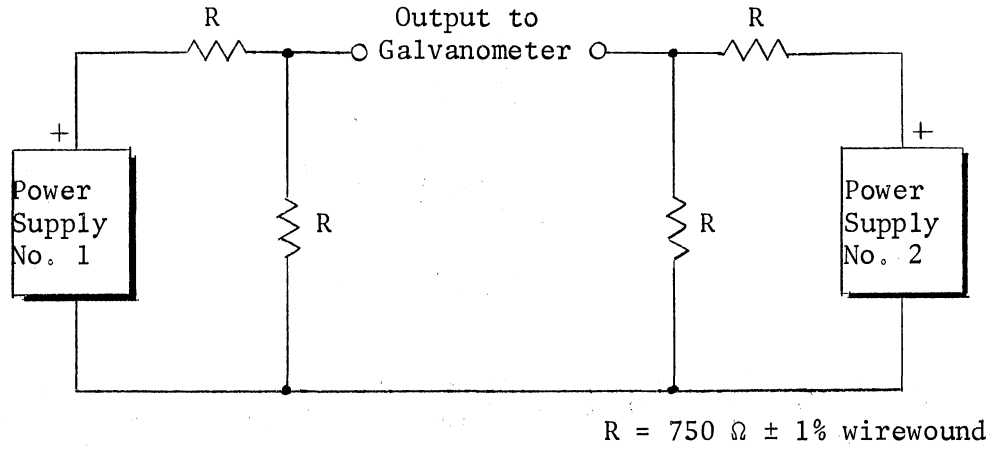

Figure 17. Diagram of Input Circuit to the Galvanometer for the Power Supply Noise Measurement

The noise voltage output to the galvanometer is assumed to represent that of a single supply with no amplitude scaling. This assumption is

valid if the random voltage fluctuations of the supplies are uncorrelated with respect to one another and their spectra are identical.

The data record for this measurement contained 16384 = 2^{14} points with a sample period of 1.12 second. The result of fitting a straight line to the data showed a linear trend of 2.6 nV/s. This corresponds to 48 μV of drift over the period of the measurement. Based on the specifications of these supplies, about 90 μV could have been expected. The spectrum shown in Figure 16 was arrived at with the following procedure. The spectral estimates were calculated as described in Chapter V. From these raw estimates, the system noise of Figure 15 was subtracted. The remaining estimates were then corrected for the roll-off characteristic of the spectrum analyzer's frequency response. Dealiasing was performed assuming a $K/f^{1.0}$ type spectral dependence.

Spectrum Analyzer Noise With Preamplifier

The noise power spectral density for the system as a unit is shown in Figure 18. This unit includes the preamplifier of Chapter IV immersed in the operating thermostat (32.26 °C), the associated preamplifier power supply, and the galvanometer and positional scanner. For this measurement both input terminals to the preamplifier were connected to the same point. A voltage divider network consisting of a Zener diode (device #302405, see Chapter VII for the characteristics of this diode) and a 995.5 Ω metal film resistor formed the input circuit with the preamplifier being connected to the diode-resistor junction. The power for the voltage divider was derived from the same supply that powered the preamplifier. The power supply voltage for this measurement was 13.5 V. A diagram showing the detail of the input connections is given in Figure 19.

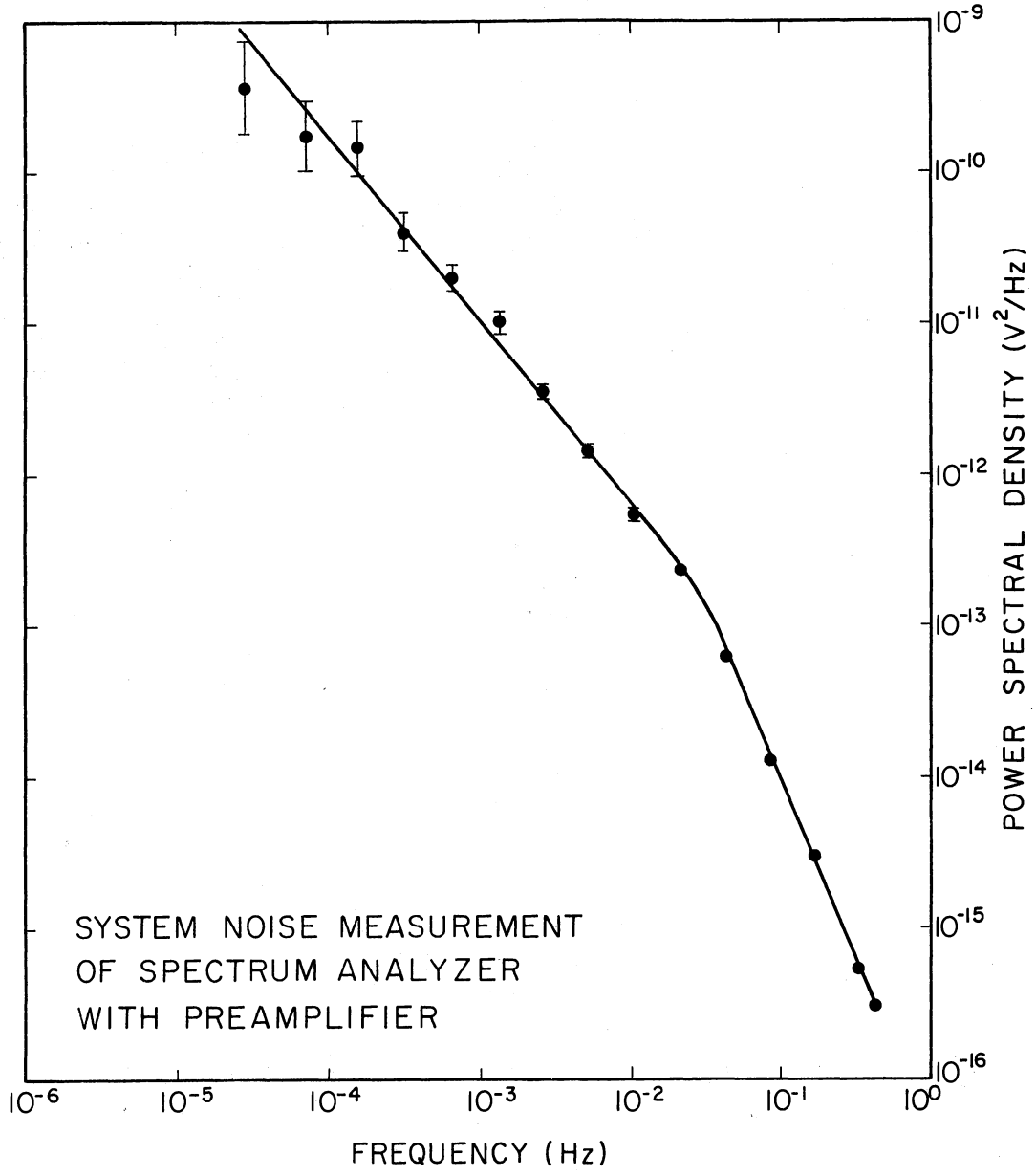

Figure 18. Spectrum Analyzer With Preamplifier Noise Power Spectrum

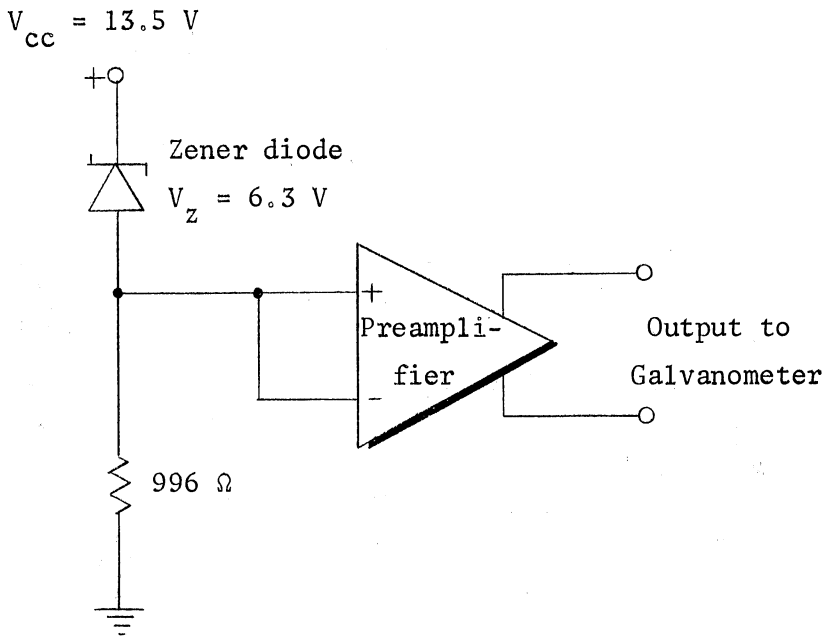

Figure 19. Diagram Showing Preamplifier Input Connections for System Noise Test

A data record of 32768 = 2^{15} points was recorded with a sample period of 1.12 second. There was for all practical purposes no discernible drift in the data. A "best" fitted straight line to the data had a slope corresponding to 14 pV/s. This for the record length of just over 10 hours corresponds to a total drift of approximately 0.5 μV which is less than a factor of 2 above the system noise voltage fluctuation of 325 nV (see Chapter II). The spectrum is in its raw estimated form with no system frequency response or aliasing corrections applied.

Spectral Estimation of Known Noise Sources

Noise Generator Noise Measurement

The measured noise power spectral density of a Quantech model 420 white noise generator is shown in Figure 21. The noise generator was connected directly to the galvanometer through a resistive attenuator. A diagram of this setup is shown in Figure 20. The gain of the loaded divider was measured and found to be 4.88×10^{-2} and its output resistance was calculated to be 765 Ω. The noise voltage level to the galvanometer, based on the output reading of the generator and the divider properties, was 9.76 $\mu V/\sqrt{Hz}$. Thus a noise signal with a white power spectral density of 9.53×10^{-11} V^2/Hz was put into the system.

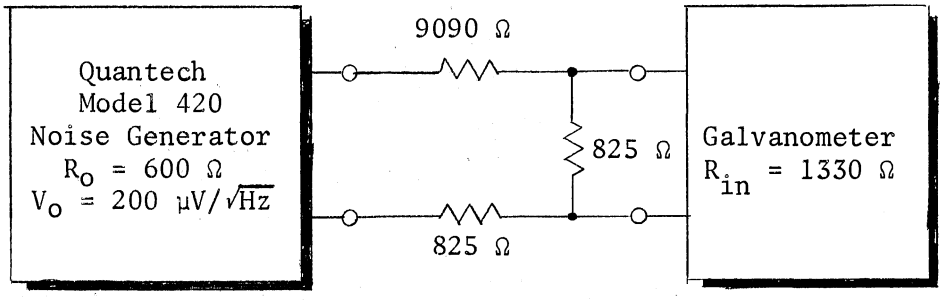

Figure 20. Diagram of Noise Generator and Galvanometer Connection

A comparison of the input noise level to the spectral estimates shows excellent agreement in that the straight line of Figure 21 corresponds to 9.40×10^{-11} V^2/Hz. These estimates were made from a $4096 = 2^{12}$

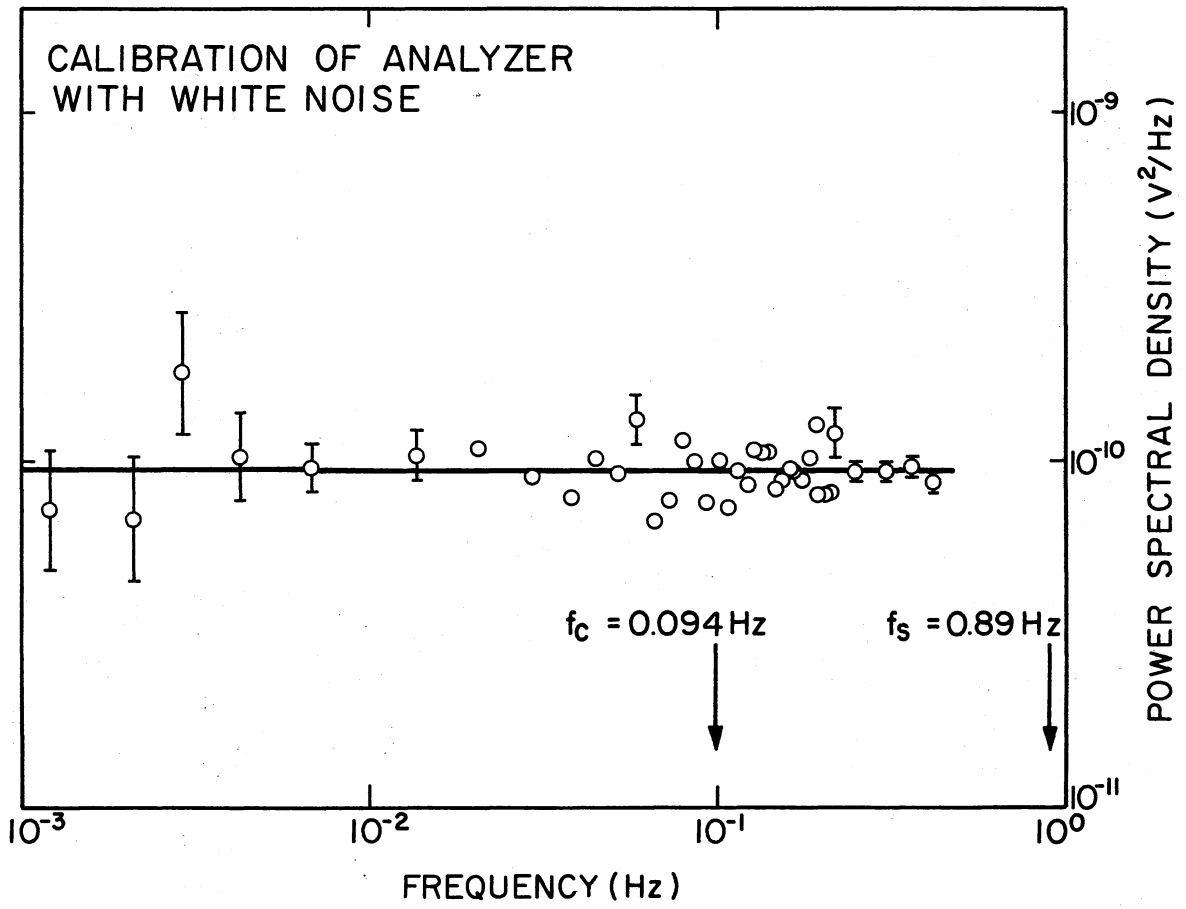

Figure 21. Power Spectral Density of Quantech Model 420 White Noise Generator

point data record. The sample period was 1.12 second which is represented in the figure as f_c. A total drift in the input signal of 1.8 μV was observed in the data record but was not removed. The calculated spectral estimates were corrected to account for the system's frequency response. The system cut-off frequency of 0.094 Hz is also shown in Figure 21. Aliasing corrections were also applied and based on an assumed constant spectral density.

Resistor Noise Measurement

Figure 23 is the result of a spectral measurement of the Nyquist noise (white) of a 10 MΩ resistor. This measurement required the use of the preamplifier and the thermostat (T = 32.26 °C). The preamplifier power supply (14.54 V for this measurement) was used to provide the necessary bias to the input. A circuit diagram of the input circuit arrangement is shown in Figure 22. The spectrum resulted from a $16384 = 2^{14}$ data point record with a sample period of 1.12 second. No discernible trend in the data was present. System frequency response corrections were made and dealiasing was done based on an assumed constant spectral density.

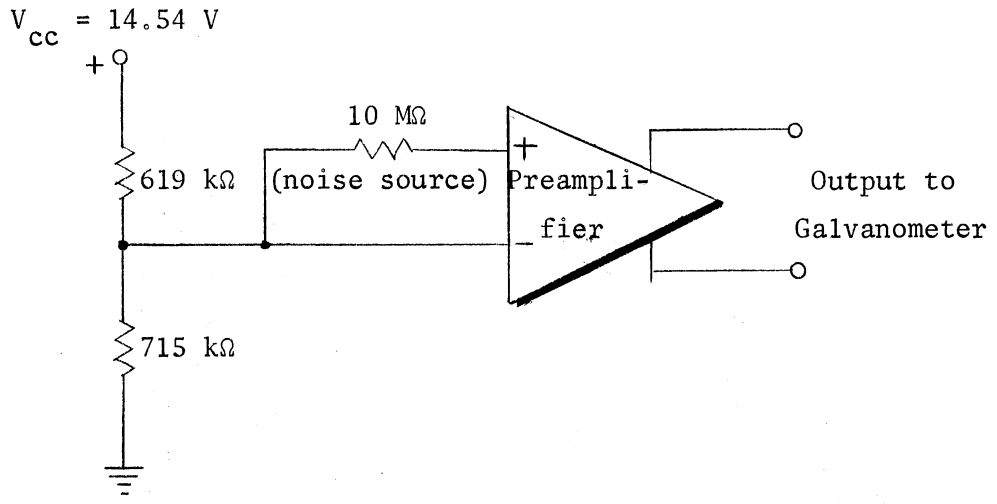

Figure 22. Diagram of Input Circuit Used for the 10 MΩ Nyquist Noise Measurement

Noise Measurement of an Ion-Implanted Resistor

The last spectral estimate in this series is a measurement of the noise power density of an ion-implanted resistor (R_{68}, device number 27 [30]). In this device only the high frequency (frequencies above 10 Hz) noise behavior was known. For further details on this see Tandon [30]. Figure 25 shows the results of the noise measurement on this device together with the known high frequency noise behavior. The frequency range, unfortunately, of the spectrum analyzer does not allow for spectral estimates at frequencies above the sampling Nyquist frequencies (f_n = 0.45 Hz). Nevertheless, the extrapolated spectra overlap and the system is taken to be calibrated against the known high frequency spectrum.

The preamplifier and thermostat (T = 32.26 °C) were used in this

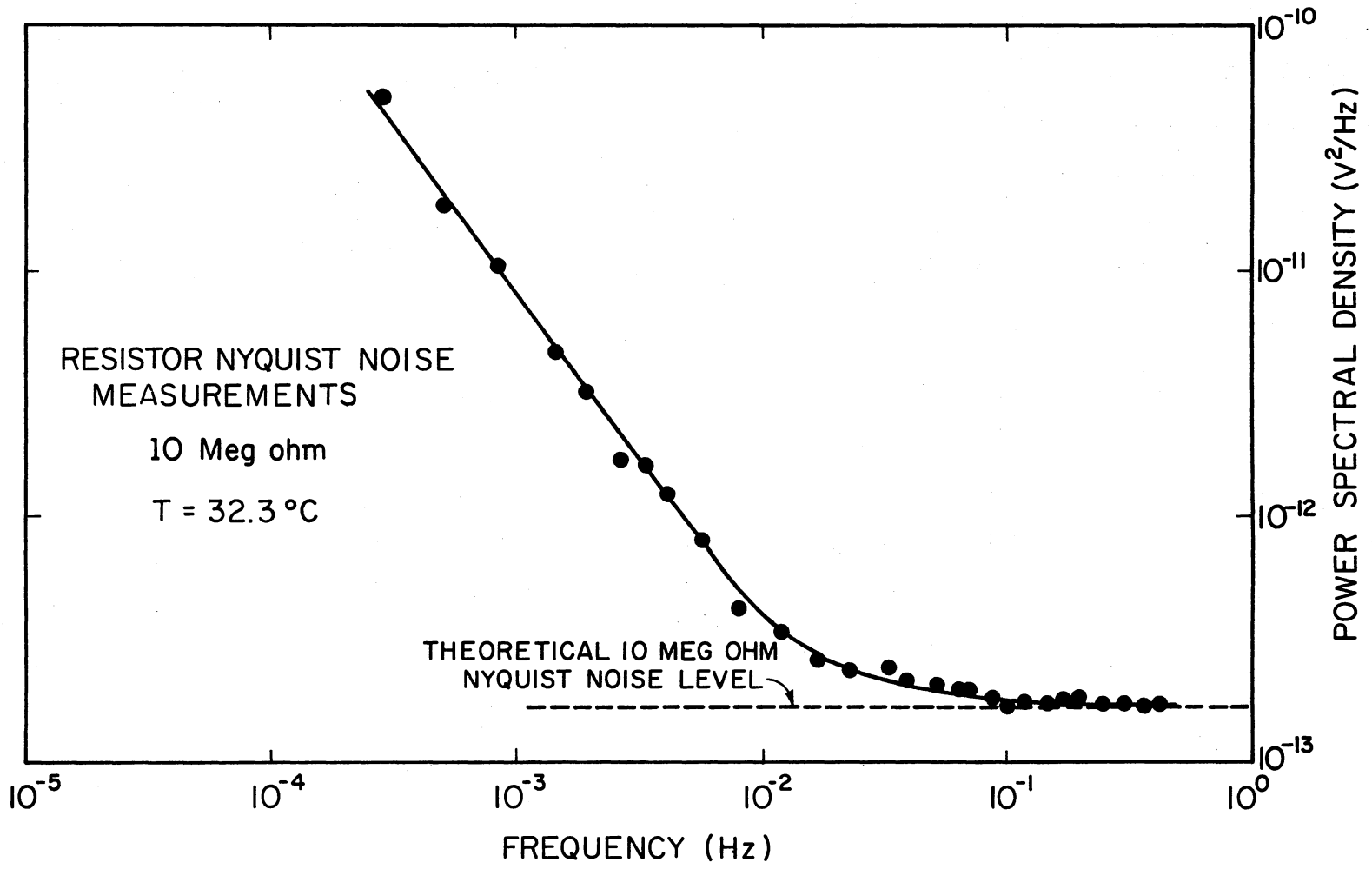

Figure 23. Power Spectral Density of a 10 MΩ Resistor

measurement. The input circuit arrangement to the preamplifier is shown in Figure 24. This arrangement allows the ion-implanted resistor to be biased without disturbing the input d.c. off-set to the preamplifier. The resistance value of R_{68} is 89.4 kΩ and its bias current was set to 6.8 μA. The other resistors used in the input network are 1% precision metal film. Two power supplies were required by this network. V_{cc} was the same supply used by the preamplifier. V_{BB} was a 1.43 V mercury battery (Mallory type RM 640) that was located inside the thermostat. The operating temperature of the thermostat was 32.26 °C.

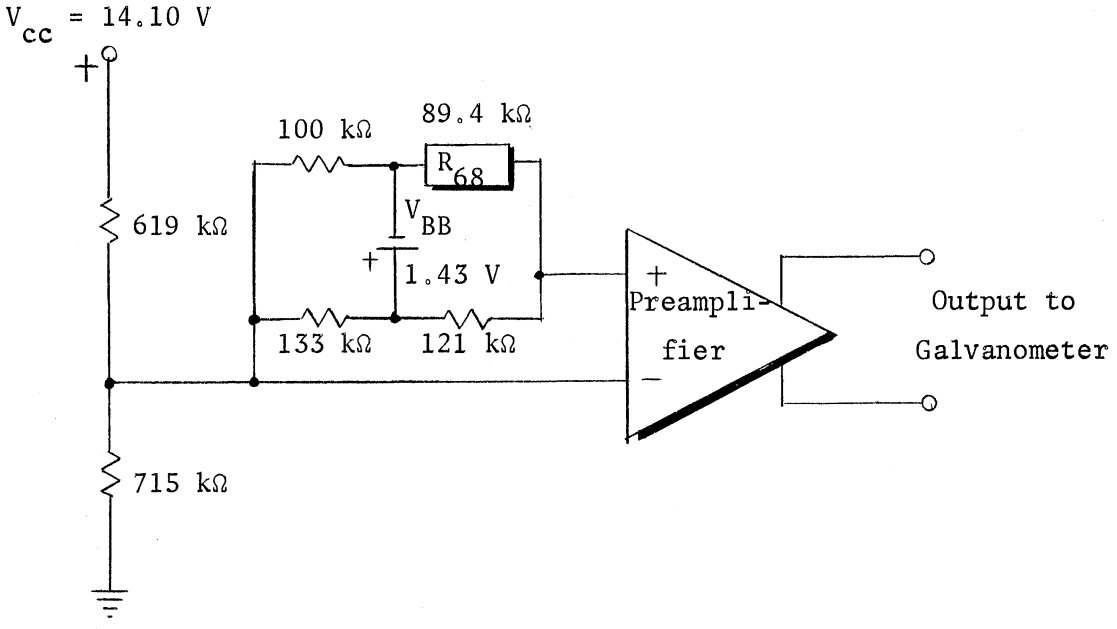

Figure 24. Diagram of Input Circuit to the Preamplifier for the Ion-Implanted Resistor Noise Measurement

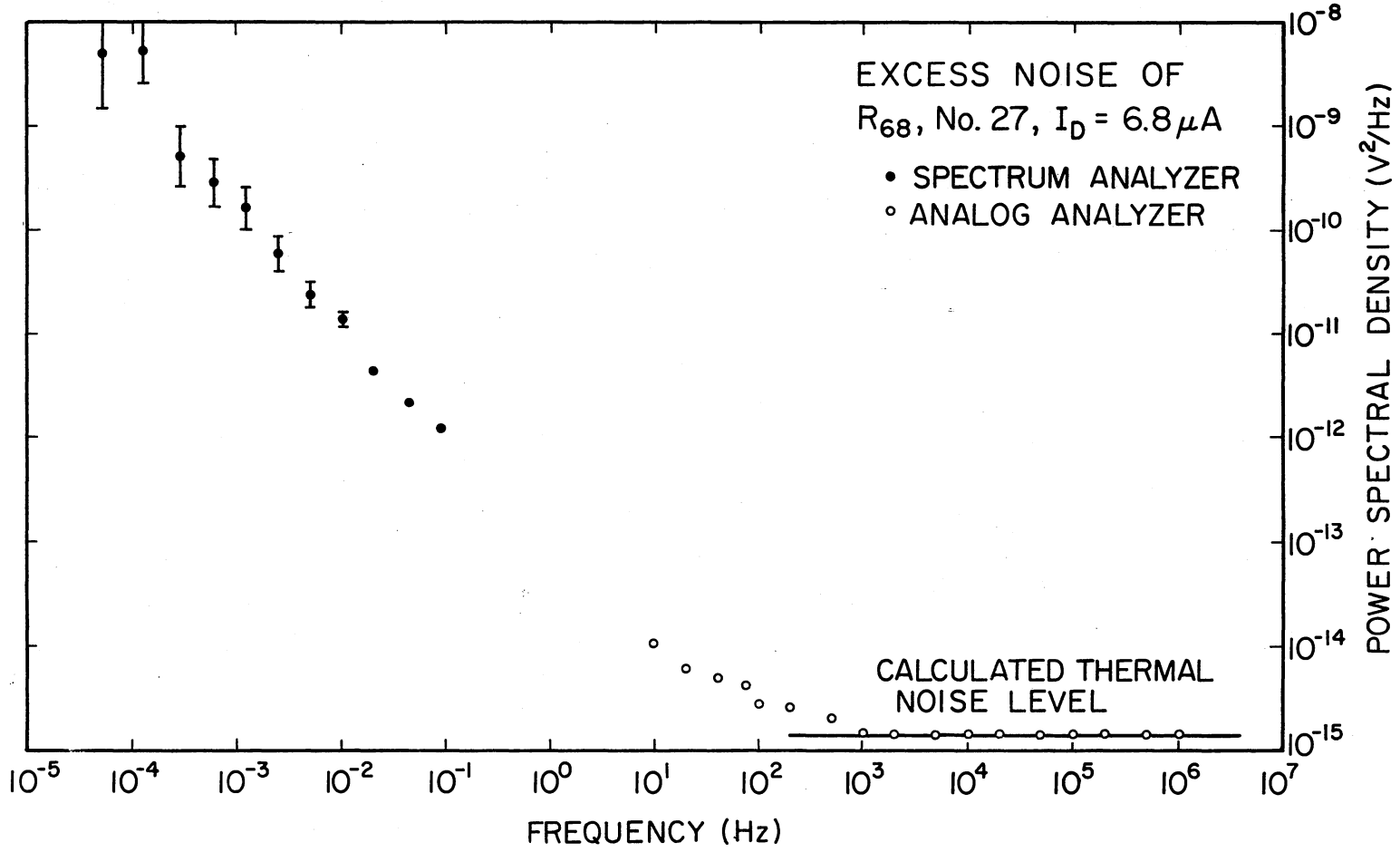

Figure 25. Power Spectral Density of an Ion-Implanted Resistor

The data record from which the spectral components were estimated contained 16384 = 2^{14} data points. The sampling period was 1.12 second. A linear trend of 0.6 nV/s (11 μV total drift for the record) was removed. The estimates were corrected for the system's frequency reponse and dealiasing was done assuming a $K/f^{1.0}$ type spectral density characteristic.

Since the analyzer measures the noise that is present at the input terminals of the preamplifier, the spectral estimates had to be multiplied by an additional factor which accounts for signal attenuation in the input circuit used (see Figure 24). A value of 5.5 was calculated for this factor. The spectral estimates shown in Figure 25 include this factor.

CHAPTER VII

LOW FREQUENCY NOISE OF ZENER DIODES

Introduction

Two low frequency noise power spectral density measurements were made using three Zener diodes. The diodes used in this study are temperature compensated, manufactured by International Rectifier. The I-V characteristics along with their temperature dependence for the Zener diodes used in the noise measurements are given in Figures 26, 27, and 28.

The first spectrum presented in this chapter represents the noise from two of these diodes and uses the preamplifier in the spectrum analyzer system. The second spectrum also used two diodes but is interpreted to represent the noise from only one of these devices. No preamplifier is used in this measurement. Both of the spectral figures presented contain a dashed curve. This curve, in each figure, represents previously published noise data for these devices which extends down to 0.1 Hz. A discussion of the spectra along with their evaluation is given in Chapter VIII.

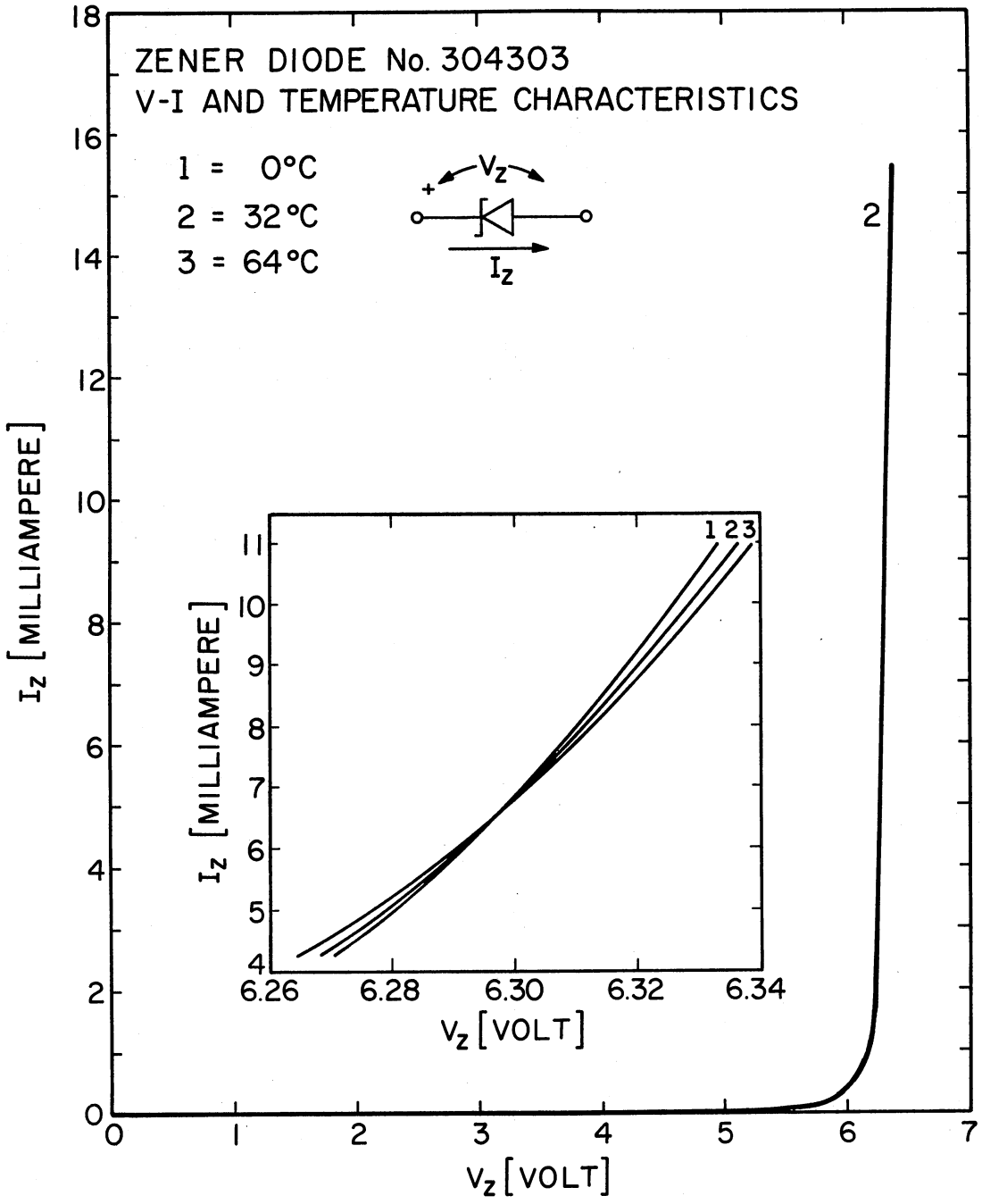

Figure 26. V-I and Temperature Characteristics of Zener Diode No. 304303

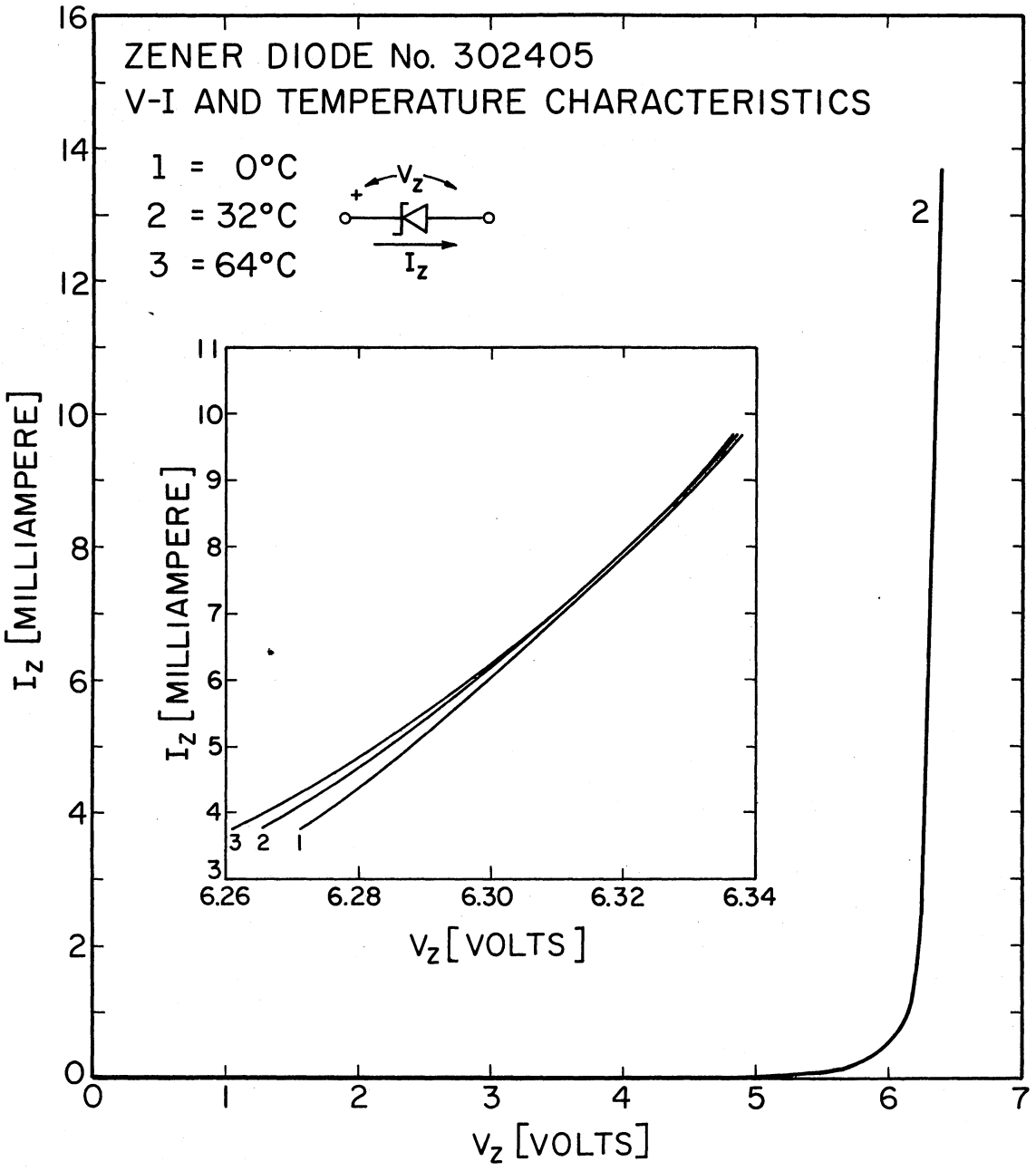

Figure 27. V-I and Temperature Characteristics of Zener Diode No. 302405

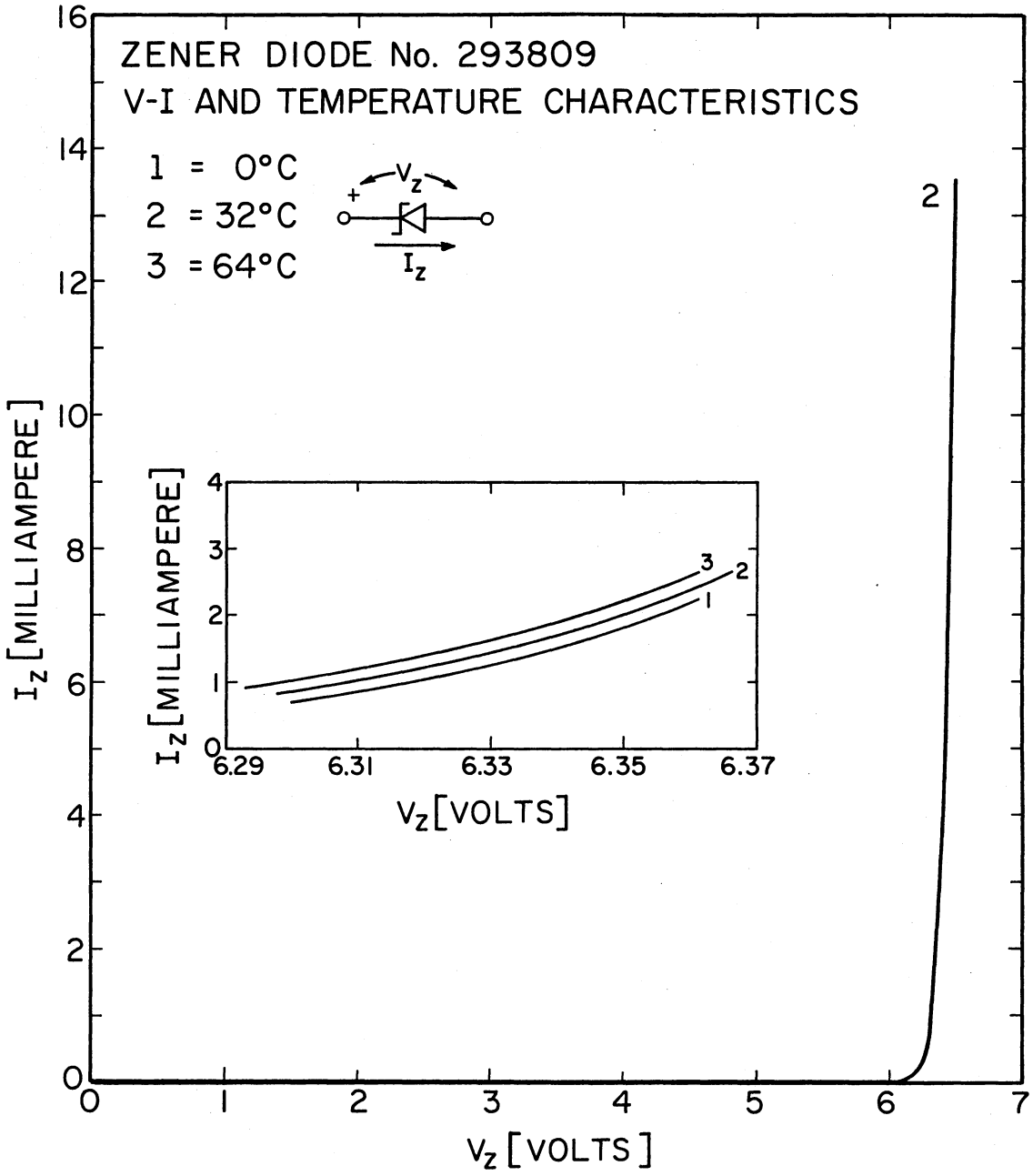

Figure 28. V-I and Temperature Characteristics of Zener Diode No. 293809

Noise Measurement of Zener Diodes

304303 and 302405

Input Circuit

The input circuit to the spectrum analyzer is shown in Figure 29. The two Zener diodes were chosen based on similar I-V characteristics and high frequency noise behavior. A two diode bridge arrangement is used to provide reasonable rejection to the common mode noise signals from the power supply. The power supply used is the same supply which powers the preamplifier (see Chapter IV) and its low frequency noise spectrum is given in Chapter VI.

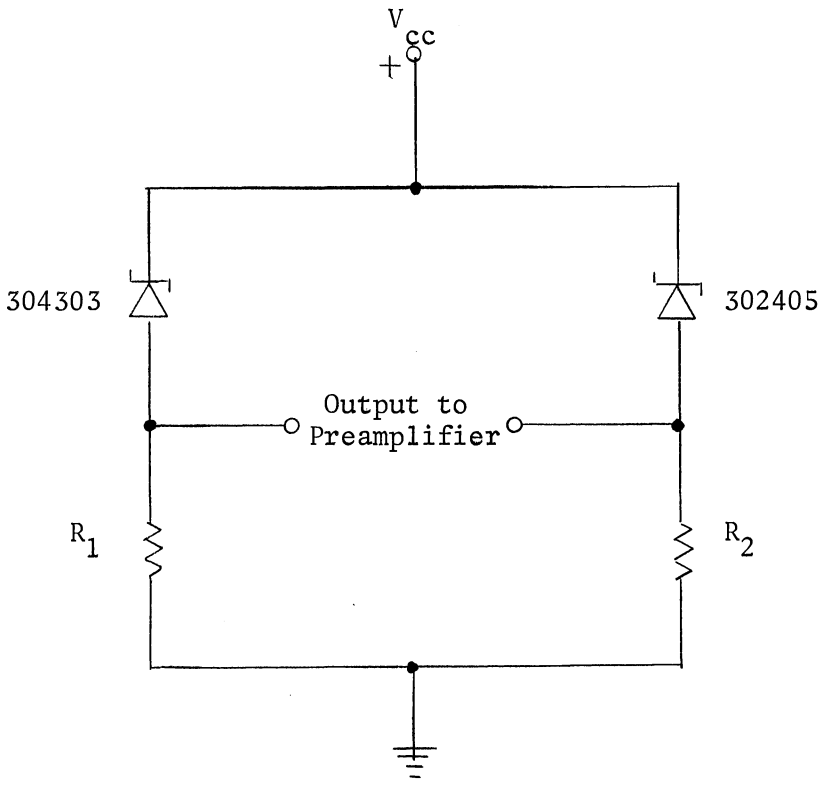

Figure 29. Input Circuit for Noise Measurement of Zener Diodes 304303 and 302405

The circuit shown in Figure 29 is mounted inside the copper enclosure (see Chapter III) along with the preamplifier. The copper enclosure was immersed in the operating thermostat during the measurements. The cathodes of the diodes were mechanically tied to the copper block to maintain them at the thermostat's temperature.

The electrical details of the circuit shown in Figure 29 are given in Table III.

TABLE III

OPERATING CONDITIONS AND SPECIFICATIONS OF INPUT CIRCUIT USED TO MEASURE NOISE OF ZENER DIODES 304303 and 302405

	Zener Diodes		Bridge
Device Number	304303	302405	
Diode Voltage [V_z(V)]	6.315	6.315	
Diode Current [I_{z_o} (mA)]	8.30	7.46	
Dynamic Resistance [r_d(Ω)]	9.30	9.86	
Voltage Temperature Coefficient [$TC = \frac{\Delta V_z}{\Delta T}\Big\vert_{I_z=I_{z_o}}$ (V/°C)]	4.8×10^{-5}	1.6×10^{-5}	
Bridge Element R_1 (Ω)			882.5
Bridge Element R_2 (Ω)			995.5
Bridge CMRR			1610
Power Supply Voltage [V_{cc}(V)] (Power Designs Inc. Model 2020)			13.615

Power Spectrum

Figure 30 shows the noise power spectral density that was obtained from measurements on diodes 304303 and 302405. This curve is interpreted to represent the noise power contribution from both diodes. It is assumed that the metal film resistors used in the bridge are relatively noiseless and therefore make no noise contribution to the measurement. The bridge CMRR of 1610 gives a noise contribution from the power supply at least four orders of magnitude down from the level shown in Figure 16.

The spectrum shown was computed from a data record of $32768 = 2^{15}$ samples. The sample period was 1.12 second ($f_s = 1.12^{-1} = 0.89$ Hz). Figure 31 shows the first 30 minutes of the recorded noise voltage output from the bridge. Although the total record length is about 10.2 hours, the 30 minute segment shown is representative of the character of the noise voltage waveform. Included in Figure 31 is a curve which represents the drift of the mean value of the recorded waveform. This curve was plotted from mean values of the data record computed over groups of 2048 samples (approximately 38 minute periods). A curve representing the fluctuations in room temperature is also given in Figure 31. A comparison of the drift and temperature curves shows that they are unrelated.

Computational Procedures

A straight line was fitted to the data record and subtracted from the record. The slope of this was found to be -45.7 pV/s which amounts to about 1.7 μV of drift over the entire data record.

The procedure for correcting the raw spectral estimates was as follows. Prior to measuring the Zener diode noise, the noise of the spectrum analyzer was measured. This was done by connecting both inputs of

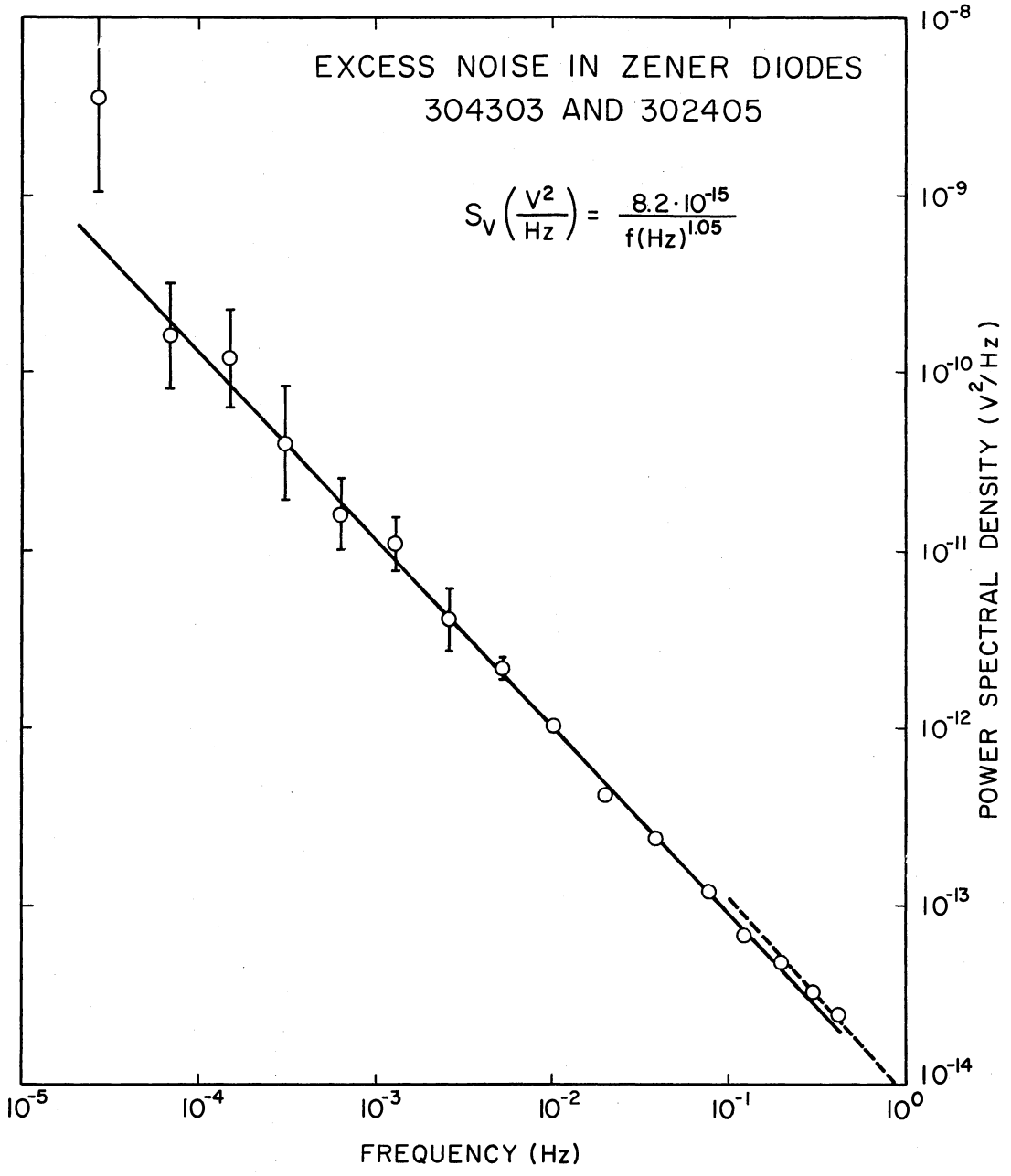

Figure 30. Power Spectral Density of Zener Diodes 304303 and 302405

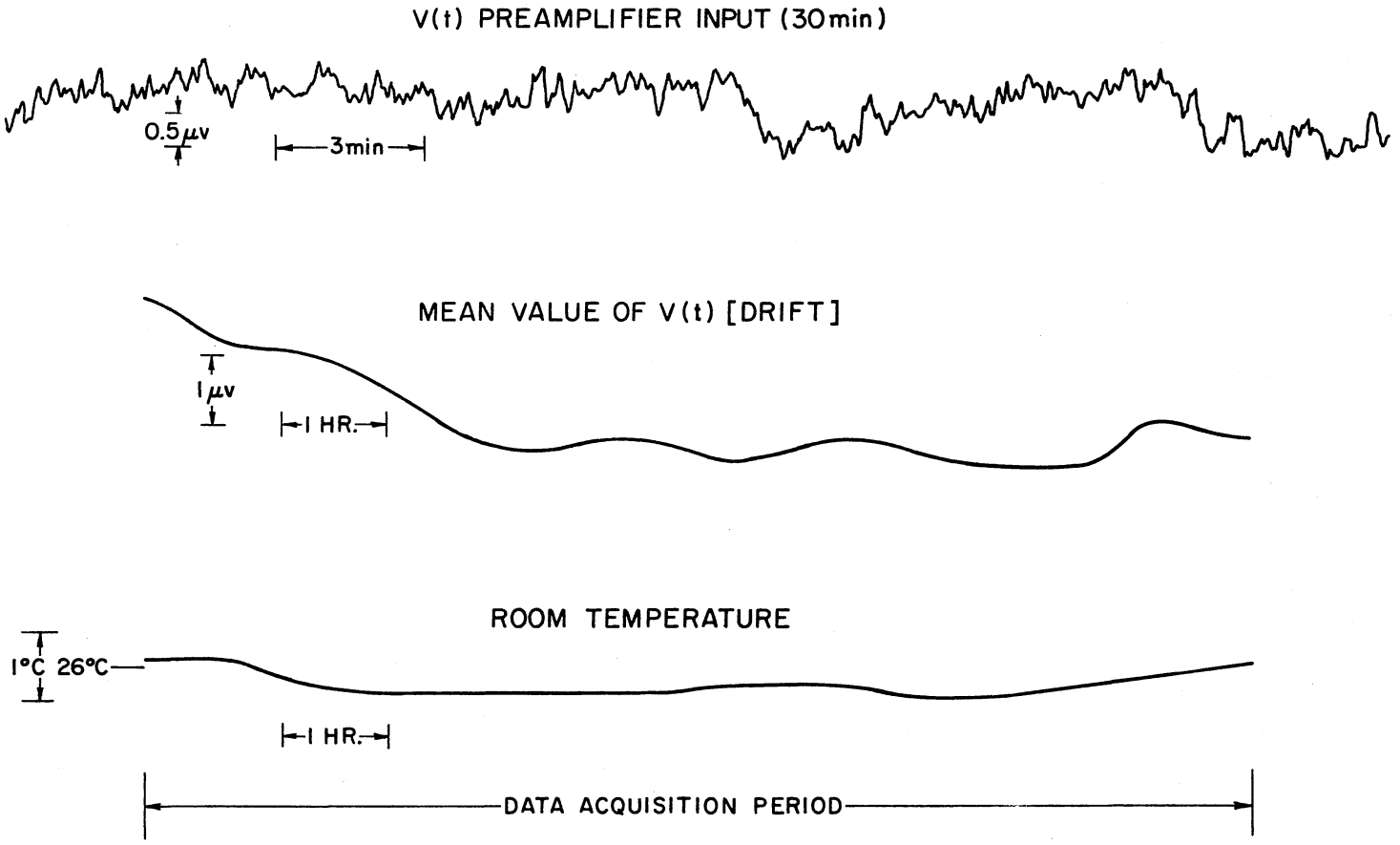

Figure 31. V(t), Mean Value Fluctuation, and Room Temperature for the Noise Measurement of Zener Diodes 304303 and 302405

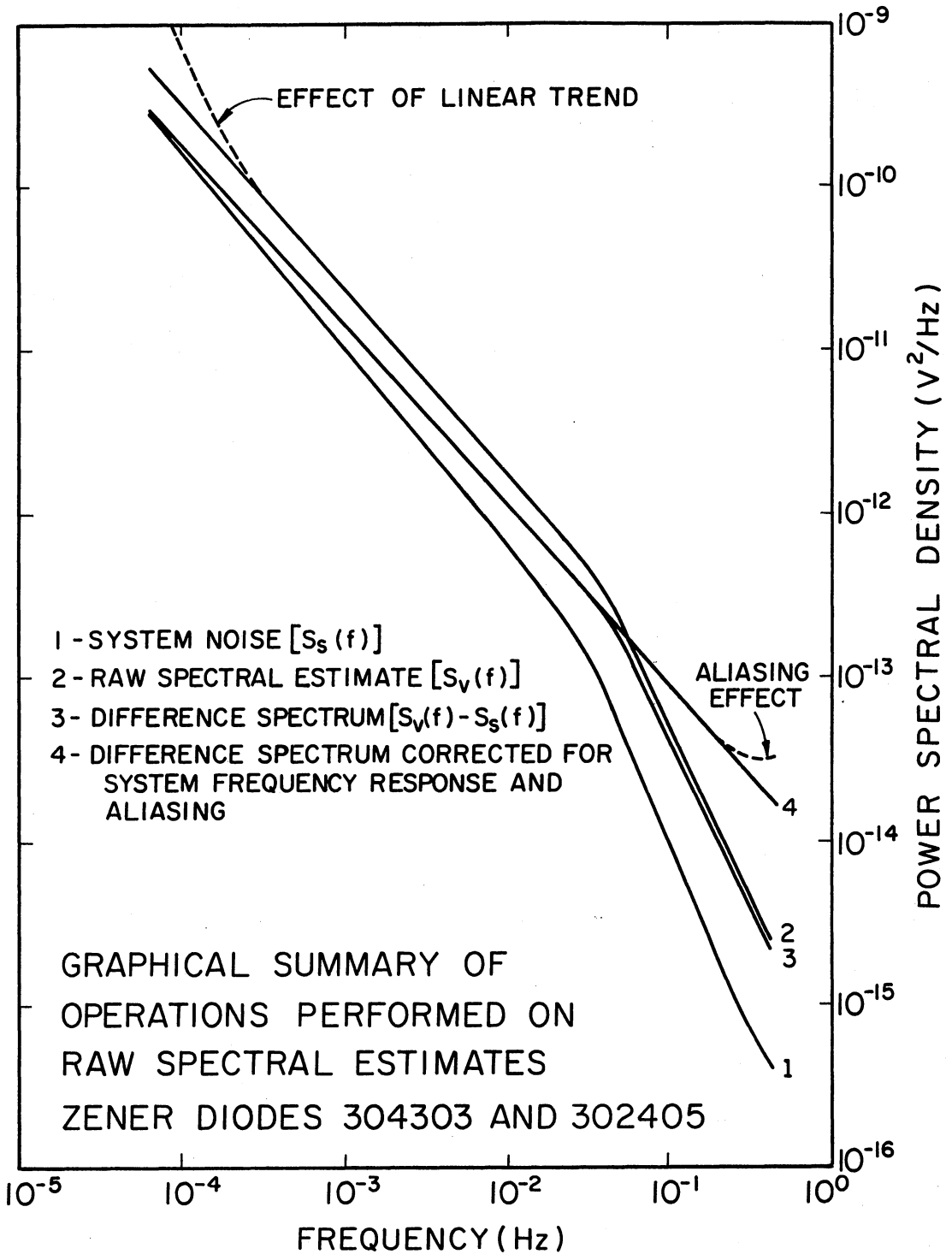

Figure 32. Graphical Summary of Operations Performed on Raw Spectral Estimates for Zener Diodes 304303 and 302405

the preamplifier to one of the two output terminals from the bridge shown in Figure 29 (further details on the measurement of the system noise can be found in Chapter VI). The resulting system noise spectrum is subtracted from the raw Zener diode spectrum. The resulting spectrum is then corrected for the spectrum analyzer's frequency response (f_c = 0.094 Hz, see Chapter II) and aliasing effects. These procedures along with their relative effects are shown in Figure 32. As a measure of the effect on the spectral estimates of not removing the calculated linear trend, the data record was also processed with no trend removal. The result of this on the raw spectrum is shown in Figure 32.

Noise Measurement of Zener Diode 293809

Input Circuit

For this measurement the input circuit shown in Figure 33 was used. A two diode bridge was used in this measurement again to minimize the effect of the common mode noise from the power supply. Although no preamplifier was used in this case, the bridge power supply is the same supply which normally powers the preamplifier described in Chapter IV. The output from the bridge is used to directly drive the galvanometer input of the spectrum analyzer.

The circuit shown in Figure 33 was mounted inside the copper enclosure and immersed into the operating thermostat during the measurement (see Chapter III). The cathodes of the two Zener diodes were mechanically fastened to the copper enclosure to insure good thermal contact.

The electrical characteristics of the bridge are summarized in Table IV.

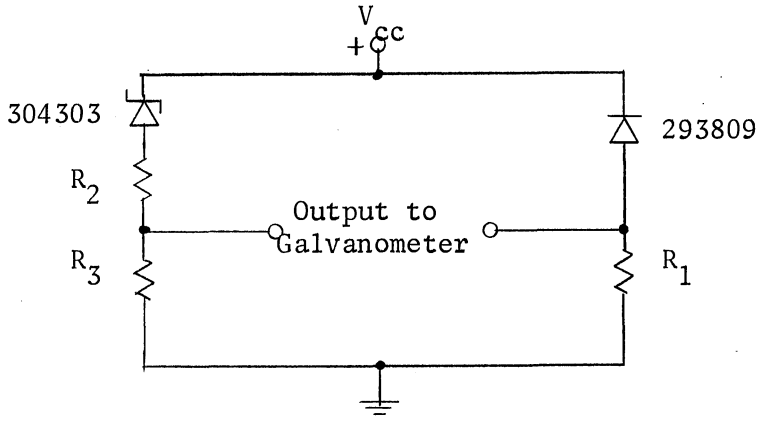

Figure 33. Input Circuit for Noise Measurement of Zener Diode 293809

TABLE IV

OPERATING CONDITIONS AND SPECIFICATIONS OF INPUT CIRCUIT USED TO MEASURE NOISE OF ZENER DIODE 293809

	Zener Diodes		Bridge
Device Number	293809	304303	
Diode Voltage [V_z(V)]	6.33	6.21	
Diode Current [I_{z_o} (mA)]	1.44	1.59	
Dynamic Resistance [r_d(Ω)]	40	46	
Voltage Temperature Coefficient [$TC = \frac{\Delta V_z}{\Delta T}\Big\|_{I_z=I_{z_o}}$ (V/°C)]	2.3×10^{-4}	2.2×10^{-4}	
Bridge Element R_1 (Ω)			998.9
Bridge Element R_2 (Ω)			74.41
Bridge Element R_3 (Ω)			904.4
Bridge CMRR			12.7
Bridge Output Resistance R_o (Ω)			145
Power Supply Voltage [V_{cc}(V)] (Power Designs Inc. Model 2020)			7.768

Power Spectrum

The noise power spectral density for Zener diode 293809 is presented in Figure 34. This spectrum is attributed solely to this diode for the following reasons. First, it can be seen on comparing the level of the noise power density of Figure 34 with that presented in Figure 30 that this spectrum is about an order of magnitude higher (note the spectrum of Figure 30 represents the noise of two diodes). The diode 304303 used in this input circuit for this measurement happens to be one of those whose noise is documented in Figure 30. From this, plus the noise voltage attenuation of 304303 by resistor R_2 and R_3 of the bridge, it is concluded that the measurement represents the noise of diode 293809. Of course it is assumed that the resistors in the bridge and power supply also make no contribution (the CMRR of 12.7 makes the noise power level from the power supply about two orders of magnitude below that shown in Figure 16).

The data record for this measurement was composed of $16384 = 2^{14}$ samples. The sample period was 1.12 second ($f_s = 1.12^{-1} = 0.89$ Hz) making for a record length of about 5 hours. Figure 35 shows 30 minutes of the voltage waveform from the bridge which is considered representative of the total record. Also in Figure 35 are curves which show the variation of the mean voltage from the bridge and the room temperature during the experiment.

Computational Procedures

The trend in the mean voltage shown in Figure 35 was removed by fitting a straight line to the data record and subtracting this line from the data. The slope of this line was computed to be -5.2 nV/s which

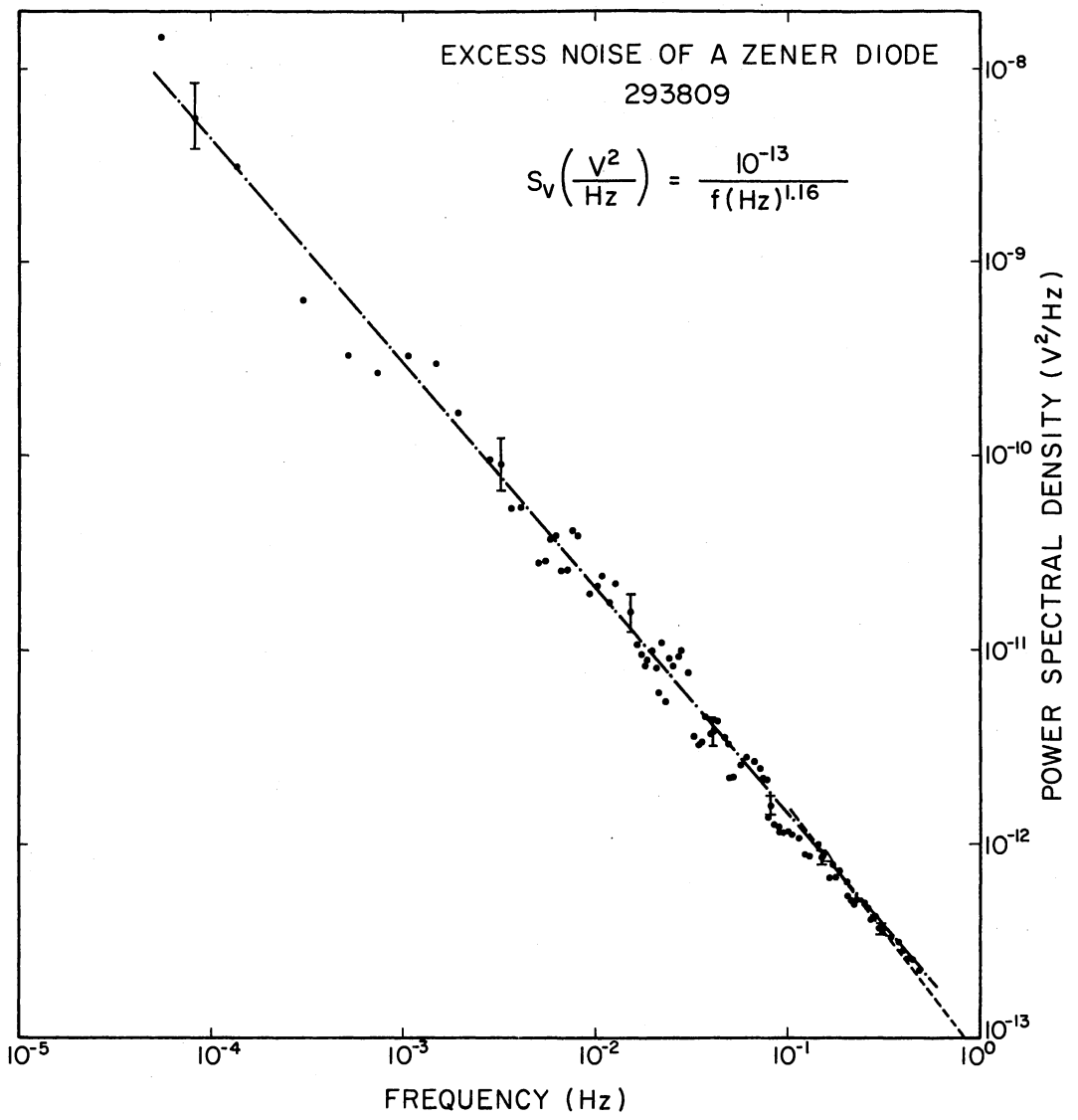

Figure 34. Power Spectral Density of Zener Diode 293809

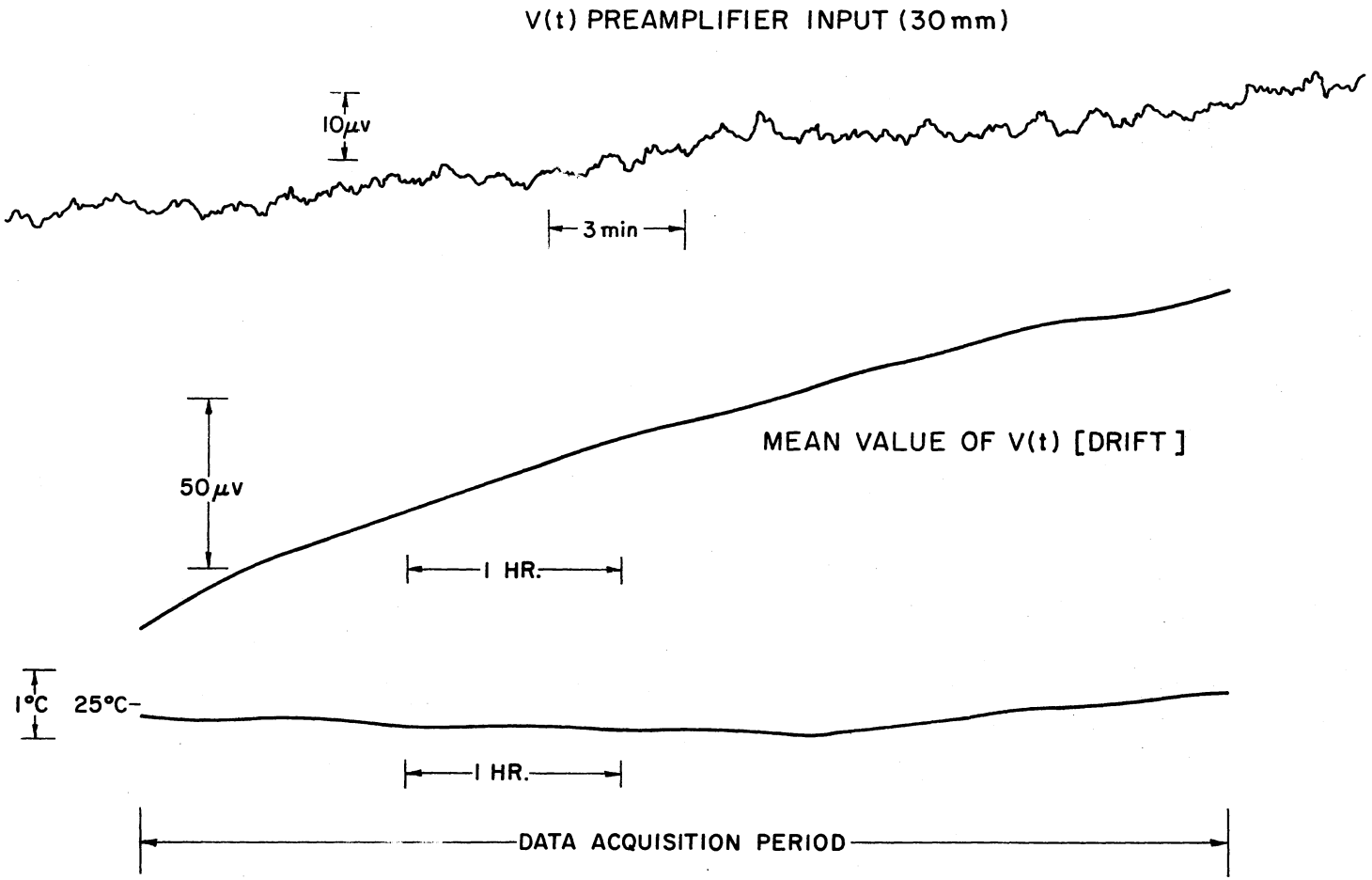

Figure 35. V(t), Mean Value Fluctuation, and Room Temperature for the Noise Measurement of Zener Diode 293809

amounts to about 95 μV of drift over the entire record. Reasons for trend removal are discussed in Chapter VIII.

The remaining procedures are identical to those outlined in the previous diode noise measurement (diodes 304303 and 302405). Figure 36 summarizes graphically the results of these procedures.

It should be noted that the output resistance of the bridge was 145 Ω. This changes the spectrum analyzer's frequency response from f_c = 0.094 Hz which occurs when the external damping of the galvanometer is 750 Ω to a lower value of about 0.07 Hz (see Chapter II). This change was considered when correcting the spectrum for the frequency response of the analyzer system.

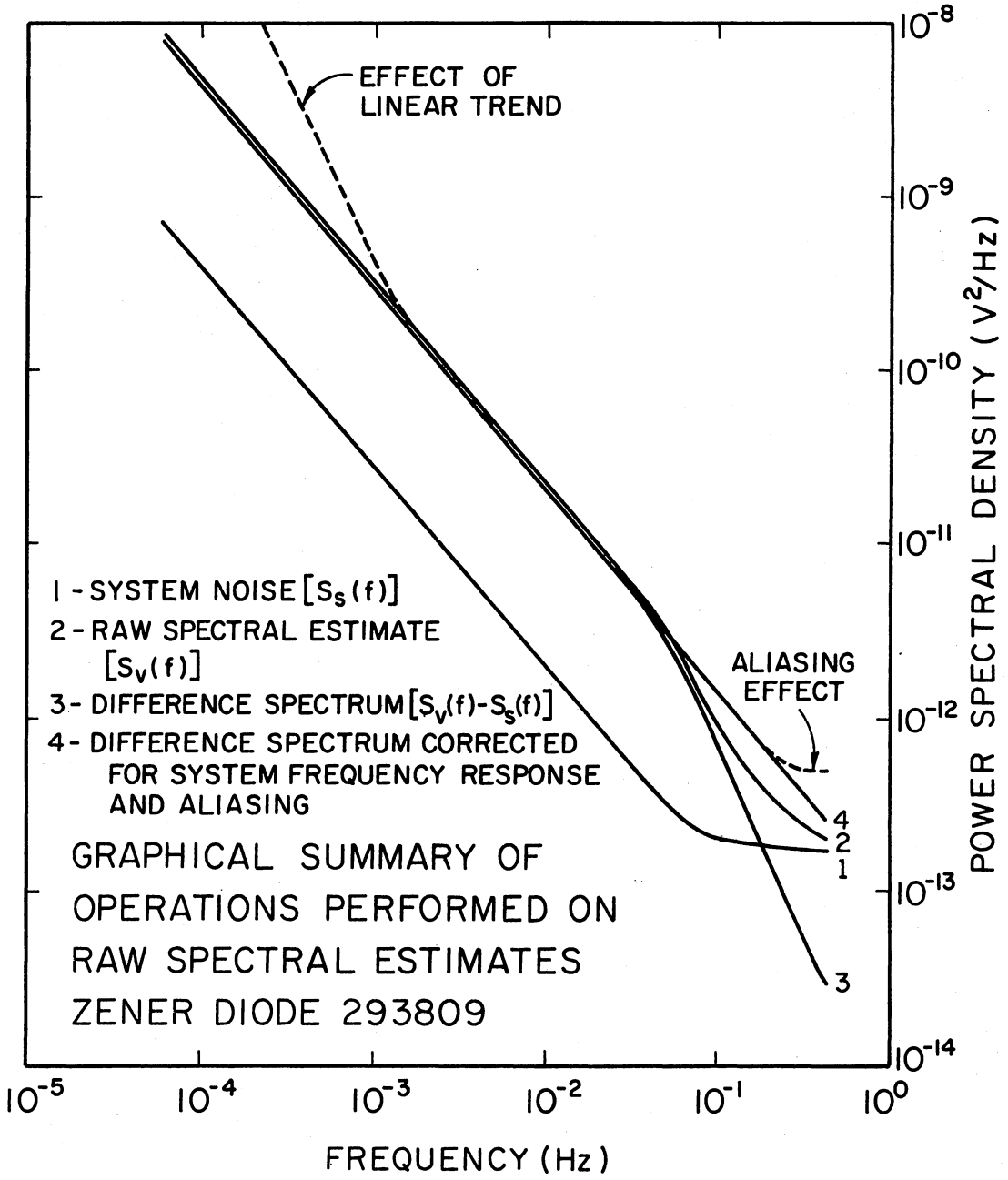

Figure 36. Graphical Summary of Operations Performed on Raw Spectral Estimates for Zener Diode 293809

CHAPTER VIII

EVALUATION OF ZENER DIODE SPECTRA

Introductory Remarks

Both Zener diode spectra presented in Chapter VII are based on noise measurements coming from the input bridge circuit. Thus, in reality, it is the noise properties of the bridge which are measured. The CMRR of the bridges used are high (1610 and 12.7, respectively) so that the contribution to the measured noise from the power supply is negligible (see power supply noise spectrum in Chapter VI). In the worst case (noise measurement of Zener diode 293809) it is down at least an order of magnitude from the level of the spectral estimates. The noise from the metal film resistors used in the bridges are assumed to make no contribution to the noise measurement. Therefore, the spectrum shown in Figure 30 is interpreted to represent the noise of Zener diodes 304303 and 302405. Based on this measurement, the noise level of the results shown in Figure 34 are taken to represent the noise of the single Zener diode 293809. This assessment is additionally supported by noise data on the diodes at frequencies above 0.1 Hz. These data suggest that the noise level of diode 293809 can be expected to be 20 to 30 times larger than either 304303 or 302405 (for details on these data see Ringo [28]).

Recorded Noise Data

Data Errors

The spectra reported in Chapter VII were computed from data records of 32768 = 2^{15} and 16384 = 2^{14} samples, respectively. The number of falsely recorded data samples that were corrected in each record (see Chapter V for details on data editing) were 21 and 8. This indicates a failure rate in the recorded data of about 0.05% (these "errors" are assumed to arise from malfunctions in the equipment that comprised the spectrum analyzer discussed in Chapter II).

Both data records appear to be free of unusually large amplitude spikes and "popcorn" noise. This is based on a computer check of the data records to see if the value of adjacent data samples varied by more than about 10 μV (the standard deviation of the data records was approximately 0.5 μV and 1.8 μV, respectively). In both cases no such "jumps" in the data were detected.

Trend Removal

A linear trend in each data record was computed by fitting a straight line (least mean square sense) to the data. This straight line was subsequently subtracted from the record. The effect of not removing this apparent trend is shown in Figures 32 and 36 in Chapter VII. It may be argued that any such operation on the data, which represent an actual noise voltage measurement, is not legitimate. However, for the spectra reported in this work, the removal of any trend from the data is necessary and probably justified.

The necessity for trend removal arises from the periodicity forced

on the data record by the FFT algorithm used in obtaining the spectral estimates. Non-removal of trend has the same effect on the voltage spectrum as if there were a "sawtooth" waveform of period equal to the data record length present in the data. This as expected, erroneously raises the spectral components at the low end of the spectrum (see Figures 32 and 36). Of course the way to avoid this problem is to record data for periods 10 to 100 times longer than the period of the lowest frequency at which an estimate is desired. However, this was not considered practical for this work.

A second reason for removing any trend is based on the argument that in measurements of this type it is not possible to realistically assess the spectral effects due to frequencies whose apparent periods are longer than the period of measurement. Therefore, since trend can be considered as a frequency lower than that which can be accommodated by the measurement, its removal seems justified.

Although the FFT algorithm forces periodicity onto the recorded random noise voltage, the effects of this are not noticeable. This statement is based on a test which involved computing the power spectrum for half the length of a data record and comparing it to the spectrum for the whole record. Both spectra were within the bounds of each other's statistical error (see Chapter V). The implication of this cursory test is that periodicity forced on a data record of a random process which goes through many "wiggles" (well over 10^3 in a 16384 point record) in the course of its recording has little if any effect on the resulting spectral density of that process.

The process of removing a linear trend in effect throws away some of the recorded information. This is verified by comparing variances

of the data before and after trend removal in a given record. In the case of Zener diode 293809 this variance was 770 $(\mu V)^2$ before removal and 3 $(\mu V)^2$ after. For the Zener diodes 304303 and 302405 measurement it was 0.5 $(\mu V)^2$ before and 0.3 $(\mu V)^2$ after. Had the trend not been removed in particular for the 293809 diode noise measurement, the resulting power spectrum would have been highly dominated by this trend rather than the random noise voltage fluctuations.

The trend that was very apparent in the 293809 diode appears to be associated with that device itself. The 95 μV drift measured over the record period is at least 15 times larger than that which could be accounted for by the power supply. Preliminary observations indicate that the drift decays with time suggesting that if the device had been kept under power at constant temperature for a few days the trend may have been considerably reduced. In fact, in the case of the other diode measurements the devices were kept under power at constant temperature for about 36 hours prior to their noise measurement. Therefore, the linear trend, although apparently a device phenomenon, is thought not to be a random process in the sense of noise and consequently it was removed from the data record.

Low Frequency Spectral Properties of the Zener Diodes

Slope

The Zener diode spectral estimates have relative errors of ± 71% at the lowest frequency estimates to about 5% at the highest frequencies. These values are based on the variance of an averaged estimate being proportional to the square root of the reciprocal of the number of

independent estimates averaged (see Chapter V). The log-log plot of the spectral estimates shown for the Zener diodes can be easily accommodated with a straight line implying that the noise properties in the measured frequency range follow a simple power law. In fact there is nothing in these spectra which even tends to suggest that a departure from the power law character should be emminent. The general form of the spectra can be expressed throughout the entire frequency range as

$$S(f) = \frac{K}{f^a} \tag{8-1}$$

where

$S(f)$ = power spectral density (V^2/Hz),

K = constant (V^2), and

f = frequency (Hz).

A value of 1.05 for "a" was determined for the 304303 and 302405 Zener diode measurement and 1.16 for diode 293809 with the value of K equal to 8.2×10^{-5} and 1.0×10^{-13}, respectively.

Stability of $S_V(f)$ Versus Time

The diodes used in this study are the very same devices reported on by Ringo [28] in 1971. The spectra shown in Chapter VII show, in addition to the measurements reported in this work, the results of Ringo on these devices. His work goes down to 0.1 Hz whereas the spectra presented in this thesis go up to 0.45 Hz. This allows for about a half decade of frequency over which direct comparison may be made. At the frequency of 0.159 Hz (ω = 1 rad/s) the magnitude of the two power densities agree to 20% and 2%, respectively. The values of "a" (exponent of f) agree to 6% and 14%. The systematic errors inherent in the

measuring apparatus are estimated to be such that absolute power spectral density values are not thought to be better than about 20%. Therefore, the Zener diode spectra are considered to be consistent with those of Ringo.

This stability in the spectra strongly suggests that some form of stationarity is present in the process or processes which give rise to their 1/f character. This form of stationarity must be different than the conventional "wide-sense" notion in that the process's associated autocorrelation function will not converge for large τ if $S_V(f)$ is assumed to strictly behave as 1/f. Thus the process cannot be "wide-sense" stationary. Nevertheless, it is concluded that these $S_V(f)$, which are interpreted as relatively short term average power spectral densities with any linear trend removed, are independent of time. This statement is made in view of the fact that the spectra for the Zener diodes presented in Chapter VII are entirely consistent with the measurements of Ringo [28] on these same devices made some 4 years earlier.

Prediction of Device Voltage Drift From its Noise Spectrum

As previously mentioned, the noise characteristics of the devices used in this study in the frequency range above 0.1 Hz are documented; in addition, a possible correlation between the 1/f noise and the voltage drift of the devices was suggested (see Ringo and Lauritsen [29]). In particular, the mean square voltage drift of these devices over a sample period of one week was computed and compared to that predicted from the measured high frequency noise power spectra extrapolated down to the corresponding frequency. The results, which showed possible correlation

in some cases, indicated a measured value about three orders of magnitude larger than that predicted. This in turn implied that a distinctive change must occur in the power spectral density curve between the frequencies of 0.1 Hz to 2 μHz in order to accommodate the measured drift data.

The power spectral estimates (after trend removal) on the three of these devices used in this study went down to frequencies below 10^{-4} Hz with no significant departure from the simple power law characteristic being noticed. It is thus concluded that if the voltage drift measurements are comparable at all, a different physical mechanism probably accounts for the observed voltage drifts and therefore such drifts are not predictable from short term device noise measurements.

CHAPTER IX

CONCLUSIONS

Accomplishments

The instrumentation necessary to make low frequency noise measurements on electronic devices has been designed and constructed. This system consists primarily of the Spectrum Analyzer, Constant Temperature Thermostat, and Preamplifier described in Chapters II, III, and IV. This system makes possible calibrated noise power studies at frequencies below 1 Hz and at voltage levels as low as 325 nV.

The spectra presented in this work appear to confirm the usefulness and validity of direct transform techniques (FFT approach) in estimating power spectral densities at low frequencies. Although these techniques and their use in themselves are not new, their application in the study of electronic noise at frequencies below 1 Hz is relatively new and only sparse information appears in the literature.

The first measurement on the spectral noise properties of Zener diodes in the frequency range of 8×10^{-5} Hz to 0.4 Hz is here reported. The results show that the 1/f character of the spectrum is preserved to at least 10^{-4} Hz. The notion that the physical process responsible for this noise is stationary at least in some sense is established by the fact that the spectra are stable. They agree well with higher frequency noise measurements made on the same devices some four years prior.

The literature shows that 1/f noise appears at frequencies at least

as low as 10^{-3} Hz in germanium filaments [31], bipolar transistors [4], and MOSFET's [23]. This type of noise is now shown to be also present, at these frequencies and lower, in devices where the physical phenomenon of "avalanching" forms the basis for their operation.

Specific Limitations and Problems

The limitations and problems encountered in this work fall into two categories, those associated with the spectrum analyzer, and those with the processing of the recorded data.

In the case of the spectrum analyzer, these center around the mechanical card punch unit. This unit limits the maximum sample rate to no more than about two samples per second thus limiting the highest frequency for spectral estimation to 1 Hz. Conventional analog spectrum analyzers typically do not go down to frequencies below 10 Hz. This clearly causes problems when trying to compare existing noise data with new measurements made with this system. The card punch unit for practical reasons, also limits the length of the data record. For data runs of 2^{15} samples, the number of cards punched is 2048. Beyond this number of samples the number of cards begin to become unmanageable (2^{16} samples = 4096 cards and so on). This, coupled with the necessity to continually monitor the card punching operation sets the practical record length to less than 24 hours (the continuous monitoring arises from having to supply fresh cards and remove punched cards about every two hours if the sample rate of approximately one sample per second is maintained).

It should be mentioned that the normal problem areas which include mechanical vibrations, thermocouple voltages, and drift in the instrumentation appear to have been avoided.

The problems in the area of data processing arise primarily from the fact that little is known about the errors that may be introduced into an estimate. These may result from the techniques used in going the direct transform route to the power spectral density of random data. In particular, the optimum choice of data "windows" for reducing leakage is an open question as is the necessity for pre-whitening data [9] whose spectral density is not constant. No pre-whitening of data was done in this study. The errors that have been discussed in this thesis are all based on the assumption that the measured data come from a physical process which is both gaussian and stationary. That this is in fact true, is also unresolved. Of course these problems can be avoided by choosing not to transform the data into the frequency domain for interpretation. An alternative is to investigate the statistics of the data directly. This idea is further discussed in the section on recommendations for further study later in this chapter.

Suggested Spectrum Analyzer Improvements

The sensitivity of the spectrum analyzer is probably its weakest point. This sensitivity is governed by the minute fluctuations in the rotating speed of the disc (positional scanner). It is felt that the sensitivity can be somewhat improved (perhaps by a factor of 3) by going to a direct drive system using a 600 rpm motor. However, the best solution to this problem appears to be a closed loop active speed control system. Such systems have reported stabilities which indicate that at least an order of magnitude of improvement in this area could be expected.

Another area in which improvement seems possible is the preamplifier

for the analyzer. The noise characteristics of this circuit are higher than expected based on high frequency noise measurements (frequencies higher than 10 Hz) made on the FET's. These measurements suggest that at least a factor of 10 reduction in noise in this circuit is possible.

Finally a major improvement in the system would be to replace the card punch data recording scheme with a magnetic tape recording system for storing data. The reliability of such systems appear to be superior, they can be left unattended, and the possibility of high density data records which extend over periods of months becomes very practical.

Recommendations for Further Study

The spectrum analyzer and thermostat make possible a multitude of low level and low frequency measurements. The validity of the noise model for FET's at frequencies below 1 Hz with gate currents less than 1 pA is one example. Drift characteristics of standard voltage cells is another. A more intriguing area though is a study of the statistical properties of random noise waveforms. Preliminary work in this area has already been reported by Bell [5], Brophy [12], and Greenstein and Brophy [15]. It is anticipated that such studies may lead to a definite identification of the process associated with 1/f noise and the properties of that process. Such information in turn may suggest a more satisfactory physical mechanism responsible for this phenomenon.

A SELECTED BIBLIOGRAPHY

(1) Abramowitz, M., and L. A. Stegun. Handbook of Mathematical Functions. U.S. Department of Commerce, NBS Applied Mathematical Series, Fourth Printing. Washington, D.C.: U.S. Government Printing Office, 1965.

(2) Akaike, H. "On the Design of Lag Window for the Estimation of Spectra." Annals of the Institute of Statistical Mathematics, Vol. 14 (1962), 1-21.

(3) Baldinger, E., and E. Nüesch. "Ein Thermostat hoher Konstanz." Zeitschrift für Angewandte Mathematik und Physik, Vol. 19 (1968), 334-344.

(4) Baldinger, E., and E. Nüesch. "Rauschen von Transistoren bei Sehr Tiefen Frequenzen." Helvetica Physica Acta, Vol. 41 (1968), 313-322.

(5) Bell, D. A. "Variance Fluctuations of 1/f Noise." Electronics Letters, Vol. 11, No. 13 (1975), 274.

(6) Bendat, Julius S., and Allan G. Piersol. Random Data: Analysis and Measurement Procedures. New York: Wiley Interscience, 1971.

(7) Bilger, H. R., J. L. Tandon, and M. A. Nicolet. "Excess Noise Measurements in Ion-Implanted Silicon Resistors." Solid State Electronics, Vol. 17 (1974), 599-605.

(8) Bingham, C., M. D. Godfrey, and J. W. Tukey. "Modern Techniques of Power Spectrum Estimation." IEEE Transactions on Audio and Electroacoustics, Vol. AU-15 (1967), 56-66.

(9) Blackman, R. B., and J. W. Tukey. The Measurement of Power Spectra From the Point of View of Communications Engineering. New York: Dover, 1958.

(10) Blakemore, David J. "Microcycle Spectral Estimation." (Unpub. Ph.D. thesis, California Institute of Technology, 1966.)

(11) Brenner, N. M. "Fast Fourier Transform of Externally Stored Data." IEEE Transactions on Audio and Electroacoustics, Vol. AU-17 (1969), 128-132.

(12) Brighan, E. Oran. The Fast Fourier Transform. Englewood Cliffs, N.J.: Prentice-Hall, Inc., 1974.

(13) Brophy, J. J. "Statistics of 1/f Noise." Physical Review, Vol. 166, No. 3 (1968), 827-831.

(14) Cooley, J. W., and J. W. Tukey. "An Algorithm for Machine Calculation of Complex Fourier Series." Math Computation, Vol. 19 (1965), 297-301.

(15) Greenstein, L. J., and J. J. Brophy. "Influence of Lower Cutoff Frequency on the Measured Variance of 1/f Noise." Journal of Applied Physics, Vol. 40, No. 2 (1969), 682-685.

(16) Haitz, R. H. "Noise of a Self-Sustaining Avalanche Discharge in Silicon: Low-Frequency Noise Studies." Journal of Applied Physics, Vol. 38, No. 7 (1967), 2935-2946.

(17) Harvey, M. E. "Precision Temperature-Controlled Water Bath." The Review of Scientific Instruments, Vol. 39, No. 1 (1968), 13-18.

(18) Herzfeld, Charles M. Temperature, its Measurement and Control in Science and Industry, Volume Three, Part 1. New York: Publishing Corp., 1962.

(19) Jenkins, G. M., and D. G. Watts. Spectral Analysis and its Applications. San Francisco: Holden-Day, 1968.

(20) Larsen, N. T. "50 Microdegree Temperature Controller." The Review of Scientific Instruments, Vol. 39, No. 1 (1968), 1-12.

(21) Lynch, Charles T. Handbook of Materials Science Volume III: Non-Metallic Materials and Applications. Cleveland: CRC Press Inc., 1975.

(22) Mansour, I. R. M., R. J. Hawkins, and G. G. Bloodworth. "Digital Analysis of Current Noise at Very Low Frequencies." The Radio and Electronic Engineer, Vol. 35, No. 4 (1968), 201-211.

(23) Mansour, I. R. M., R. J. Hawkins, and G. G. Bloodworth. "Measurement of Current Noise in M. O. S. Transistors From 5 x 10^{-5} to 1 Hz." The Radio and Electronics Engineer, Vol. 35, No. 4 (1968), 212-216.

(24) Miller, S. A. Ethylene and its Industrial Derivatives. London: Ernest Benn Limited, 1969.

(25) Motchenbacher, C. D., and F. C. Fitchen. Low-Noise Electronic Design. New York: Wiley Interscience, 1973.

(26) Otnes, Robert K., and Loren Enochson. Digital Time Series Analysis. New York: Wiley Interscience, 1972.

(27) Parzen, E. Stochastic Processes. San Francisco: Holden-Day, 1962.

(28) Ringo, John A. "Low Frequency Noise in Reference Diodes." (Unpub. Ph.D. thesis, University of Washington, 1971.)

(29) Ringo, J. A., and P. O. Lauritsen. "Voltage Drift Related to Low-Frequency Noise in Reference Diodes." Proceedings IEEE, Vol. 60 (1972), 236-237.

(30) Tandon, Jawahar Lal. "Excess Noise Spectral Analysis of Boron Implanted Layers in Silicon." (Unpub. M.S. thesis, Oklahoma State University, 1973.)

(31) Templeton, I. M., and B. W. Rollin. "Noise in Germanium Filaments at Very Low Frequencies." Proceedings Physical Society B, Vol. 67 (1954), 271.

(32) Weast, Robert C. Handbook of Chemistry and Physics 54th Edition. Cleveland: CRC Press Inc., 1973.

(33) van der Ziel, A. Fluctuation Phenomena in Semi-Conductors. London: Butterworths Scientific Publications, 1959.

APPENDIX A

POSITIONAL SCANNER CIRCUIT DIAGRAM

This appendix contains the circuit diagram of the electronic circuitry associated with the positional scanner discussed in Chapter II. The power for the circuit is obtained from two HP 721A power supplies set for + and - 15 V, respectively.

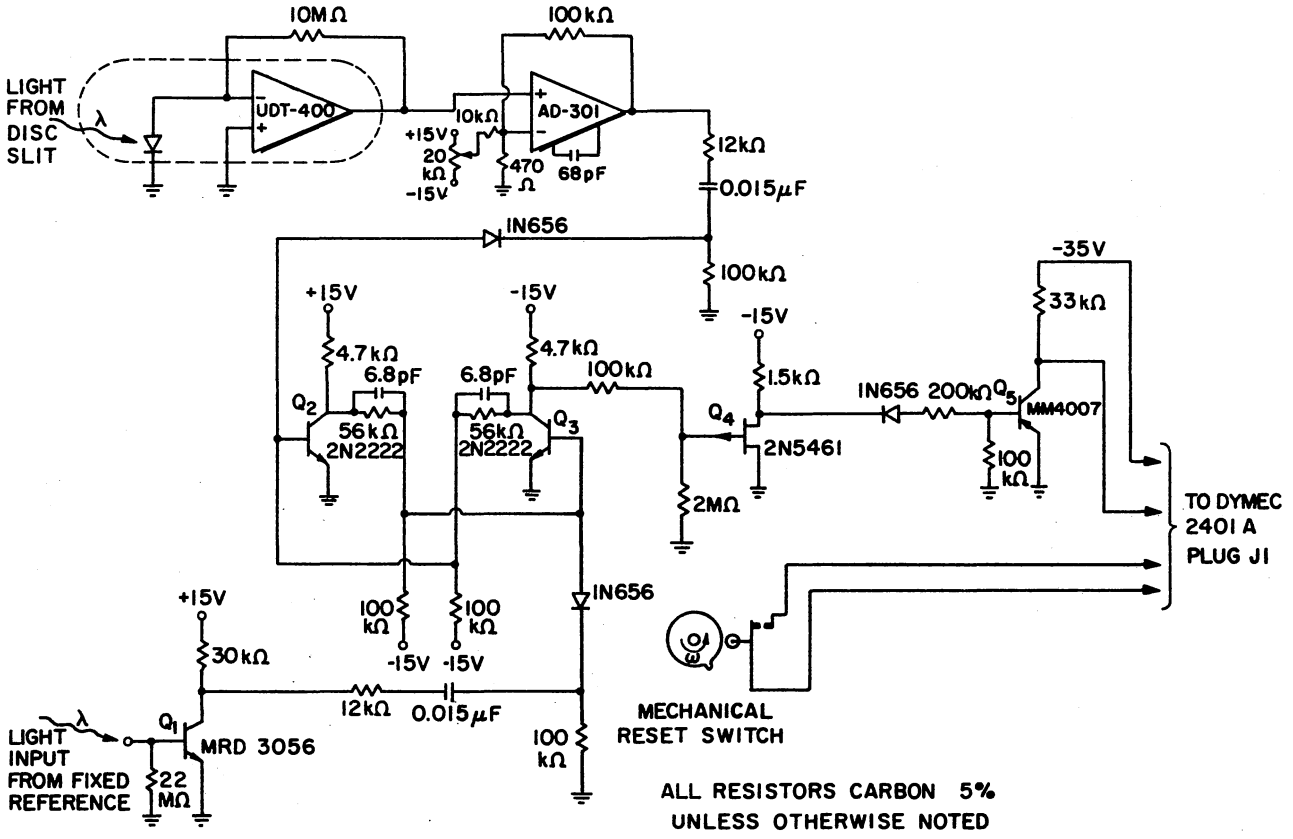

Figure 37. Positional Scanner Circuit Diagram

APPENDIX B

CONSTANT TEMPERATURE THERMOSTAT

CIRCUIT DIAGRAMS

Contained in this appendix are the electronic circuit diagrams of the circuitry associated with the thermostat presented in Chapter III. This circuitry is presented in four separate schematic diagrams with a fifth diagram detailing the interconnections. The power for the circuits presented is supplied by two Harrison Labs 865C power supplies which are set for + and - 15 V, respectively. The reference oscillator signal is supplied by a Wavetek 133 low frequency function generator.

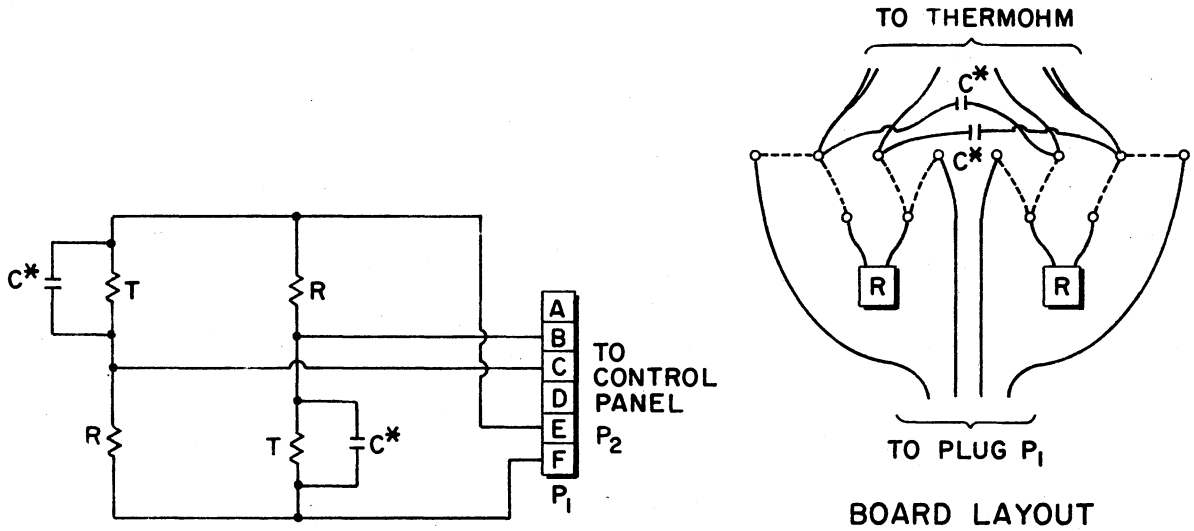

T - L & N No. 8922-44-00-0-22-S
DUAL 100Ω PLATINUM THERMOHM

R - VISHAY TYPE S102
113Ω, 0.01%, T.C.- 1 PPM

C* - SELECTED FOR VALUE NECESSARY
TO BALANCE BRIDGE

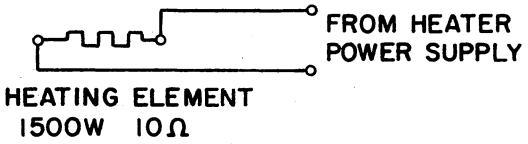

Figure 38. Circuit Diagram of Temperature Sensitive Bridge and Heater Element

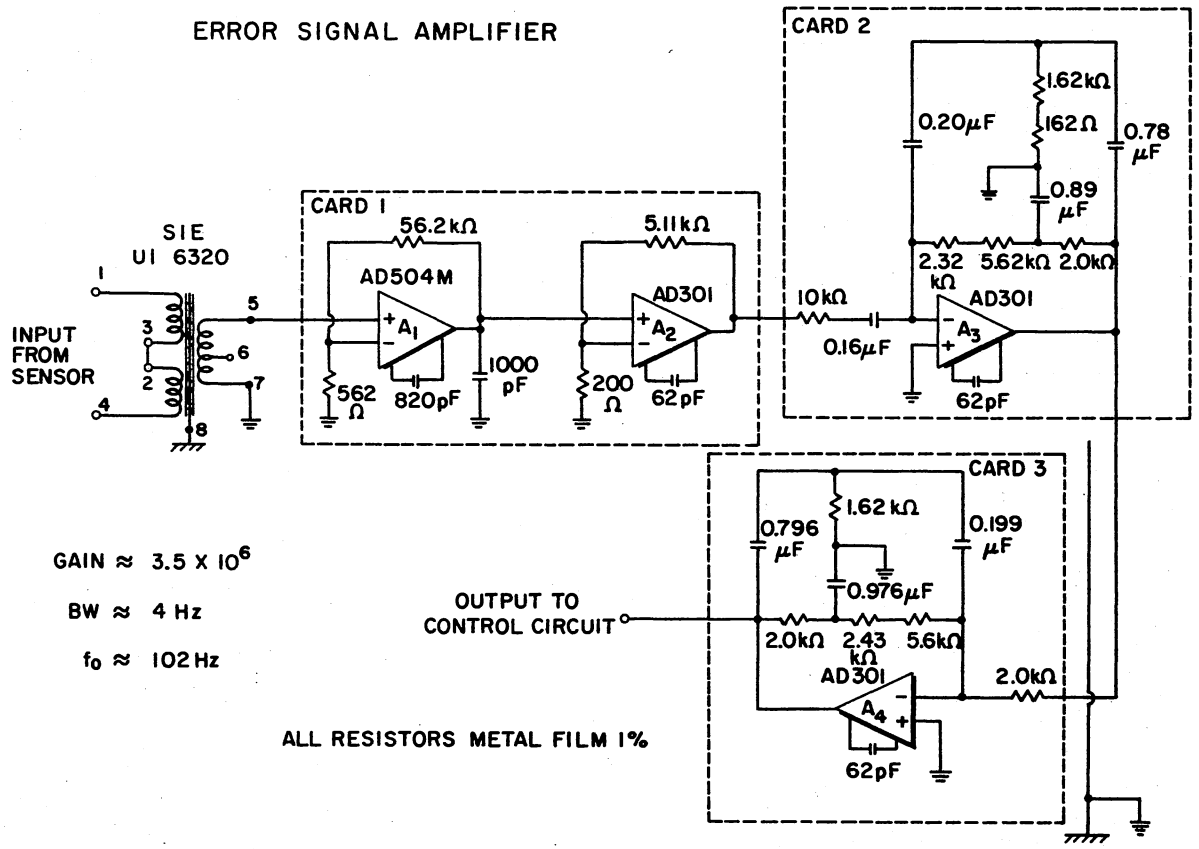

Figure 39. Circuit Diagram of Error Signal Amplifier

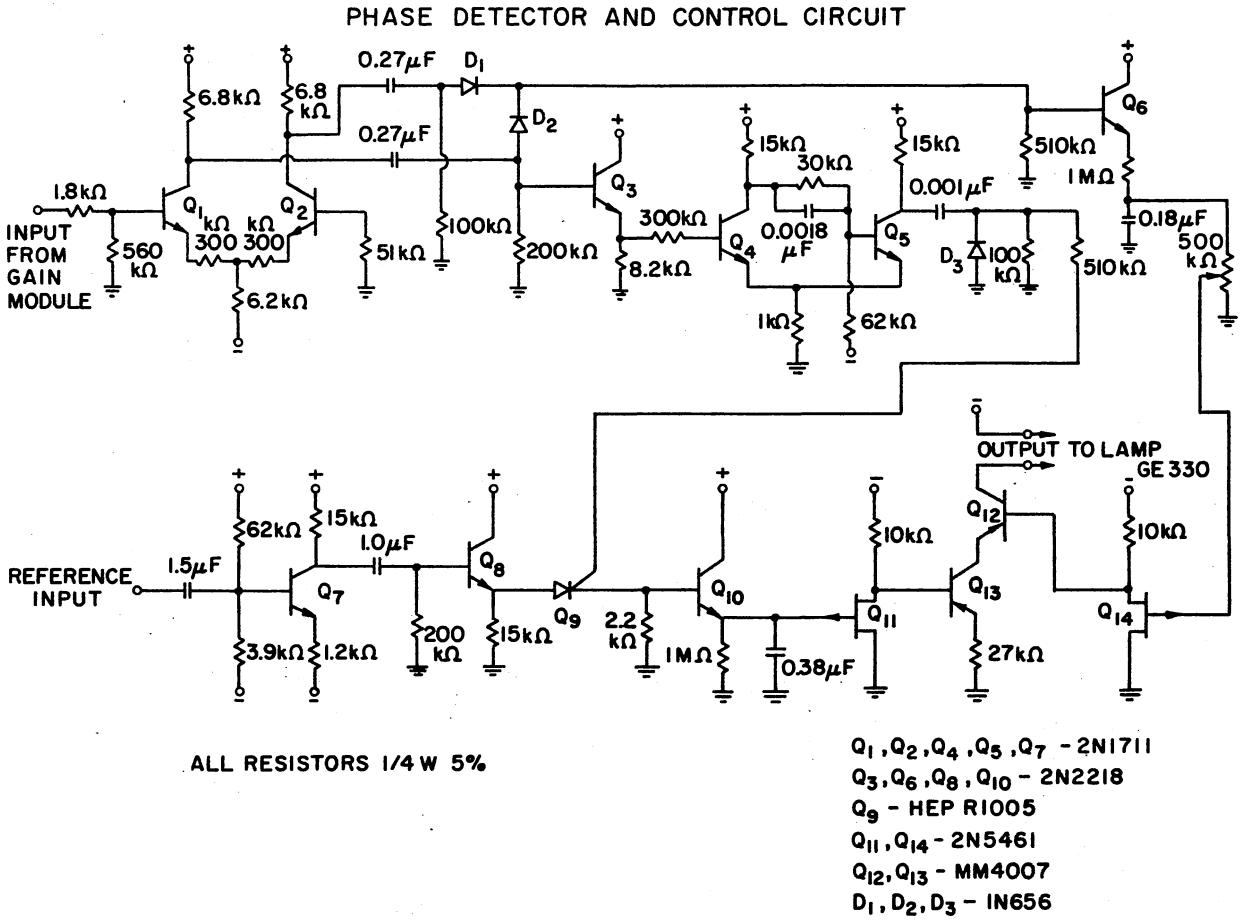

Figure 40. Circuit Diagram of Phase Detector and Control Circuit

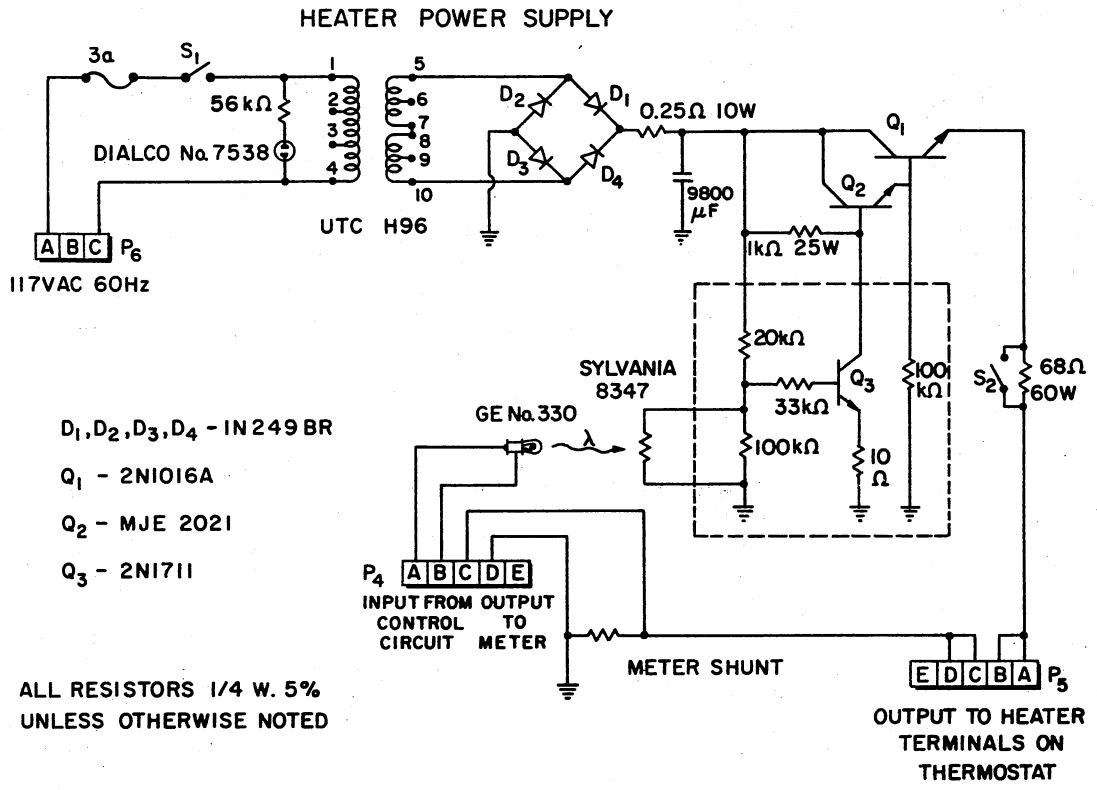

Figure 41. Circuit Diagram of Heater Power Supply

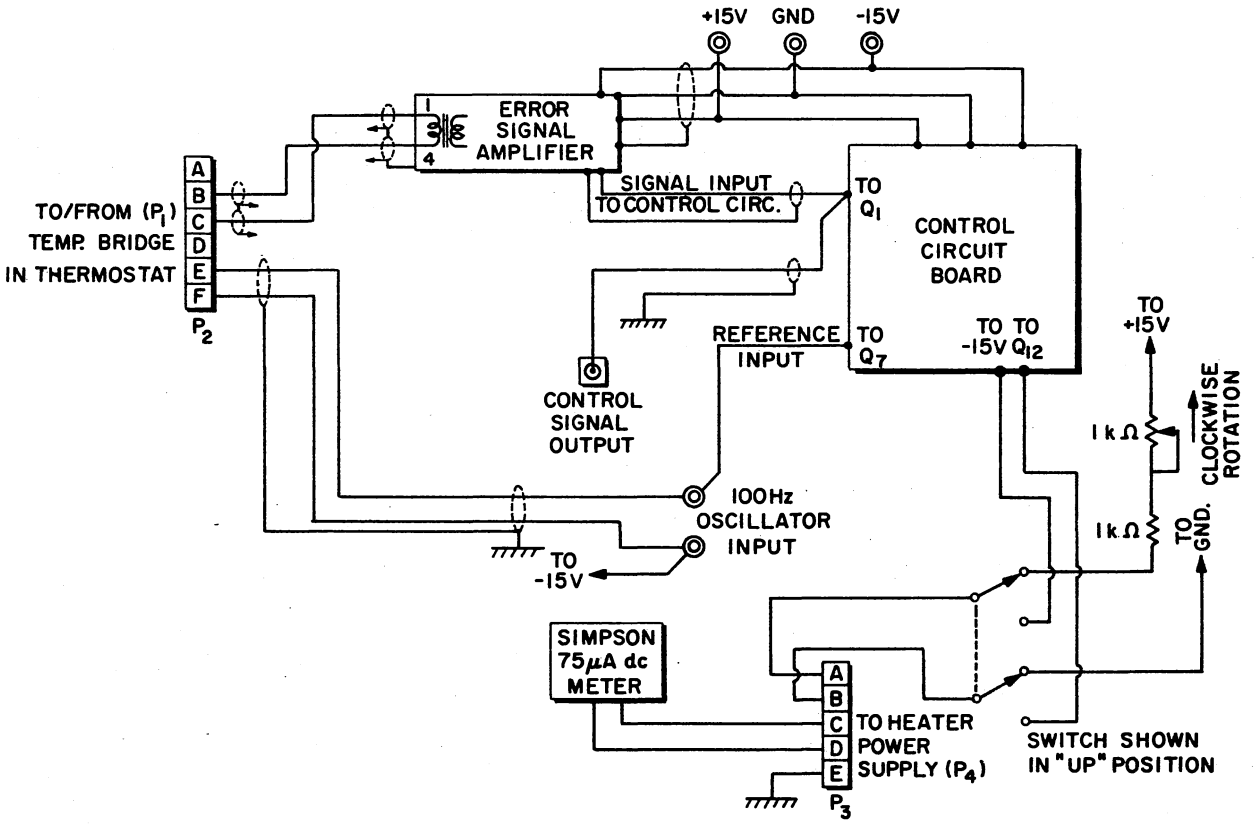

Figure 42. Interconnection Diagram for the Circuits Used in the Thermostat Control System

APPENDIX C

FORTRAN LISTING OF PROGRAM USED FOR NOISE DATA PROCESSING

The complete program that was used to process the noise voltage data and described in Chapter V is listed in this appendix. The programming language used for this program is FORTRAN IV. The FFT (Fast Fourier Transform) routine used is contained in the library of subroutines of the computational facility at Oklahoma State University. The calling name for the FFT is FOUR2.

The input data set for this program consists of two cards and the measured noise data. The first card is simply a title card which normally contains information identifying the noise data set. It is read according to a 20A4 format. The second card contains the values for the following variables in the order given. These variables are: NN - the number of samples in the data set, DUL - the upper allowable limit on each data value, DLL - the lower allowable limit on each data value, DXR - the maximum allowable change in value between adjacent data samples, POD - the data sample period in seconds, YL - a sensitivity parameter for the spectrum analyzer, IXT - a flag denoting if the data set should be corrected for a linear trend (IXT $\neq$ 0 if this is desired), and IAC - a flag denoting if program output is desired on punched cards (IAC $\neq$ 0 if punched card output is desired). The values of these variables are

punched on the second card according to a 1I10,5F10.0,2I5 format. The noise data set, which follows, is read according to a 16F5.0 format.

```
FORTRAN IV G LEVEL  21                MAIN                DATE = 75302          15/46/11

0001                  REAL*8 XAV, DNN
0002                  DIMENSION Q(20), X(32770)
0003                1 FORMAT (1H1)
0004                2 FORMAT (20A4)
0005                3 FORMAT (1H1,15X,20A4,////,1H0,15X,23HNUMBER OF DATA POINTS =,1I7,/
                     1,1H0,15X,15HSAMPLE PERIOD =,1F7.4,2X,7HSECONDS,/,1H0,15X,21HUPPER
                     2LIMIT ON DATA =,1F8.1,/,1H0,15X,21HLOWER LIMIT ON DATA =,1F8.1,///
                     3/,1H0,31X,11HDATA ERRORS,/,1H+,31X,11(1H_),/,1H0,15X,9HPOINT NO.,5
                     4X,10HDATA VALUE,4X,15HCORRECTED VALUE,/,1H+,15X,9(1H_),5X,10(1H_),
                     54X,15(1H_),/)
0006                4 FORMAT (1H ,12X,1I10,5X,1F10.0,7X,1F10.1)
0007                5 FORMAT (1H0,15X,18HNUMBER OF ERRORS =,1I6,///)
0008                6 FORMAT (1I10,5F10.0,2I5)
0009                7 FORMAT (1H1,1I10,3F10.1,2F15.4,2I10,//)
0010                8 FORMAT (16F5.0)
0011                9 FORMAT (1H0,15X,20HMEAN VALUE OF DATA =,1E14.6,3X,11HMICRO-VOLTS)
0012                  READ (5,2) (Q(L),  L=1,20)
0013                  READ (5,6) NN, DUL, DLL, DXR, POD, YL, IXT, IAC
0014                  READ (5,8) (X(I),  I=1,NN)
0015                  WRITE (6,7) NN, DUL, DLL, DXR, POD, YL, IXT, IAC
0016                  WRITE (6,3) (Q(L),  L=1,20), NN, POD, DUL, DLL
0017                  TP = (1.0E+05)*POD
0018                  NOE = 0
0019                  DO 13 I=2,NN
0020                  XX = X(I)
0021                  IF(DUL-XX)12,12,10
0022               10 IF(XX-DLL)12,12,11
0023               11 AVX = ABS(X(I)-X(I-1))
0024                  IF(DXR-AVX)12,12,13
0025               12 X(I) = (X(I-1) + X(I+1))/2.0
0026                  NOE = NOE + 1
0027                  WRITE (6,4) I, XX, X(I)
0028               13 CONTINUE
0029                  WRITE (6,5) NOE
0030                  CALL TCTD(NN,TP,X)
0031                  CALL CTPU(NN,TP,YL,X)
0032                  XAV = 0.0
0033                  DO 14 I=1,NN
0034                  XAV = XAV + X(I)
0035               14 CONTINUE
0036                  DNN = NN
0037                  XAV = XAV/DNN
0038                  WRITE (6,9) XAV
0039                  DO 15 K=1,NN
0040                  X(K) = X(K) - XAV
0041               15 CONTINUE
0042                  CALL PITD(NN,X)
0043                  IF(IXT)16,17,16
0044               16 CALL SLRM(NN,POD,X)
0045                  CALL PITD(NN,X)
0046               17 CALL SDVAM(NN,X)
0047                  CALL PHORT(NN,IAC,POD,Q,X)
0048                  STOP
0049                  END
```

```
FORTRAN IV G LEVEL  21                TCTD              DATE = 75302          15/46/11

0001                  SUBROUTINE TCTD(N,TP,X)
0002                  DIMENSION Z(3), T(3), X(1)
0003                  DO 7 K=2,N
0004                  Z(1) = X(K-1)
0005                  Z(2) = X(K)
0006                  IF(N-K)1,1,2
0007                1 Z(3) = 2.0*Z(2) - Z(1)
0008                  GO TO 3
0009                2 Z(3) = X(K+1)
0010                3 T(1) = Z(1)
0011                  T(2) = Z(2) + TP
0012                  T(3) = Z(3) + 2.0*TP
0013                  TX = Z(1) + TP
0014                  GX = 0.0
0015                  DO 6 L=1,3
0016                  XL = 1.0
0017                  DO 5 J=1,3
0018                  IF(L-J)4,5,4
0019                4 XL = XL*(TX - T(J))/(T(L) - T(J))
0020                5 CONTINUE
0021                  GX = GX + XL*Z(L)
0022                6 CONTINUE
0023                  X(K) = GX
0024                7 CONTINUE
0025                  RETURN
0026                  END
```

```
FORTRAN IV G LEVEL  21                  CTPU                DATE = 75302          15/46/11

0001                  SUBROUTINE CTPU(NN,TP,YL,X)
0002                  DIMENSION X(1)
0003                  PI = 3.14159265
0004                  A = 2.0*PI/TP
0005                  DO 1 I=1,NN
0006                  X(I) = YL*COTAN(A*X(I))
0007                1 CONTINUE
0008                  RETURN
0009                  END
```

```
FORTRAN IV G LEVEL  21                  PITD                DATE = 75302          15/46/11

0001                  SUBROUTINE PITD(NN,X)
0002                  DIMENSION X(1)
0003                1 FORMAT (1HO,15X,35HPOWER IN THE TIME DOMAIN WAVEFORM =,1P1E14.6,3X
                     1,24H(MEAN MICROVOLT SQUARED))
0004                  DNN = NN
0005                  M = NN - 1
0006                  A = X(1)*X(1) + X(NN)*X(NN)
0007                  DO 2 I=2,M
0008                  A = A + X(I)*X(I)
0009                2 CONTINUE
0010                  POW = A/DNN
0011                  WRITE (6,1) POW
0012                  RETURN
0013                  END
```

```
FORTRAN IV G LEVEL  21                SLRM              DATE = 75302          15/46/11

0001                  SUBROUTINE SLRM(N,SP,X)
0002                  DIMENSION X(1)
0003                1 FORMAT (1HO,/,1HO,15X,55HLINEAR TREND REMOVED FROM DATA  (LEAST ME
                     1AN SQUARE FIT),/,1HO,15X,21HTIME AXIS INTERCEPT =,1P1E14.6,3X,11H(
                     2MICROVOLT),/,1HO,15X,7HSLOPE =,1P1E14.6,3X,18H(MICROVOLT/SECOND))
0004                  DN = N
0005                  A = DN*(DN + 1.0)/2.0
0006                  B = A*(2.0*DN + 1.0)/3.0
0007                  AB = DN*B - A*A
0008                  T = 0.0
0009                  SX = 0.0
0010                  SXY = 0.0
0011                  DO 2 K=1,N
0012                  T = T + 1.0
0013                  SX = SX + X(K)
0014                  SXY = SXY + T*X(K)
0015                2 CONTINUE
0016                  Q = (B*SX - A*SXY)/AB
0017                  R = (DN*SXY - A*SX)/AB
0018                  RN = R/SP
0019                  WRITE (6,1) Q, RN
0020                  T = 0.0
0021                  DO 3 I=1,N
0022                  T = T + 1.0
0023                  X(I) = X(I) - (Q + R*T)
0024                3 CONTINUE
0025                  RETURN
0026                  END
```

```
FORTRAN IV G LEVEL  21                SDVAM              DATE = 75302          15/46/11

0001                  SUBROUTINE SDVAM(NN,X)
0002                  DIMENSION XM(150), VS(150), X(1)
0003                1 FORMAT (1H1,9X,21HDATA POINTS PER SET =,1I5,/,1H0,9X,16HNUMBER OF
                     1SETS =,1I5,//,1H0,9X,10HSET NUMBER,6X,4HMEAN,7X,8HVARIANCE,6X,18HS
                     2TANDARD DEVIATION,/)
0004                2 FORMAT (1H ,5X,1I10,7X,1P1E10.3,3X,1P1E10.3,8X,1P1E10.3)
0005                3 FORMAT (1H0,10X,8HALL SETS,4X,1P1E10.3,3X,1P1E10.3,8X,1P1E10.3,//)
0006                  K = 256
0007                  N = NN/K
0008                  WRITE(6,1) K, N
0009                  AN = N
0010                  AK = K
0011                  BK = AK - 1.0
0012                  ANK = NN
0013                  BNKR = 1.0/(ANK - 1.0)
0014                  JI = 1
0015                  JK = K
0016                  DO 12 I=1,N
0017                  XX = 0.0
0018                  DO 10 J=JI,JK
0019                  XX = XX + X(J)
0020               10 CONTINUE
0021                  XX = XX/AK
0022                  XM(I) = XX
0023                  SS = 0.0
0024                  DO 11 J=JI,JK
0025                  YY = (X(J) - XX)*(X(J) - XX)
0026                  SS = SS + YY
0027               11 CONTINUE
0028                  SS = SS/BK
0029                  VS(I) = SS
0030                  SD = SQRT(SS)
0031                  WRITE(6,2) I, XX, SS, SD
0032                  JI = JI + K
0033                  JK = JK + K
0034               12 CONTINUE
0035                  XT = 0.0
0036                  DO 13 II=1,N
0037                  XT = XT + XM(II)
0038               13 CONTINUE
0039                  XT = XT/AN
0040                  VT = 0.0
0041                  DO 14 JJ=1,N
0042                  ZZ = (XT - XM(JJ))*(XT - XM(JJ))
0043                  VT = VT + BK*VS(JJ) + AK*ZZ
0044               14 CONTINUE
0045                  VT = BNKR*VT
0046                  SDT = SQRT(VT)
0047                  WRITE(6,3) XT, VT, SDT
0048                  RETURN
0049                  END
```

```
FORTRAN IV G LEVEL  21                PHORT              DATE = 75302          15/46/11

0001                  SUBROUTINE PHORT(NN,IPUN,TP,AEQ,X)
0002                  DIMENSION N(1), AEQ(1), X(1)
0003                1 FORMAT (1H1)
0004                2 FORMAT (20A4)
0005                3 FORMAT (2I10,1F10.5)
0006                4 FORMAT (4E20.6)
0007                5 FORMAT (1H1,15X,20A4,///,1HO,15X,23HNUMBER OF DATA POINTS =,II7,/,
                     11HO,15X,15HSAMPLE PERIOD =,1F7.4,2X,7HSECONDS)
0008                  WRITE (6,5) (AEQ(I),  I=1,20), NN, TP
0009                  N(1) = NN
0010                  CALL WNFN(NN,X)
0011                  CALL FOUR2(X,N,1,-1,0)
0012                  B = 1.142857
0013                  DNN = NN
0014                  NPO = NN + 1
0015                  TFQ = 0.0
0016                  DTFQ = 1.0/(DNN*TP)
0017                  TPSB = 2.0*TP*TP*DTFQ*B
0018                  DO 6 I=1,NPO,2
0019                  II = I + 1
0020                  X1 = X(I)
0021                  X2 = X(II)
0022                  X(I) = TFQ
0023                  X(II) = (X1*X1 + X2*X2)*TPSB
0024                  TFQ = TFQ + DTFQ
0025                6 CONTINUE
0026                  CALL PRFD(NN,DTFQ,X)
0027                  CALL AGEO(NN,TP,X)
0028                  CALL AVFC(NN,TP,KL,X)
0029                  IF(IPUN)7,8,7
0030                7 WRITE (7,2) (AEQ(L),  L=1,20)
0031                  WRITE (7,3) KL, NN, TP
0032                  WRITE (7,4) (X(II),  II=1,KL)
0033                8 WRITE (6,1)
0034                  RETURN
0035                  END
```

```
FORTRAN IV G LEVEL  21                    WNFN                DATE = 75302          15/46/11

0001                  SUBROUTINE WNFN(NN,X)
0002                  DIMENSION X(1)
0003                  DNN = NN
0004                  PI = 3.14159265
0005                  B = 0.5
0006                  A = 10.0*PI/DNN
0007                  CC = COS(A)
0008                  CMO = 1.0
0009                  CMZ = CC
0010                  X(1) = 0.0
0011                  X(NN) = 0.0
0012                  IL = NN/10
0013                  IU = NN - 1
0014                  DO 1 K=2,IL
0015                  SS = B*(1.0 - CMZ)
0016                  X(K) = SS*X(K)
0017                  X(IU) = SS*X(IU)
0018                  CMT = CMO
0019                  CMO = CMZ
0020                  CMZ = 2.0*CMO*CC - CMT
0021                  IU = IU - 1
0022                1 CONTINUE
0023                  II = IL + 1
0024                  B = 2.0*B
0025                  DO 2 J=II,IU
0026                  X(J) = B*X(J)
0027                2 CONTINUE
0028                  RETURN
0029                  END
```

```
FORTRAN IV G LEVEL  21                PRFD              DATE = 75302          15/46/11

0001                  SUBROUTINE PRFD(NN,DTFQ,X)
0002                  DIMENSION X(1)
0003                1 FORMAT (1H0,15X,31HPOWER IN THE FREQUENCY DOMAIN =,1P1E14.6,3X,24H
                     1(MEAN MICROVOLT SQUARED))
0004                  A = (X(2) + X(NN+2))/2.0
0005                  B = 0.0
0006                  DO 2 I=4,NN,2
0007                  B = B + X(I)
0008                2 CONTINUE
0009                  POW = DTFQ*(A + B)
0010                  WRITE (6,1) POW
0011                  RETURN
0012                  END
```

```
FORTRAN IV G LEVEL  21                AGEO                DATE = 75302          15/46/11

0001                  SUBROUTINE AGEO(NN,TP,X)
0002                  DIMENSION X(1)
0003                1 FORMAT (1H , ///,16X,52HPOINTS  =  NUMBER OF RAW SPECTRAL ESTIMATE
                     1S AVERAGED,/,1HO,15X,57HBANDWIDTH  =  BANDWIDTH OF THE SPECTRAL ES
                     2TIMATE  (HERTZ),/,1HO,15X,76HFREQUENCY  =  APPROXIMATE CENTER FREQ
                     3UENCY OF THE SPECTRAL ESTIMATE  (HERTZ),/,1HO,15X,76HESTIMATE  =
                     4VALUE OF THE POWER SPECTRAL ESTIMATE  (MICROVOLT SQUARED/HERTZ),//
                     5//,1HO,24X,38HPOWER SPECTRAL DENSITY ANALYSIS OUTPUT,/,1H+,24X,38(
                     61H_),/,1HO,15X,6HPOINTS,6X,9HBANDWIDTH,9X,9HFREQUENCY,9X,8HESTIMAT
                     7E,/,1H+,15X,6(1H_),6X,9(1H_),9X,9(1H_),9X,8(1H_))
0004                2 FORMAT (1HO,10X,1I9,1P3E18.5)
0005                  NNN = NN
0006                  NE = -3
0007                  DO 4 M=1,20
0008                  IF(NNN)5,5,3
0009                3 NNN = NNN/2
0010                  NE = NE + 1
0011                4 CONTINUE
0012                5 DNN = NN
0013                  BW = 1.0/(DNN*TP)
0014                  L = 1
0015                  CFQ = 0.0
0016                  WRITE (6,1)
0017                  WRITE (6,2) L, BW, BW, X(4)
0018                  L = 6
0019                  MM = 2
0020                  DO 7 J=1,NE
0021                  SUM = 0.0
0022                  DO 6 I=1,MM
0023                  SUM = SUM + X(L)
0024                  L = L + 2
0025                6 CONTINUE
0026                  DMM = MM
0027                  SUM = SUM/DMM
0028                  MTT = 2*MM
0029                  DMT = MTT
0030                  FRQ = BW*(DMT + DMM - 1.0)/2.0
0031                  BWA = DMM*BW
0032                  WRITE (6,2) MM, BWA, FRQ, SUM
0033                  MM = MTT
0034                7 CONTINUE
0035                  RETURN
0036                  END
```

```
FORTRAN IV G LEVEL  21                AVFC                DATE = 75302          15/46/11

0001                  SUBROUTINE AVFC(NN,TP,KL,X)
0002                  DIMENSION X(1)
0003                1 FORMAT (1H1, ///,16X,52HPOINTS  =  NUMBER OF RAW SPECTRAL ESTIMATE
                     1S AVERAGED,/,1HO,15X,57HBANDWIDTH  =  BANDWIDTH OF THE SPECTRAL ES
                     2TIMATE  (HERTZ),/,1HO,15X,76HFREQUENCY  =  APPROXIMATE CENTER FREQ
                     3UENCY OF THE SPECTRAL ESTIMATE  (HERTZ),/,1HO,15X,76HESTIMATE  =
                     4VALUE OF THE POWER SPECTRAL ESTIMATE  (MICROVOLT SQUARED/HERTZ),//
                     5//,1HO,24X,38HPOWER SPECTRAL DENSITY ANALYSIS OUTPUT,/,1H+,24X,38(
                     61H_),/,1HO,15X,6HPOINTS,6X,9HBANDWIDTH,9X,9HFREQUENCY,9X,8HESTIMAT
                     7E,/,1H+,15X,6(1H_),6X,9(1H_),9X,9(1H_),9X,8(1H_))
0004                2 FORMAT (1HO,10X,1I9,1P3E18.5)
0005                3 FORMAT (1H ,37X,1P2E18.5)
0006                  WRITE (6,1)
0007                  DNN = NN
0008                  BW = 1.0/(DNN*TP)
0009                  FS = 1.5*BW
0010                  BWA = 4.0*BW
0011                  NPA = 4
0012                  K = 2
0013                  DO 11 I=2,NN,8
0014                  X(K) = (X(I) + X(I+2) + X(I+4) + X(I+6))/4.0
0015                  K = K + 2
0016               11 CONTINUE
0017                  DO 12 J=1,7,2
0018                  X(J) = FS
0019                  FS = FS + BWA
0020               12 CONTINUE
0021                  WRITE (6,2) NPA, BWA, X(1), X(2)
0022                  WRITE (6,3) (X(L),X(L+1),  L=3,7,2)
0023                  KK = 9
0024                  K = 10
0025                  L = 10
0026                  LF = 32
0027                  III = 18
0028                  FS = 1.5*BW + 4.0*BWA
0029               13 NPA = 2*NPA
0030                  NPATT = 2*NPA
0031                  FS = FS + 0.5*BWA
0032                  BWA = 2.0*BWA
0033                  NM = NPA/4
0034                  DNM = NM
0035                  DO 19 II=1,III
0036                  LF = LF + NPATT
0037                  IF(NN-LF)22,14,14
0038               14 SUM = 0.0
0039                  DO 15 JJ=1,NM
0040                  SUM = SUM + X(L)
0041                  L = L + 2
0042               15 CONTINUE
0043                  X(K) = SUM/DNM
0044                  X(KK) = FS
0045                  IF(II-1)16,16,17
0046               16 WRITE (6,2) NPA, BWA, X(KK), X(K)
0047                  GO TO 18
0048               17 WRITE (6,3) X(KK), X(K)
0049               18 K = K + 2
0050                  KK = KK + 2
0051                  FS = FS + BWA
0052               19 CONTINUE
0053                  IF(2048-LF)20,20,21
0054               20 III = 16
0055               21 GO TO 13
0056               22 KL = K - 2
0057                  RETURN
0058                  END
```

VITA

Telva Joe Boehm

Candidate for the Degree of

Doctor of Philosophy

Thesis: A NOISE SPECTRUM ANALYZER FOR FREQUENCIES LESS THAN ONE HERTZ AND INVESTIGATION OF LOW FREQUENCY ZENER DIODE NOISE

Major Field: Electrical Engineering

Biographical:

Personal Data: Born on August 30, 1943, Shiner, Texas, the son of Mr. and Mrs. A. J. Boehm.

Education: Attended primary and secondary schools in Shiner, Texas and graduates from Shiner High School in May, 1961; received Bachelor of Science in Electrical Engineering degree from The University of Texas - Austin, Austin, Texas in January, 1965; received Master of Science degree from Oklahoma State University, Stillwater, Oklahoma in May, 1970; completed requirements for Doctor of Philosophy degree at Oklahoma State University, Stillwater, Oklahoma in December, 1975.

Professional Experience: Employed as Staff Electronics Engineer by Phillips Petroleum Company, Bartlesville, Oklahoma, January, 1965 to July, 1966 and February, 1967 to September, 1969; Research Engineer with the Electro-Mechanics Company, Austin, Texas, July, 1966 to February, 1967; Instructor in Electrical Engineering at Texas A & I University, Kingsville, Texas, September, 1970 to July, 1972; Instructor in Electrical Engineering (part time) at Oklahoma State University, Stillwater, Oklahoma, September, 1973 to September, 1975.

Professional Memberships: Phi Kappa Phi; Eta Kappa Nu; and Sigma Tau.